

**VEHICLE-TO-VEHICLE CHANNEL MODELING AND
REAL TIME SIMULATOR DESIGN**

BY

MUHAMMAD IMRAN AKRAM

A Dissertation Presented to the
FACULTY OF THE COLLEGE OF GRADUATE STUDIES
KING FAHD UNIVERSITY OF PETROLEUM & MINERALS
DHAHRAN, SAUDI ARABIA

In Partial Fulfillment of the
Requirements for the Degree of

DOCTOR OF PHILOSOPHY

In

ELECTRICAL ENGINEERING

SEPTEMBER 2012

KING FAHD UNIVERSITY OF PETROLEUM & MINERALS
DHAHRAN 31261, SAUDI ARABIA

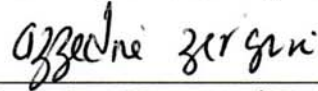
DEANSHIP OF GRADUATE STUDIES

This dissertation, written by **MUHAMMAD IMRAN AKRAM** under the direction of his dissertation adviser and approved by his dissertation committee, has been presented to and accepted by the Dean of Graduate Studies, in partial fulfillment of the requirements for the degree of **DOCTOR OF PHILOSOPHY IN ELECTRICAL ENGINEERING**.

Dissertation Committee



Dr. Asrar U. H. Sheikh (Adviser)



Dr. Azzedine Zerguine (Member)



Dr. Samir H. Abdul-Jauwad
(Member)



Dr. Ali H. Muqaibel (Member)



Dr. Tareq Y. Al-Naffouri (Member)



Dr. Ali A. Al-Shaikhi
Department Chairman



Dr. Salam A. Zummo
Dean of Graduate Studies



126/11/12

Date

©Muhammad Imran Akram
2012

Dedicated to the loving memories of my beloved parents

ACKNOWLEDGMENTS

In the name of Allah, the Most Gracious, the Most Merciful

All praise and thanks to Almighty Allah for His countless blessings

I am indebted to my university, King Fahd University of Petroleum and Minerals for my admission to its PhD program, and providing access to its scholarly faculty members and educational environment.

I would like to convey my deep thanks and appreciation to my adviser, Dr. Asrar U. H. Sheikh, whose experience, knowledge and persistence provided me a valuable support to accomplish my PhD goal. I appreciate his skills in many areas specially in channel modeling and simulator design. Dr. Sheikh supported me through out my course work, built my confidence, encouraged me to a challenging dissertation topic, and guided me technically with his experience.

I would also like to thank my dissertation committee members Dr. Azzedine Zerguine, Dr. Tareq Al-Naffouri, Dr. Ali H. Muqaibel and Dr. Samir H. Abdul-Jauwad for their guidance, constructive and positive feedback. I would also like to thank Dr. Maan A. G. Kousa my graduate adviser, for his precious support and advice during my time at KFUPM.

Finally, I would like to thank my parents, wife, siblings and my friends specially Khurram Masood, Muhammad Omer Bin Saeed, Fouad Zaro and Raza Umar for their prayers and their support.

TABLE OF CONTENTS

LIST OF TABLES	x
LIST OF FIGURES	xi
NOMENCLATURE	xiv
ABSTRACT (ENGLISH)	xviii
ABSTRACT (ARABIC)	xx
CHAPTER 1. INTRODUCTION	1
1.1 Background	3
1.1.1 Wireless Channel Modeling	3
1.1.2 V2V Channel Modeling	6
1.1.3 V2V Applications	9
1.1.4 Channel Simulators	10
1.2 Literature Survey	12
1.2.1 Large Scale Channel Models	12
1.2.2 Small Scale Channel Models	12
1.2.3 Composite Channel Models	13
1.2.4 Wideband Channel Models	13
1.2.5 V2V Channel Models	14
1.2.6 Non-Isotropic Scattering	14
1.2.7 Channel Simulators	15

1.2.8	Channel Emulators	16
1.3	Dissertation Contributions	18
1.4	Dissertation Layout	18
CHAPTER 2. NAKAGAMI HOYT V2V CHANNEL MODEL		20
2.1	First Order Statistics	22
2.2	Second Order Statistics	24
2.2.1	Spatial Time Correlation Function	24
2.2.2	Power Spectral Density	28
2.2.3	Level Crossing Rate and Average Duration of Fade	29
2.2.4	Squared Time Autocorrelation Function	31
2.3	Simulation and Results	32
2.4	Summary	41
CHAPTER 3. V2V HOYT CHANNEL MODEL UNDER NON- ISOTROPIC SCATTERING		43
3.1	Second Order Statistics	44
3.1.1	Spatial Time Correlation Function	44
3.1.2	Power Spectral Density	48
3.1.3	Level Crossing Rate and Average Duration of Fade	49
3.1.4	Squared Time Autocorrelation Function	51
3.2	Simulation and Results	53
3.3	Summary	63
CHAPTER 4. V2V HOYT CHANNEL MODEL WITH DIF- FUSED LINE OF SIGHT		64
4.1	Introduction	64
4.2	The Proposed Channel Model	65
4.3	First Order Statistics	66
4.4	Second Order Statistics	69
4.4.1	Spatial Time Correlation Function	69

4.4.2	Power Spectral Density	72
4.4.3	Level Crossing Rate and Average Duration of Fade	74
4.4.4	Squared Time Autocorrelation Function	77
4.5	Simulation and Results	79
4.6	Summary	88
CHAPTER 5. CHANNEL EMULATOR DESCRIPTION		89
5.1	Design Philosophy	90
5.2	Emulator Design Specification	91
5.3	Channel Emulator Functionality	92
5.3.1	Baseband Data Acquisition	93
5.3.2	Primary Secondary Board Interface	96
5.3.3	Tap Delay Line Filtering	99
5.3.4	Channel Gains Generations	103
5.4	Results and Comparison	110
5.5	Summary	117
CHAPTER 6. CONCLUSIONS AND FUTURE RECOMMENDATIONS		118
6.1	Conclusions	118
6.2	Future Recommendations	119
VITAE		144

LIST OF TABLES

5.1	Four Taps TDL Resources Allocation for Main Loop	104
5.2	Various Channel Models for Simulation	107
5.3	MSE of Various Quantities for $\alpha=0.5$	116

LIST OF FIGURES

1.1	Electromagnetic Waves Propagation	4
1.2	V2V Communications with Obstructed LoS	8
2.1	Block Diagram of IFFT Based Simulator	34
2.2	Output of the Hoyt Simulator	36
2.3	Hoyt Amplitude PDF Plot	36
2.4	Hoyt Phase PDF Plot	37
2.5	PSD Plot for $q=0.5$	37
2.6	Autocorrelation Function of Real Part of Envelope	39
2.7	Level Crossing Rate for $a=0.5$	39
2.8	Average Fade Duration for $a=0.5$	40
2.9	Squared Time Autocorrelation Function for $q=0.5$	40
2.10	Mean Square Error of Autocorrelation Function	42
3.1	Von Mises PDF Showing Non-Isotropic Scattering	45
3.2	Output of the Hoyt Simulator	56
3.3	Hoyt Amplitude PDF Plot	56
3.4	Hoyt Phase PDF Plot	57
3.5	PSD Plot for $q=.5$	57
3.6	Autocorrelation Function of Real Part of Envelop	58
3.7	Autocorrelation Function of Real Part of Envelop for $q=0.5,k=3$	58
3.8	Squared Autocorrelation Function of Real Part for $q=0.5,k=3$	59
3.9	Level Crossing Rates for $q=1$	59
3.10	Level Crossing Rates for $q=0.5$	60

3.11	Level Crossing Rates for $q=0.3$	60
3.12	Average Duration of Fade for $q=1$	61
3.13	Average Duration of Fade for $q=0.5$	61
3.14	Average Duration of Fade for $q=0.3$	62
3.15	Mean Square Error of Autocorrelation Function	62
4.1	Block Diagram of the Simulator Using Proposed Model	80
4.2	Envelope Output of the Simulator	80
4.3	Envelope PDF Plot	82
4.4	Phase PDF Plot	82
4.5	PSD Plot for $q=0.5$	83
4.6	Autocorrelation Function of Real Part of Envelope	83
4.7	Level Crossing Rate for $a=0.5$	84
4.8	Average Fade Duration for $a=0.5$	84
4.9	Normalized Squared Autocorrelation Function of envelope $q =0.5$	85
4.10	Mean Square Error of Autocorrelation Function	87
5.1	Channel Emulator Block Diagram	94
5.2	ORS-114 Block Diagram [145]	94
5.3	Block Diagram Showing Input Output Operations	97
5.4	Timing Diagram	97
5.5	MCBSP Connection Between the Two DSPs	98
5.6	Pointer Manipulation Using Circular Addressing	102
5.7	Tap Delay Line Filter Model	102
5.8	Single Tap Generation Using Filter Method	107
5.9	Frequency Response of IIR Filter $q=0.5$ $a=0$	108
5.10	Frequency Response of IIR Filter $q=0.5$ $a=0.5$	108
5.11	Frequency Response of IIR Filter $q=0.5$ $a=1.0$	109
5.12	Channel Magnitude Impulse Response	111
5.13	Input Data on Both I and Q Channel	111
5.14	TDL Filter Output Magnitude Plot	113

5.15 TDL Filter Output Phase Plot	113
5.16 PDF Plot for Envelope	114
5.17 PDF Plot for Phase	114
5.18 PDF Plot for LCR	115
5.19 PDF Plot for ADF	115
5.20 BER Plot, BPSK Modulation $q=1, q=0.5, q=0.3$	116

Nomenclature

Abbreviations

ACF	:	Autocorrelation Function
ADC	:	Analog to Digital Converter
ADF	:	Average Duration of Fade
AoA	:	Angle of Arrival
AoD	:	Angle of Departure
B2V	:	Base-to-Vehicle
DAC	:	Digital to Analog Converter
DSK	:	DSP Starter Kit
DSP	:	Digital Signal Processing
EDMA	:	Enhanced Direct Memory Access
EMIF	:	External Memory Interface
FPGA	:	Field Programmable Gate Array
IC	:	Integrated Circuit
IDFT	:	Inverse Discrete Fourier Transform
IFFT	:	Inverse Fast Fourier Transform
LAN	:	Local Area Network
LCD	:	Liquid Crystal Display
LCR	:	Level Crossing Rate
LoS	:	Line of Sight

MATLAB	:	Matrices Laboratory
MIMO	:	Multiple Input Multiple Output
MSE	:	Mean Square Error
NLoS	:	Non-Line of Sight
PCIE	:	Peripheral Component Interconnect Express
PSD	:	Power Spectral Density
QoS	:	Quality of Service
RMS	:	Root Mean Square
SoS	:	Sum of Sinusoids
SNR	:	Signal to Noise Ratio
SS-MSD	:	Steady-State Mean Square Deviation
SVD	:	Singular Value Decomposition
TDL	:	Tap Delay Line
TI	:	Texas Instrument
V2V	:	Vehicle-to-Vehicle
WSN	:	Wireless Sensor Network

Notations

i	:	Iteration number
d	:	Doppler value
$E[.]$:	Expectation operator
q	:	Hoyt Parameter
μ	:	Complex Gaussian process
ζ	:	Hoyt envelope process
ν	:	Hoyt phase process
	:	Mean direction of angle of arrival
σ	:	Standard deviation of complex Gaussian process
σ_1	:	Standard deviation of in-phase component
σ_2	:	Standard deviation of quadrature component
$ \cdot $:	L2 norm
N_p	:	Number of multipath components
N_f	:	Number of frequency points
r_n	:	Uniformly distributed amplitude of n^{th} multipath component
ϕ_n	:	Uniformly distributed phase of n^{th} multipath component
V_1	:	Receiver velocity
V_2	:	Transmitter velocity
f_{d1}	:	Maximum Doppler frequency of receiver
f_{d2}	:	Maximum Doppler frequency of transmitter

R	:	Space time correlation function of Hoyt process
N_ζ	:	Level crossing rate of envelope ζ
N	:	Maximum number of taps
$\bar{\tau}$:	Average duration of fade
$S(f)$:	Power spectral density
M	:	Number of time samples
$K(.)$:	Elliptical integral of second order
K	:	Constant $\frac{2\pi}{\lambda}$
J_0	:	Zero order Bessel function
α	:	Angle of arrival or angle of Departure
κ	:	Concentration parameter
H	:	Hoyt process with diffused LoS
A	:	Direct LoS component
ρ	:	Lognormally distributed component
r_0	:	Normalized envelope
T_s	:	Sampling Time
p	:	Probability density function
P	:	Probability distribution function

DISSERTATION ABSTRACT

NAME: Muhammad Imran Akram

TITLE OF STUDY: Vehicle-to-Vehicle Channel Modeling and Real Time Simulator Design

MAJOR FIELD: Electrical Engineering

DATE OF DEGREE: September 2012

Recently, wireless channel modeling and simulation has gained considerable attention in the field of wireless communications. To design a reliable and efficient wireless system, it is essential to understand the behavior of wireless channels in different environments. Due to the time varying and dispersive nature of wireless channels, accurate statistical channel modeling is a challenging task. To understand the nature of wireless channel, many researchers reported results of measurements under different environments and several channel models have been proposed on the basis of these measurements. This dissertation investigates the application of Nakagami-Hoyt channel model to Vehicle-to-Vehicle (V2V) communications under different scattering conditions.

Initially, a V2V Nakagami-Hoyt model that assumes isotropic scattering at both the transmitter and receiver antennas is proposed. Then, a generalized model is proposed with non-isotropic scattering assumption. Finally, a V2V Hoyt model with diffused Line of Sight (LOS) under isotropic scattering is investigated.

The proposed model is analyzed for first order statistics that include amplitude and phase Probability Density Functions (PDF) and mathematical expressions are derived for second order statistics including Spatial Time Correlation Function (STCF), Power Spectral Density (PSD), Squared Time Autocorrelation Function (STACF), Level Crossing Rate (LCR) and Average Duration of Fades (ADF). The proposed models are validated by an Inverse Fast Fourier Transform (IFFT) based simulator.

Finally, a real time wideband channel simulator (also known as emulator) is designed and implemented. The implemented emulator uses a floating point (TMS320C6713) and a fixed point (TMS320C6416) DSP. The emulator has 8 taps and baseband bandwidth of 20 MHz. It provides flexibility to test various channel models under different conditions. The baseband data is applied at the emulator input and output data is analyzed and compared with the analytical results in order to validate the emulator functionality.

Keywords: *Vehicle-to-vehicle, Nakagami-Hoyt, Spatial time correlation function, Power spectral density, Wideband channel simulator.*

ملخص الرسالة

الاسم: محمد عمران أكرم

عنوان الأطروحة: تصميم محاكي و أنمذجة القناة من مركبة الى مركبة

التخصص: هندسة الاتصالات

تاريخ الحصول على الدرجة: أيلول 2012

في الآونة الأخيرة، اكتسبت أنمذجة ومحاكاة القناة اللاسلكية اهتماما كبيرا في مجال الاتصالات اللاسلكية. ولتصميم نظام لاسلكي ذو موثوقية وفعالية من الضروري أن نفهم سلوك القنوات اللاسلكية في بيئات مختلفة. نظرا لطبيعة وتنوع وقت التشنت فإن أنمذجة القنوات اللاسلكية مهمة صعبة. ولفهم طبيعة القنوات اللاسلكية، أفاد العديد من الباحثين نتائج القياسات تحت بيئات مختلفة ونماذج قناة وقد اقترحت عدة نماذج على أساس هذه القياسات. هذه الأطروحة تدرس في تطبيق نموذج قناة نكاكامي-هويت في الاتصالات (V2V) في ظل ظروف مختلفة نشر.

في البداية، نموذج نكاكامي-هويت يقترح V2V و يفترض النموذج الذي نشر موحد الخواص على حد سواء في الارسال والهوائيات المتلقية. ثم، يقترح نموذجا المعمم مع افتراض نشر غير موحد الخواص. وأخيرا، تم التحقيق نموذجا هويت V2V مع الخط موزع البصر (LOS) في إطار موحد الخواص نشر.

النموذج المقترح حلل للإحصاءات الدرجة الأولى التي تشمل السعة وظائف المرحلة الكثافة الاحتمالية (PDF) والتعبيرات الرياضية وتستمد لإحصاءات الدرجة الثانية بما في ذلك وظيفة التوقيت المكاني الارتباط

(STCF)، كثافة الطاقة الطيفية (PSD)، تربيع دالة ترابط تلقائي الوقت (STACF)، المستوى معبر قيم (LCR) ومتوسط مدة رحيل (ADF). يتم التحقق من صحة النماذج المقترحة من قبل تحويل فورييه السريع العكسي (IFFT) استنادا على المحاكي.

وأخيرا، تم تصميم وتنفيذ جهاز محاكاة حقيقي ذو قناة نطاق عريضة (المعروف أيضا باسم المضاهاة). المضاهاة تنفذها يستخدم الفاصلة العائمة (TMS320C6713) ونقطة ثابتة (TMS320C6416 DSP). محاكي يحتوي على 8 الصنابير وعرض النطاق الترددي القاعدي من 20 ميغاهرتز. أنها توفر المرونة لاختبار نماذج مختلفة في ظل ظروف مختلفة. يتم تطبيق بيانات القاعدي في إدخال البيانات وإخراج المضاهاة وتحليلها ومقارنتها مع النتائج التحليلية من أجل التحقق من صحة وظيفة المحاكي.

كلمات البحث: مركبة الى مركبة، نكاامي-هويت، وظيفة التوقيت المكاني الارتباط، كثافة الطاقة

الطيفية، محاكاة حقيقي ذو قناة نطاق عريضة.

CHAPTER 1

INTRODUCTION

Radio communication is the option which makes communication on the move possible. Suitable technology and radio spectrum were the two major hurdles in the way of making communication accessible to common man although radio communication was invented more than a century ago. In 1895, Guglielmo Marconi was the first who established a radio link when he transmitted the morse code of the letter *S* from his backyard over a distance of 100 meters. Today, after more than 100 years, wireless communication is replacing old wired networks. The recent applications of wireless communication include but not limited to Wireless Local Area Networks (WLAN), messaging, wireless sensor networks, automated highways, industrial automation, smart homes, cordless and cellular telephone systems, satellite systems, Femtocells, Bluetooth and Zigbee devices etc. The wireless devices are also used as remote controlling devices for cars, home television systems, walkie-talkies etc [1]-[3].

In the conventional wireless communication systems, all the mobile stations

communicate with each other using a fixed station (base station) which is normally located at an elevated location. The mobile station is likely to be surrounded by assortment of objects having different shapes and scattering may occur near the mobile station which results in multipath fading channel and a direct path between the base and mobile may not always be present. Moreover, due to the motion of mobile station or changes in the surrounding environment, the channel may also vary with time.

Furthermore, two vehicles may directly communicate with each other while moving in the same or different directions and speeds avoiding the use of base station. V2V communications as it is called, finds its applications in mobile ad-hoc wireless networks, intelligent highway systems, emergency, military and security vehicles. The V2V communications is expected to enhance road safety (resulting in fewer accidents), improve traffic flow and share real time data without involving the cellular network which leads to greater fuel efficiency and reduce travel time.

To evaluate the design and performance of a communication system, it is desirable to evaluate it in realistic conditions. Although, experiments can be performed while driving vehicles through different environments but, this is a time-consuming and expensive exercise. In addition, the field trials can be affected by unintended and uncontrolled circumstances. The alternative is inexpensive and flexible option in use of a real time channel simulator (emulator) and it allows for measurement of the performance in a laboratory environments as in [4]-[6].

1.1 Background

1.1.1 Wireless Channel Modeling

Wireless communications are inherently unreliable due to their adverse time varying nature, multipath propagations and severe interference from other transmissions. Every communication system has to overcome these propagation effects to deliver acceptable performance. Unless specific measurements are taken, substantially higher power must be transmitted in order to overcome these severities. To design reliable and efficient wireless systems, it is essential to understand the nature of channels in different environments.

Electromagnetic waves propagate through these environments where they traverse unobstructed (free space) or reflected, scattered, and diffracted by terrain irregularities like walls, buildings, and other objects. Reflections occur when the dimension of the surface are larger than the wavelength of the incident wave. When the incident waves with wavelength in the order of or larger than the dimension of the incident object with irregular shape, scattering takes place and the signal energy is directed in many directions. These phenomenon are shown in Figure 1.1. The details of this propagation can be obtained by solving Maxwell's equations applying boundary conditions related to the physical and electromagnetic characteristics of the obstructing objects [7]. The solution to these equations are usually hard to obtain except under simpler geometry of the objects and under such circumstances approximations are usually made. Ray tracing are sometimes employed towards simplification of analytical solution.

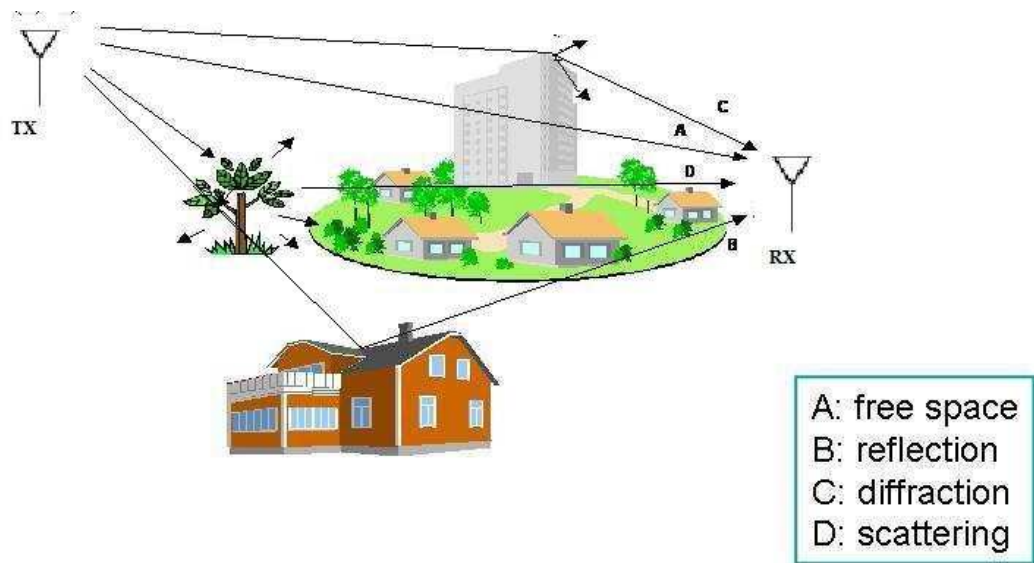


Figure 1.1: Electromagnetic Waves Propagation

Due to the complexity and time varying nature of wireless channel, it becomes hard to obtain an accurate deterministic channel model and researchers resort to statistical channel models, which plays an important role in the design of wireless communication system. Gaining understanding of the propagation channel is the first step towards an efficient wireless system design. The purpose of channel modeling is to estimate the first and the higher order statistical parameters of the fading channel and measure the performance of a transmission system. These parameters include Doppler spread, the time statistics of fading (average fade duration, level crossing rates), amplitude probability densities functions and the coherence bandwidth. For this purpose, extensive measurements have been made in different environments to characterize the channel. Over the past few decades, a number of experiments have been performed to characterize mobile channels in urban, suburban, mountainous, wooded and highway environments [8]-[25]. Based on these measurements, several statistical channel models have been proposed and investigated. These include pure short term fading models like the well-known Rayleigh, Rice [26], Hoyt [27], Nakagami-m [28], the mixed models Rice-lognormal Model [29], the Nakagami-Rice Model [30], the Nakagami-lognormal Model [31], the K distribution which is a substitute for the Rayleigh-lognormal distribution [32] and Weibull [33] and pure long term lognormal fading model [13], [34].

1.1.2 V2V Channel Modeling

In this dissertation the focus is on V2V channel modeling and simulation. V2V communication is a rapidly growing field these days. Measurements are being taken to characterize V2V channels along with their modeling and simulation. The aim of this dissertation is to use the findings of these measurement to develop a generalized statistical channel model and channel simulator.

In V2V communications, the transmitter and receiver directly communicate with each other without using a base station (BS). The antennas are mounted on the top or inside the vehicles and the speed of vehicles and their directions may be different thereby generating a time varying channel with the presence of Doppler spread. The buildings and other vehicles around act as scatterers hence generating multipath channel. Depending upon the vehicular locations the line of sight (LoS) may or may not be present. The transmitter and receiver communicating with each other are normally at the same height but surrounded by different set of scatterers. This scenario differs from the base to mobile communication where the BS is usually free of scatterers.

In V2V communications the LoS is not usually present and it may be partially obstructed which results in a diffused LoS component creating a phenomenon called Shadowing. Figure 1.2 presents a typical V2V communications scenarios. The direct component may or may not be present depending on the presence or absence of obstacles between the transmitter and the receiver. The direct component may be further divided into the case where a clear LoS between the

receiver and the transmitter exists or a diffused LoS is present. The value of diffused LoS is negligible when the buildings are of steel or reinforced concrete but it may be present in the case of buildings made of wood and bricks. Typical values of attenuations are mentioned in [36]. Moreover, indirect component may result from either scattering or diffractions or reflections or all of these from nearby and distant building and other obstacles.

The small-scale fading statistics in V2V communications have been of considerable interest in literature. Cheng et al [35] shows that for the distance between the Tx and Rx less than 5 m, the channel can be modeled as Nakagami- m with large value of m (3-4) whereas for the distance exceeding 70-100 meter the m factor was found to be less than unity which indicates severe fading which is worse than Rayleigh ($m=1$). This type of channel where $m \leq 1$ can be modeled as Nakagami-Hoyt (q) model. Youssef et al [25] validates the model after taking the measurements in the rural environment and states that the channel is more accurately modeled only when the variances of in-phase and quadrature components are not equal.

Previous V2V research was restricted to Rayleigh model and did not cover the generic cases where LoS is present. The above discussion leads the author to present a more generalized scenario and hence this model has been considered in this dissertation for investigation. In Chapter 2 to 4, the proposed model has been analyzed in detail for various first and second degree statistical parameters.

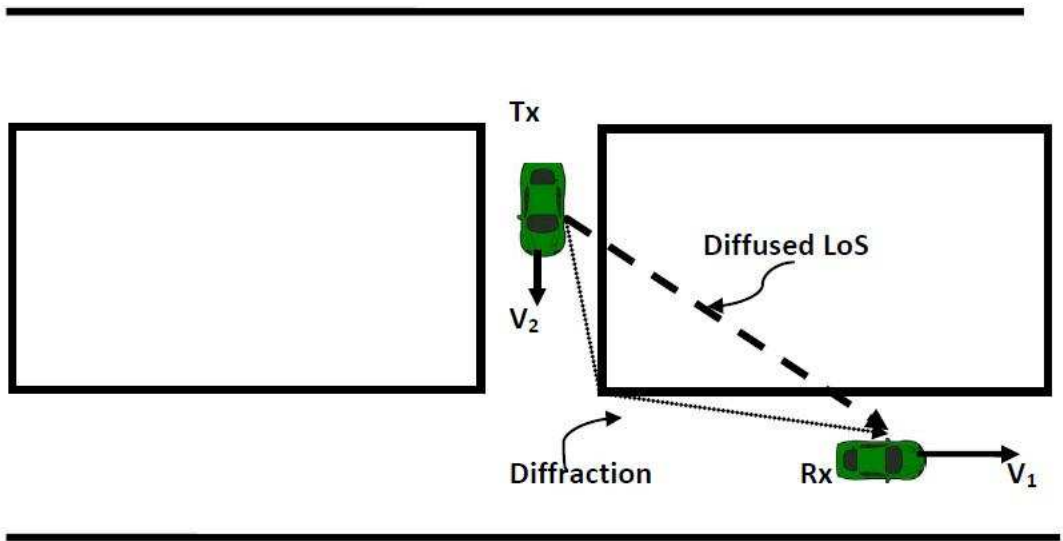


Figure 1.2: V2V Communications with Obstructed LoS

1.1.3 V2V Applications

V2V communication finds its applications in many fields. The main motivation behind using V2V technology is road safety and collision avoidance that can result in saving millions of human lives every year. In this section, some V2V applications are described.

Road Safety

Vehicles coordinate with other vehicles on the road to inform possible obstacle or danger. Car sensors can detect abrupt changes in path or speed and send them to the neighboring one. Vehicles can notify close vehicles of the direction they are taking so the drivers can make better decisions; a more advanced version of turn signals. In more advanced systems, at intersections the system can decide which vehicle has the right to pass first and alert all the drivers. Other applications include obstacle detection, reporting accidents, lane change alert etc.

Autonomous Vehicles

Recently, autonomous vehicles (self-driving cars), have been introduced and tested by different companies. Autonomous vehicle system is now legalized in California, Nevada and Florida states. These vehicles are safer than manually driven vehicles and can lead to increase in highways capacity by a factor of two or three through better controlled driving.

Military Applications

V2V communications can be used in battle fields where its main applications include surveillance, convoy communications, unmanned aerial vehicles (UAV) and video monitoring. In a typical convoy scenario, multiple vehicles are linked via broadband, with both the front and rear vehicles connected to the command post via satellite uplink [37].

Traffic Management

V2V communication is also used to remove traffic congestion or to ease traffic flow. Depending upon the traffic conditions, the traffic signal durations can be made adaptable. The traffic intersection control can also be enhanced to prevent accidents at road intersections.

1.1.4 Channel Simulators

Designing a reliable wireless communication system is a challenging task that communication engineers have to face. Customer's satisfaction must be met. The Quality of Service (QoS) includes good voice quality, having a low tolerance for busy signals or dropped connections, and desired error-free high-speed data transmission. For a system to efficiently meet these requirements, it must perform well in many different environments where the radio propagation characteristics vary considerably. Ensuring a products performance requires not only analysis and simulation, but also prototyping and testing. Such circumstances require a

large number of field trials and theoretical analysis to be performed. Field tests in a mobile environment are considerably more expensive and may require permission of regulatory authorities. A much more practical approach is to use a real-time channel simulator (emulator) that may be configured to simulate the various radio propagation characteristics encountered in the real world.

Simulation is generally defined as emulation of real system. The act of simulation of a system generally requires representation of certain key characteristics or behaviors of that system. Simulation can be used to show the behavior of the real system under different conditions that represent the real operating conditions. While simulation is used primarily for performance evaluation and design tradeoff studies (parameter optimization), simulation can also be used to establish test procedures and benchmarks, end-of-life predictions, and investigations of design anomalies after the system is deployed in the field.

Wireless channel simulators play important role in testing radio system components and devices in mobile environments. The aim behind the development of the channel simulator is to provide tools to test the system in the presence of controlled laboratory environment and in real time the highly dispersive propagation conditions of the multipath mobile radio channel caused by reflection and scattering.

The commercially available channel emulators such as *Spirent* [52], *Propsim* [53], *Azimuth RF* [54] etc. may not offer the user enough flexibility when configuring the wireless channel parameters to test the system under different environ-

mental conditions. A low cost channel emulator is therefore required that models different scenarios and at the same time provides the user flexibility to measure the performance of the wireless transceiver under environmental conditions.

1.2 Literature Survey

Channel modeling is the first step towards the efficient wireless simulator design. Over the past many years several mobile channel models have been proposed for links between fixed base station and mobile station. These include large scale, small scale, composite and wideband fading models. V2V channel models were also proposed between two mobile stations. Based on these models several software simulators and hardware simulators (emulators) were developed.

1.2.1 Large Scale Channel Models

Large scale fading models for path loss prediction include Okumara [55], Hata [56], Maciel [57], Ikegami [58], Xia [59], Walfisch-Bertoni [60], COST-231 [61] models. Several combinations of these models were also considered where different path loss terms from different models were used.

1.2.2 Small Scale Channel Models

Small scale fading models like the well-known Rayleigh, Rice [26], Hoyt [27], Nakagami-m [28] and Weibull [33] and for longer term lognormal [13], [34] fading models were used.

1.2.3 Composite Channel Models

Several composite fading models combining the short and long term models include Nakagami-lognormal [28], Suzuki [38] and Rice-lognormal [39]. For Satellite communications, Mehrina and Hashemi [40] proposed a model which is a combination of Rice and Nakagami-Hoyt channel, Loo in [41] proposed a mobile satellite model for the rural environment and Lutz [42] proposed a two state model Rice plus Rayleigh-Lognormal. Furthermore during the past decade, the statistical properties of the Generalized Rice [43],[44], Extended generalized Rice [80], Generalized Rice Hoyt[46], Nakagami-m fading [47], [48] were studied.

1.2.4 Wideband Channel Models

Several wideband channel models were also developed. These include Saleh and Valenzuela model [49] which is based on Turin [13] where a cluster of paths arrive in a unit time are modeled as a Poisson process. Each cluster is composed of clusters of sub-paths having exponential decay of the power. This model is known as Poisson-Poisson model. COST 207 [50] first introduced Tap Delay Line (TDL) models for the wideband propagation channels where number of paths were fixed and their average powers were modeled by Power Delay Profile (PDP). The maximum number of paths varied depending upon the system bandwidth from environment to environment. The TDL model was used by many standardized systems. These include GSM, WIFI, IMT2000, UMTS etc.

1.2.5 V2V Channel Models

During the last decade, large number of research projects were done on V2V communications [116]-[124]. V2V measurements over 5 GHz were performed by [119],[120] and the channel model was proposed in [121]. A detailed survey of the vehicular channel characterization under different environments (highway, rural, urban and suburban) was presented in [123]. The path loss exponent, RMS delay spread and mean Doppler spread under these conditions were shown.

The statistical model for V2V communication was first proposed by Akki and Haber [114] with the statistical properties described in [115]. This model covered Rayleigh distribution where both in-phase and quadrature components had equal variances. Matolak et al [125] performed measurement in five different cities and based on the results, modeled the channel as Weibull fading channel.

1.2.6 Non-Isotropic Scattering

In many real world scenarios, however, non-isotropic scattering is often experienced by the propagation wave. It was shown in [51]-[67] that in dense urban and indoor environments, non-isotropic scattering around the mobile station exists. Therefore, the autocorrelation function of Rice process under non-isotropic condition was derived [69]. The second order statistics of V2V Ricean fading channel under non-isotropic conditions were also derived and the theoretical results were compared with the measured data [68]. Zheng et al [70] presented V2V model for Rayleigh fading under non-isotropic condition. Many non-uniform distributions

were derived for different Angles of Arrival (AoA) and Angles of Departure (AoD). These include Gaussian, Laplacian, quadratic and Von Misses distributions. Von Misses distribution (assumed in [70]), a generic case described in [51], covers the other distributions (Gaussian, Laplacian, cosine and uniform distributions) as its special cases.

1.2.7 Channel Simulators

The simulators developed on the basis of above models are classified into three categories. The first category based on Jake's model uses the Sum of Sinusoid (SoS) approach for generating the fading channel coefficients. This approach has the drawback of multiple *Sine* function calls which make it computationally expensive to implement in real time. Secondly, this kind of simulators do not produce the channel behavior in time having statistical properties that match accurately with the theoretical values. Over the past two decades, significant research has been done to improve the model in order to generate the channel coefficients with statistical properties that are closer to the ones predicted by theoretical expressions [126]-[136]. The second class of simulator based on Clarke's model uses IFFT/IDFT based approach to generate the required channel coefficients. Although this approach is computationally efficient but it works on the block of data and hence for the streaming data in real time, it can not be used. The development of such simulators started in 1975 when [137] developed an IFFT based simulator in FORTRAN. The third approach that is also used in this dissertation

is the filter based approach. This is computationally efficient as well as it produces channel coefficients with more accurate statistical properties.

Cox et al [15] presented a discrete line spectrum based approach to simulate the channel. The work in [139] was based on sum of sinusoids (SoS) approach for simulator design. In [140] the simulation of MIMO V2V was presented. The simulator proposed in [141] was based on Kullback-Leibler divergence which was compared with IFFT based simulator design. Borries et al [113] used Gaussian quadrature rules for simulator design. Zaji et al [143] proposed an efficient SoS based approach for V2V simulator design. All the simulator design approaches mentioned above were restricted to only V2V Rayleigh fading channel.

1.2.8 Channel Emulators

Over the past four decades, efforts have been made to design and implement simulators in real time. Early efforts of emulator development were based on analog components [83]-[88]. The development of channel emulator started in 1973 when [82] developed the first Rayleigh based channel emulator. The emulator used Zener diode to generate Gaussian random variable. The analog components including op-amp, capacitors and resistors were used to generate the pulse shaping filter. With the advent of digital computers, micro-controllers, fast Analog to Digital Converters (ADCs) and Digital to Analog Converters (DACs), the analog components were replaced by digital thereby increasing the reliability and flexibility of emulators. Comroe et al [89] first used discrete digital logic in its emulator. Later

with the development of high speed Digital Signal Processors (DSPs), the DSP based channel emulators were developed these include a 16 bit fixed point DSP based emulator for implementation and simulation of the Gaussian quadrature components along with the log-normally distributed LoS component [90], an SoS based hardwired emulator [91] to verify the level crossing rate and distribution function expressions of Rayleigh, TMS320 E15 DSP chip based emulator [92], a fast and accurate simulator by Kominakis [98] and a C6713 DSP and PCIE-6259 hardware based emulator [100]. In addition to these, several wideband emulators were also developed, these include TMS32050 DSP and IMSA110 IC based emulator [93] having a baseband bandwidth of 10 MHz and maximum Doppler frequency of 100 Hz, TMS320C31 DSP based emulator [94], a 6 taps channel emulator having maximum signal bandwidth of 20 MHz using two 32 bit DSP floating point processors [95], a hybrid DSP FPGA architecture based 12 taps channel emulator [96] having baseband bandwidth of 5 MHz, a satellite Channel emulator [97] using TMS320C6701 DSP platform, a 5 MHz 12 taps emulator using 12 DSPs (1 for each tap) for the generation of complex coefficients [99] and a MIMO channel emulator using TMS320C55 DSP [101]. Over the last decade, the use of Field Programmable Gate Arrays (FPGAs) in DSP applications has become quite common. The FPGA based emulators were also developed. Implementation of channel emulators over FPGAs were described in [102]-[113].

1.3 Dissertation Contributions

The dissertation main contributions can be summarized as follows:

1. A novel channel model (Nakagami-Hoyt V2V) is proposed and its statistical properties are derived assuming both isotropic and non-isotropic scattering cases. A MATLAB based simulator is developed for this purpose to validate the derived results.
2. A generalized channel model (Nakagami-Hoyt V2V with diffused LoS) is proposed and its statistical properties are also derived assuming isotropic scattering. The model is validated using a MATLAB based simulator.
3. A wideband channel emulator is designed and implemented, it simulates the above channel models. The designed emulator in this dissertation is a modified form of the simulator described in [98]. The proposed emulator is a generalized real time version to model the wideband Nakagami-Hoyt channel found in V2V communication environment. The frequency selective channel is modeled as TDL filter. Efficient implementation of TDL filter is performed using TMS320C6416 DSP processor. To the best of author's knowledge, to date no such channel emulator has been developed and implemented.

1.4 Dissertation Layout

The remainder of this dissertation is organized as follows. Chapter 2 describes the Nakagami-Hoyt V2V channel model. The statistical properties of the proposed

model have been derived under the assumption of isotropic scattering (omnidirectional antennas) at both receiver and transmitter. The IFFT based simulator which has been developed to validate the chosen model is described. Chapter 3 discusses a generalized Nakagami-Hoyt V2V model under non-isotropic scattering. Again, the statistical properties for this model are derived and the simulator is developed to validate this model. In Chapter 4, the statistical properties of Nakagami-Hoyt V2V model with diffused LoS component are derived and a simulator is developed to validate the mathematical results. Chapter 5 describes the design philosophy behind the channel emulator and its implementation. Finally, Chapter 6 lists the research contributions made and it is followed by recommendations for future research. The chapter ends with concluding remarks.

CHAPTER 2

NAKAGAMI HOYT V2V CHANNEL MODEL

In this Chapter, we briefly describe and review the first and second order statistics of Hoyt fading narrow-band channel under the assumptions that the receiver and transmitter are moving with velocities V_1 and V_2 , respectively and under the isotropic scattering (i.e, omnidirectional antennas have been used at both end). The first order (probability density function of envelop and phase, mean and RMS values) and second order (spatial-time correlation function, time autocorrelation function, power spectral density, squared time autocorrelation function, level crossing rate and average duration of fade) statistical properties are derived and a MATLAB based simulator is developed to validate these properties. Finally, mean square error between the estimated and theoretical time autocorrelation function is also obtained as a function of number of frequency points of the simulator.

The Nakagami-Hoyt (also known as q) distribution is the distribution of the modulus of a complex Gaussian random variable $\mu(t)$ whose components are independent with zero mean and unequal variances.

$$\mu(t) = \mu_1(t) + j\mu_2(t) \quad (2.1)$$

and $\zeta(t)$ defines the modulus of the process, i.e.,

$$\zeta(t) = |\mu(t)| \quad (2.2)$$

where $\mu_1(t)$ and $\mu_2(t)$ are the Gaussian random processes with zero mean and variances σ_1^2 and σ_2^2 , respectively. $|\cdot|$ indicates the l_2 norm. The model parameters q and a are defined as

$$q = \frac{\sigma_1}{\sigma_2} \quad (2.3)$$

and

$$a = \frac{V_2}{V_1} \quad (2.4)$$

Reference [114] proposed a statistical model for the V2V Rayleigh fading channel. This model is modified for Nakagami-Hoyt frequency flat fading channel. The baseband equivalent channel components may be written as

$$\mu_1(t) = \sum_{n=1}^{N_p} r_n \cos[(w_{1n} + w_{2n})t + \phi_n] \quad (2.5)$$

Also,

$$\mu_2(t) = \frac{1}{q} \sum_{n=1}^{N_p} r_n \sin[(w_{1n} + w_{2n})t + \phi_n] \quad (2.6)$$

where N_p is the number of propagation paths, r_n and ϕ_n are respectively the uniformly distributed amplitude and phase of n^{th} path. w_{in} is given by

$$w_{in} = 2\pi f_{di} \cos(\alpha_{in}), \quad i = 1, 2 \quad (2.7)$$

where f_{d1} and f_{d2} are the maximum Doppler frequencies due to the motion of receiver and transmitter respectively. α_{1n} and α_{2n} are the AoA and AoD of the n^{th} path with respect to the velocity vector of receiver and transmitter, respectively.

2.1 First Order Statistics

The probability density function of a random variable is defined as the likelihood of the random variable to take on a given value. The PDF of the envelope $\zeta(t)$ is given by [27]

$$p_\zeta(x) = \frac{x}{\sigma_1 \sigma_2} e^{-\frac{x^2}{4}(\frac{1}{\sigma_1^2} + \frac{1}{\sigma_2^2})} I_0\left[\frac{x^2}{4}\left(\frac{1}{\sigma_1^2} - \frac{1}{\sigma_2^2}\right)\right], \quad x \geq 0 \quad (2.8)$$

where $I_0(\cdot)$ denotes the zeroth-order modified Bessel function of the first kind.

The PDF of the corresponding phase process $\nu(t) = \arctan[\mu_2(t)/\mu_1(t)]$ is given by [27]

$$p_\nu(\theta) = \frac{\sigma_1 \sigma_2}{2\pi(\sigma_2^2 \cos^2 \theta + \sigma_1^2 \sin^2 \theta)}, \quad 0 \leq \theta < 2\pi \quad (2.9)$$

when variances of in-phase and quadrature components are equal i.e. $\sigma_1=\sigma_2=\sigma$,

(2.8) becomes

$$p_\zeta(x) = \frac{x}{\sigma^2} e^{-\frac{x^2}{2\sigma^2}}, \quad x \geq 0 \quad (2.10)$$

which is Rayleigh PDF and (2.9) becomes

$$p_\nu(\theta) = \frac{1}{2\pi}, \quad 0 \leq \theta < 2\pi \quad (2.11)$$

which is Uniform distribution PDF.

Since the PDFs are independent of time so they will remain the same for V2V Nakagami-Hoyt channels. The mean m_μ and RMS R_{rms} values can be easily obtained as

$$\begin{aligned} m_\mu = E[\mu(t)] &= E[\mu_1(t)] + jE[\mu_2(t)] \\ &= 0 \end{aligned} \quad (2.12)$$

$$\begin{aligned} R_{rms} = \sqrt{E[\mu(t)^2]} &= \sqrt{E[\mu_1(t)^2] + E[\mu_2(t)^2]} \\ &= \sqrt{\sigma_1^2 + \sigma_2^2} \\ &= \sigma_2 \sqrt{1 + q^2} \end{aligned} \quad (2.13)$$

2.2 Second Order Statistics

The first-order PDFs of the envelope and phase do not provide information about the coherence or rapidity of the signal fades, as both PDFs are blind to the channels correlation properties. In this section, we shall derive the second order statistics of the proposed model. These include the spatial time correlation function, power spectral density, level crossing rate, the average duration of fade and squared time autocorrelation function. These quantities are useful in the measurement of burst error, bit and symbol interleaving schemes, mobile velocity estimation and Markov modeling of fading channels [71], [72], [78] and [73].

2.2.1 Spatial Time Correlation Function

Spatial time correlation function is defined as a statistical correlation between random variables at two different points that are separated in space and time. It is useful in different fields like communication and signal processing, astronomy, statistical mechanics, financial analysis etc.

For the derivation of spatial time correlation function of Nakagami-Hoyt V2V channel, [114] is used as a reference. The reference [114] describes the case when the fading is Rayleigh distributed. The results are obtained for more general case where $\sigma_1 \neq \sigma_2$.

The spatial time correlation function of the envelope is given by [74]

$$R(x_1, x_2, t_1, t_2) = \frac{1}{2} E[\mu_{x_2}(t_2) \mu_{x_1}^*(t_1)] \quad (2.14)$$

where $E[\cdot]$ is the statistical average, $\mu_{x_1}(t_1)$ and $\mu_{x_2}(t_2)$ are the complex envelope received at positions x_1 and x_2 at times t_1 and $t_2 = t_1 + \Delta t$ respectively. The envelope $\mu_{x_1}(t_1)$ may be written as,

$$\begin{aligned}\mu_{x_1}(t_1) &= \sum_{i=1}^{N_p} r_i \cos[(\omega_{1i} + \omega_{2i})t_1 + \phi_i] \\ &+ j \frac{1}{q} \sum_{i=1}^{N_p} r_i \sin[(\omega_{1i} + \omega_{2i})t_1 + \phi_i]\end{aligned}\quad (2.15)$$

Also,

$$\begin{aligned}\mu_{x_2}(t_2) &= \mu_{x_2}(t_1 + \Delta t) \\ &= \sum_{i=1}^{N_p} r_i \cos[(\omega_{1i} + \omega_{2i})(t_1 + \Delta t) + \phi_i + \psi_i] \\ &+ j \frac{1}{q} \sum_{i=1}^{N_p} r_i \sin[(\omega_{1i} + \omega_{2i})(t_1 + \Delta t) + \phi_i + \psi_i]\end{aligned}\quad (2.16)$$

where $\psi_i = \frac{2\pi}{\lambda} \Delta x \cos \alpha_{1i}$, $\omega_{li} = 2\pi f_{ml} \cos \alpha_{li}$ for $l = 1, 2$, ϕ_i is the uniformly distributed phase, α_{1i} and α_{2i} are AoA and AoD of the i th component respectively, $K = \frac{2\pi}{\lambda}$, $\Delta t = t_2 - t_1$ and $\Delta x = x_2 - x_1$. Therefore, we obtain,

$$\begin{aligned}R(x_1, x_2, t_1, t_2) &= \frac{1}{2} E \left[\sum_{i=1}^{N_p} \sum_{j=1}^{N_p} r_i r_j \right. \\ &\quad \left. \{ \cos[(\omega_{1i} + \omega_{2i})(t_1 + \Delta t) + \phi_i + \psi_i] \cos[(\omega_{1j} + \omega_{2j})t_1 + \phi_j] \right. \\ &\quad + \frac{1}{q^2} \sin[(\omega_{1i} + \omega_{2i})(t_1 + \Delta t) + \phi_i + \psi_i] \sin[(\omega_{1j} + \omega_{2j})t_1 + \phi_j] \\ &\quad + j \frac{1}{q} \sin[(\omega_{1i} + \omega_{2i})(t_1 + \Delta t) + \phi_i + \psi_i] \cos[(\omega_{1j} + \omega_{2j})t_1 + \phi_j] \\ &\quad \left. \left. - j \frac{1}{q} \cos[(\omega_{1i} + \omega_{2i})(t_1 + \Delta t) + \phi_i + \psi_i] \sin[(\omega_{1j} + \omega_{2j})t_1 + \phi_j] \right\} \right]\end{aligned}$$

AoA and AoD of i^{th} component are independent of each others and depends on the position of scatterers around the Rx and Tx only. They are also independent of the envelope and phase distributions. Hence, it is assumed that ϕ_i , α_{1i} , α_{2i} and r_i are mutually independent. Further, due to isotropic scattering assumption, α_{1i} and α_{2i} have uniform distributions for all i . Since ϕ_i is assumed to be uniformly distributed with zero mean, therefore $E[e^{j(\phi_i - \phi_j)}] = 0$ for all $i \neq j$. Also, for $i = j$, $E[e^{j(\phi_i - \phi_j)}] = 1$ and we get,

$$R(\Delta x, \Delta t) = \frac{1}{2} E \left[\sum_{i=1}^{N_p} r_i^2 \left\{ \left(1 + \frac{1}{q^2}\right) \cos[(\omega_{1i} + \omega_{2i})\Delta t + \psi_i] + j \frac{2}{q} \sin[(\omega_{1i} + \omega_{2i})\Delta t + \psi_i] \right\} \right]$$

It follows that,

$$\sigma_1^2 = \frac{1}{2} E[\sum_{i=1}^{N_p} r_i^2]$$

It is easy to see that the general form of the spatial time correlation function is written as,

$$R(\Delta x, \Delta t) = \frac{1 + q^2}{2q^2} \sigma_1^2 J_0(KV_2\Delta t) J_0(KV_1\Delta t + K\Delta x) \quad (2.17)$$

where $J_0(\cdot)$ is the zero-order Bessel function. $R(\Delta x, \Delta t)$ is the correlation functions of two signal envelopes obtained at two locations Δx apart, and at two time

instant Δt apart.

It can be shown that for $q = 1$, the space time correlation function for V2V Rayleigh fading channel is obtained

$$R(\Delta x, \Delta t) = \sigma_1^2 J_0(KV_2\Delta t)J_0(KV_1\Delta t + K\Delta x) \quad (2.18)$$

which matches with the result of [114]. Further by setting $V_2 = 0$ (i.e transmitter stationary) in (2.18), we get Tx (stationary) and Rx (mobile) B2V Rayleigh channel,

$$R(\Delta x, \Delta t) = \sigma_1^2 J_0(KV_1\Delta t + K\Delta x) \quad (2.19)$$

The time correlation is obtained by setting $\Delta x = 0$ in (2.18)

$$R_\mu(\Delta t) = R(0, \Delta t) = \frac{1 + q^2}{2q^2} \sigma_1^2 J_0(KV_2\Delta t)J_0(KV_1\Delta t) \quad (2.20)$$

The spatial correlation function is obtained by setting $\Delta t = 0$ in (2.18).

$$R_\mu(\Delta x) = R(\Delta x, 0) = \frac{1 + q^2}{2q^2} \sigma_1^2 J_0(K\Delta x) \quad (2.21)$$

Similarly for Rayleigh fading, the time and spatial correlation functions are obtained as

$$R_\mu(\Delta t) = \sigma_1^2 J_0(KV_2\Delta t)J_0(KV_1\Delta t) \quad (2.22)$$

$$R_\mu(\Delta x) = \sigma_1^2 J_0(K\Delta x) \quad (2.23)$$

2.2.2 Power Spectral Density

The power spectral density $S(f)$ of a signal is a quantity describes how the power of the signal is distributed in a range of frequency. It is useful in identifying the periodicity in a signal. For example, in speech processing it is used to find the pitch (fundamental frequency) and higher order harmonics. It is also useful in designing digital filters to suppress unwanted frequency components.

For a Wide Sense Stationary (WSS), process power spectral density is obtained by taking the Fourier Transform of the time autocorrelation function $R_\mu(\Delta t)$.

$$S(f) = \int_{-\infty}^{\infty} R_\mu(\Delta t) e^{-j2\pi f \Delta t} d\Delta t \quad (2.24)$$

$$S(f) = \frac{1+q^2}{2q^2} \sigma_1^2 \int_{-\infty}^{\infty} J_0(KV_2 \Delta t) J_0(KV_1 \Delta t) e^{-j2\pi f \Delta t} d\Delta t \quad (2.25)$$

The integral is evaluated using table in [76] and its reduced form is,

$$S(f) = \frac{1+q^2}{2q^2 \pi^2 f_{m1} \sqrt{a}} \sigma_1^2 \times K \left[\frac{(1+a)}{2\sqrt{a}} \sqrt{1 - \left(\frac{f}{(1+a)f_{m1}} \right)^2} \right], \quad a \neq 0, |f| < (1+a)f_{m1} \quad (2.26)$$

where $K(\cdot)$ is the elliptical integral function of first kind, f_{m1} , f_{m2} are the maximum Doppler shifts due to the motion of the receiver and transmitter respectively with $f_{mi} = \frac{V_i}{\lambda}$. Therefore, $f_{m2} = a f_{m1}$

Now, for the case $a = 0$, we have $V_2 = 0$. Hence, the PSD is obtained as

$$S(f) = \frac{1+q^2}{2q^2} \sigma_1^2 \int_{-\infty}^{\infty} J_0(KV_1\Delta t) e^{-j2\pi f\Delta t} d\Delta t \quad (2.27)$$

which is evaluated in [76] as

$$S(f) = \frac{1+q^2}{2q^2} \frac{\sigma_1^2}{\pi \sqrt{f_{m1}^2 - f^2}}, \quad |f| < f_{m1} \quad (2.28)$$

which is the expression for PSD of B2V Hoyt channel. Again the Rayleigh B2V PSD expression is obtained by setting $q = 1$ in eq (2.28),

$$S(f) = \frac{\sigma_1^2}{\pi \sqrt{f_{m1}^2 - f^2}}, \quad |f| < f_{m1} \quad (2.29)$$

2.2.3 Level Crossing Rate and Average Duration of Fade

The level crossing rate $N_\zeta(r)$ of stochastic process describes how often the process crosses a given level r for positive and negative slopes within unit time. It describes the rapidity of fading. Its main application include optimizing receiver parameters like modulation format, frame length, automatic gain control, estimating receiver velocity etc.

The level crossing rate of the process $\zeta(t)$ is obtained by solving the following integral [81]

$$N_\zeta(r) = \int_0^\infty \dot{z} p_{\zeta\dot{\zeta}}(r, \dot{z}) d\dot{z} \quad (2.30)$$

where $p_{\zeta\dot{\zeta}}$ is the joint PDF of $\zeta(t)$ and its time derivative $\dot{\zeta}(t)$. From [25], LCR

for B2V Hoyt envelope is given by

$$\begin{aligned}
N_{\zeta}(r) &= \frac{r}{(2\pi)^{3/2}\sigma_1\sigma_2} \\
&\times \int_0^{2\pi} e^{\left[-\frac{r^2}{2\sigma_1^2\sigma_2^2}(\sigma_2^2\cos^2(\theta)+\sigma_1^2\sin^2(\theta))\right]} \\
&\times \sqrt{\beta_1\cos^2(\theta) + \beta_2\sin^2(\theta)}d\theta
\end{aligned} \tag{2.31}$$

where $\beta_i = -\ddot{R}_{ii}(0)$ for $i = 1, 2$ and R_{11} & R_{22} are the autocorrelation functions of real and imaginary parts of the process, respectively.

For V2V Hoyt channel, using the values of $\beta_1 = (\sqrt{2\pi}\sigma_1f_{m1})^2(1 + a^2)$, $\beta_2 = \beta_1/q^2$ and $r_0 = r/R_{rms}$, the expression becomes,

$$\begin{aligned}
N_{\zeta}(r_0) &= \frac{\sqrt{(1 + a^2)(q^2 + 1)}f_{m1}r_0}{2q\sqrt{\pi}} \\
&\times \int_0^{2\pi} e^{\left[-\frac{r_0^2(q^2+1)}{2q^2}(\cos^2(\theta)+q^2\sin^2(\theta))\right]} \\
&\times \sqrt{q^2\cos^2(\theta) + \sin^2(\theta)}d\theta
\end{aligned} \tag{2.32}$$

It is easy to see that by substituting $a = 0$ and $q = 1$ the above equation will be reduced to the expression for B2V Rayleigh LCR as given in [75].

The average duration of fade of a signal is defined as average duration of time for which the signal envelope r spends below a specified threshold R_0 . It is useful in the estimation of burst error rate. It is given by [81]

$$\bar{\tau} = \frac{P(r < R_0)}{N_{\zeta}(r)} \tag{2.33}$$

where $P(r < R_0)$ is the Cumulative Density Function obtained by

$$P(r < R_0) = \int_0^{R_0} p_\zeta(x) dx \quad (2.34)$$

This is obtained by integrating (2.8). Hence substituting (2.32) and (2.34) in (2.33), ADF can be directly obtained.

2.2.4 Squared Time Autocorrelation Function

Squared time autocorrelation function is defined as time autocorrelation of the square of the envelope of a signal. It is used in computation of carrier to noise ratio (CNR),

$$R_{\mu^2}(\Delta t) = E[|\mu(t)|^2 |\mu(t + \Delta t)|^2] \quad (2.35)$$

$$\begin{aligned} R_{\mu^2}(\Delta t) &= E[|\mu(t)|^2 |\mu(t + \Delta t)|^2] \\ &= E[(\mu_1^2(t) + \mu_2^2(t))(\mu_1^2(t + \Delta t) + \mu_2^2(t + \Delta t))] \\ &= E[\mu_1^2(t)\mu_1^2(t + \Delta t) + \mu_2^2(t)\mu_2^2(t + \Delta t) \\ &\quad + \mu_1^2(t)\mu_2^2(t + \Delta t) + \mu_2^2(t)\mu_1^2(t + \Delta t)] \end{aligned} \quad (2.36)$$

All the Gaussian processes in the above equation are assumed zero mean i.e., $E[\mu_i(t)] = E[\mu_i(t + \Delta t)] = 0$. Since $\mu_1(t)$ and $\mu_2(t)$ are independent. Therefore

$$E[\mu_1^2(t)\mu_2^2(t)] = E[\mu_1^2(t)]E[\mu_2^2(t)] = \sigma_1^2\sigma_2^2 \quad (2.37)$$

Also, we have

$$\begin{aligned}
E[\mu_i^2(t)\mu_i^2(t + \Delta t)] &= E[\mu_i^2(t)]E[\mu_i^2(t + \Delta t)] & (2.38) \\
&+ 2\{E[\mu_i(t)\mu_i(t + \Delta t)]\}^2 \\
&= \sigma_i^4[1 + 2J_0^2(w_{m1}\Delta t)J_0^2(w_{m2}\Delta t)]
\end{aligned}$$

Substituting (2.37) and (2.38) in (2.36) results in

$$R_{\mu^2}(\Delta t) = 2\sigma_1^2\sigma_2^2 + (\sigma_1^4 + \sigma_2^4)(1 + 2J_0^2(w_{m1}\Delta t)J_0^2(w_{m2}\Delta t))$$

where, $w_{mi} = 2\pi f_{mi}$ is the angular frequency in radians per second.

The squared power spectral density is defined as the Fourier transform of the squared time autocorrelation function, i.e.,

$$S_{\mu^2}(f) = \int_{-\infty}^{\infty} R_{\mu^2}(\Delta t)e^{-j2\pi f\Delta t}d\Delta t \quad (2.39)$$

The integral in (2.39) is solved numerically

2.3 Simulation and Results

The simulator described in this thesis uses Smith spectrum method mentioned in [77]. This method requires frequency domain generation and processing of random signal followed by IFFT to obtain a time domain sequence with the desired properties. This method is IFFT based and was slightly modified to generate Hoyt

fading signal envelope simulator. The block diagram of the proposed simulator is shown in Figure 2.1. The simulator is implemented in MATLAB by following the steps given below.

1. Input the number of *frequency* samples (N_f) and *time* samples (M).
2. Specify maximum Doppler frequency due to the mobility of the receiver f_{m1} in Hz.
3. Specify the value of parameter a which defines the maximum Doppler frequency due to the mobility of the transmitter $f_{m2} = af_{m1}$.
4. Specify the value of q
5. Generate two $N_f/2$ samples Gaussian quadrature components with zero mean and unity variance. Generate the remaining $N_f/2$ components by conjugating them. This forms the negative frequency components.
6. Generate N_f points spectrum $\sqrt{S(f)}$ using (2.26).
7. The frequency spacing between the adjacent spectral lines are given by $\Delta f = 2f_{m1}(1+a)/N_f$. The time resolution is given by $1/\Delta f(M-1)$
8. Multiply the in-phase and quadrature components by $\sqrt{S(f)}$ and perform the IFFT of the resultant individual. Normalize both the resulting in-phase and quadrature to make their variance unity.
9. Quadrature component will yield μ_2 while in-phase component after multiplying with q will yield μ_1 .

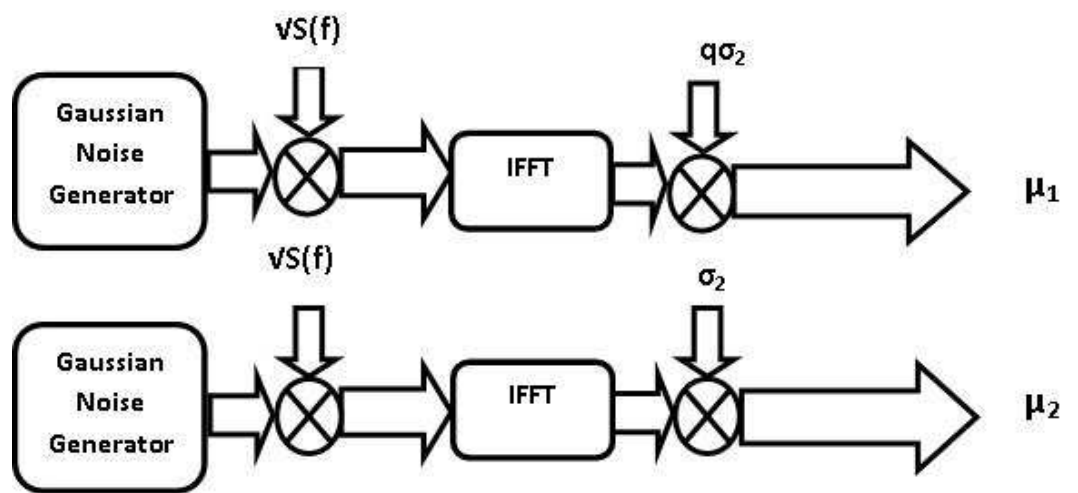


Figure 2.1: Block Diagram of IFFT Based Simulator

10. The square root of the sum of squared envelopes of both will generate random variable having Nakagami-Hoyt distribution for the given value of q .
11. The phase distribution is obtained by using the phase random variable $\tan^{-1}(\mu_1/\mu_2)$

The simulation was run with the following parameters, carrier frequency $f = 900MHz$, velocity of receiver $V_1 = 72km/hr$ which means $f_{m1} = 60Hz$, three different values of $q = 1, 0.5, 0.3$, three different values of $a = 1, 0.5, 0$ and $N_f = 8192$ samples.

The simulator sample output for $q = 0.5$ and $a = 0.5$ is shown in Figure 2.2. It shows the envelope time variation in dB .

The amplitude and phase PDFs plots are shown in Figure 2.3 and 2.4 respectively. The corresponding theoretical outputs of (2.8) and (2.9) respectively were also plotted for comparison. For $q = 1$, the plots obtained matches with Rayleigh envelope and phase PDFs [75].

The PSD plots for $a = 1, 0.5, 0$ and $q = 0.5$ are shown in Figure 2.5. It is evident from the plot that $S(f)$ has peaks at $f = \pm(f_{m1} - f_{m2})$ due to the characteristics of elliptical integral function $K(\cdot)$. The plots are symmetric which is the case of isotropic scattering when the correlation between the real and imaginary part is zero. For $a = 0$, the curve is U shaped which is the PSD plot of B2V communication.

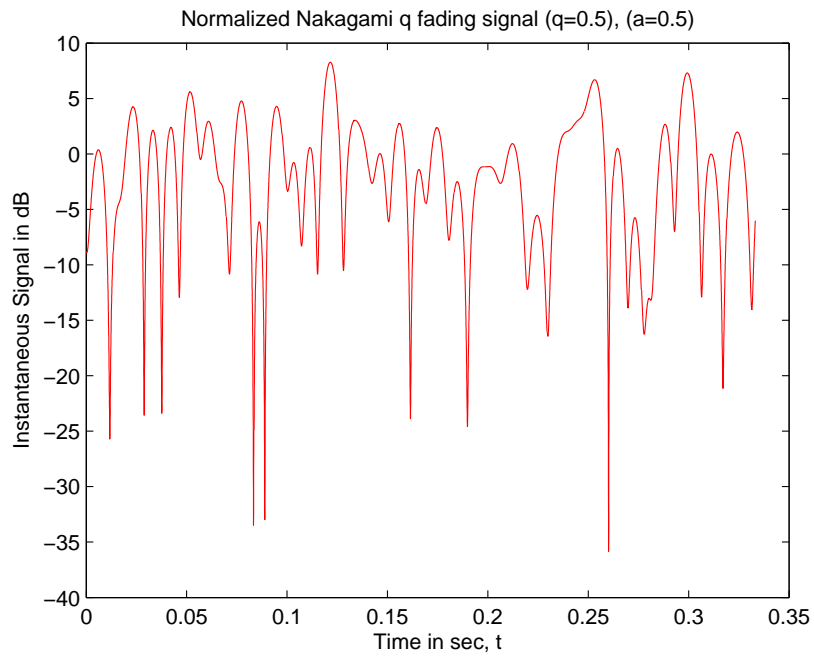


Figure 2.2: Output of the Hoyt Simulator

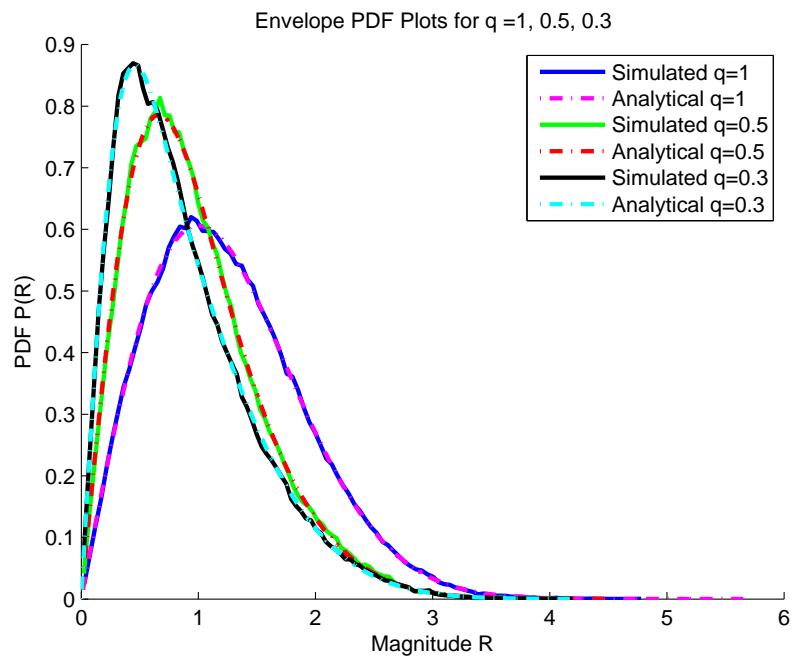


Figure 2.3: Hoyt Amplitude PDF Plot

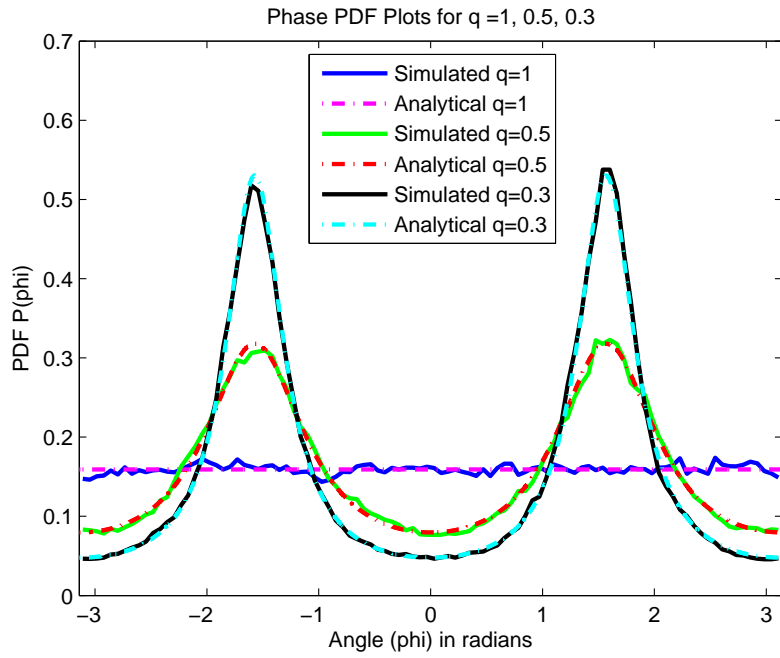


Figure 2.4: Hoyt Phase PDF Plot

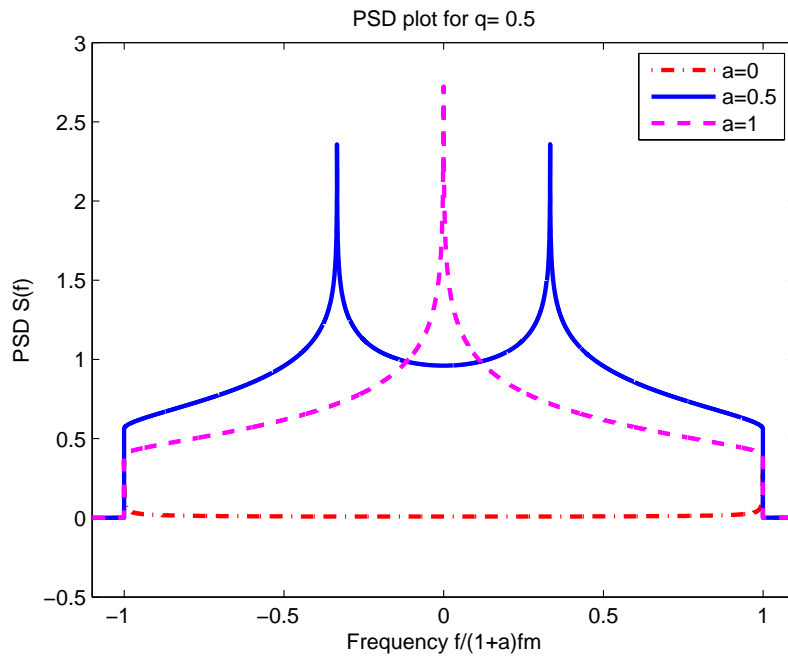


Figure 2.5: PSD Plot for $q=0.5$

The normalized ACF plots are shown in Figure 2.6. The plots for $a = 1, 0.5, 0$ are compared with the theoretical results obtained using expression of (2.20) for $q = 0.5$. Since the real and imaginary components are Gaussian, it can be found from the plots that the normalized ACF are still Bessel but with different shape than the one shown in [115].

The LCR and ADF for $q = 1, 0.5, 0.3$ are plotted in Figure 2.7 and 2.8 respectively for $a = 0.5$. The curves are matched with their theoretical expressions given by (2.32) and (2.33). It can be inferred from these curves that for a particular value of threshold r_0 , a decrease in value of q (i.e., increase in fading severity) results in higher LCR and lower ADF. It is also shown in Figure 2.7 that starting from higher values of threshold r_0 , LCR first start increasing till it reaches its maximum value at around -5 dB and then starts decreasing onward. The threshold at which LCR is maximum can be obtained by taking the derivative of (2.32) and equating it to 0.

The normalized squared autocorrelation function plots are shown in Figure 2.9. The plots for $a = 1, 0.5, 0$ are compared with the theoretical results obtained using expression of (2.39) with $q = 0.5$.

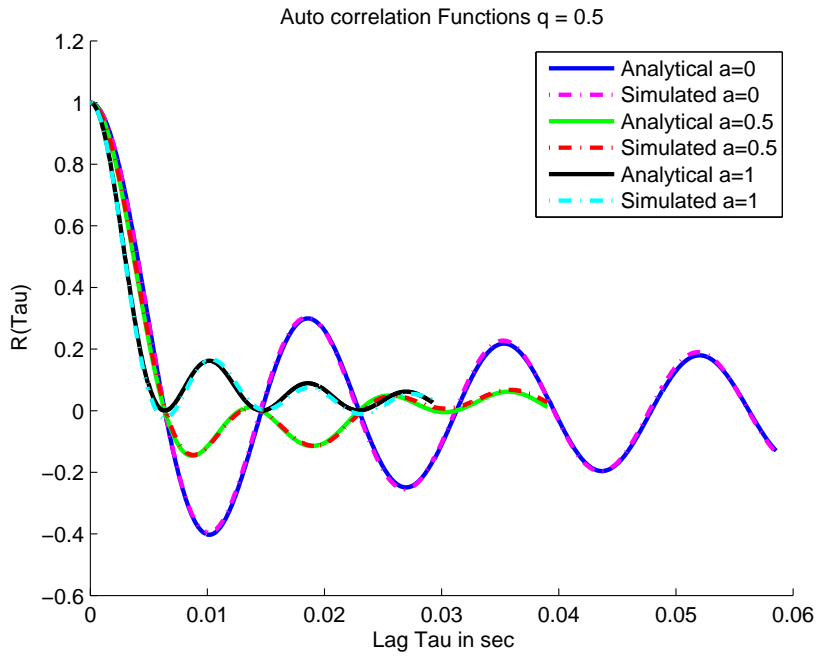


Figure 2.6: Autocorrelation Function of Real Part of Envelope

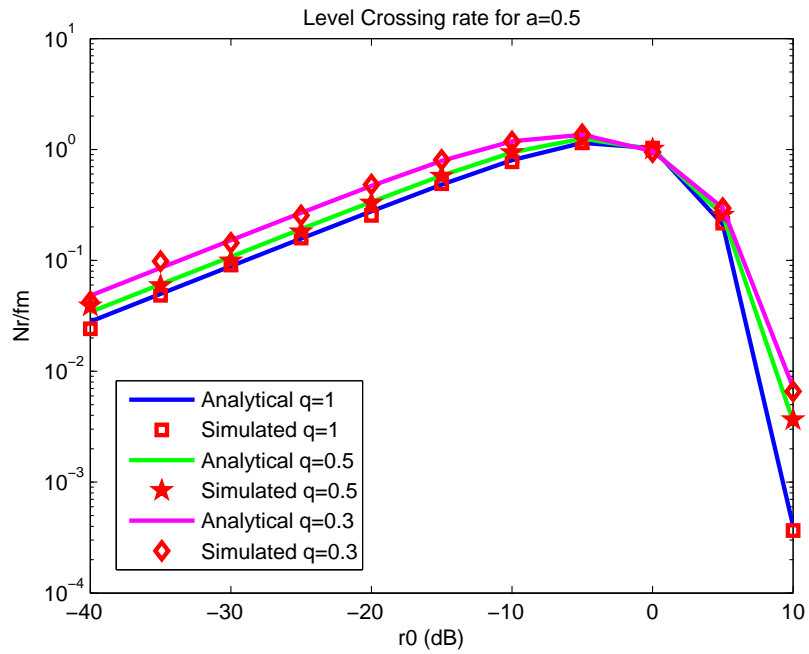


Figure 2.7: Level Crossing Rate for $a=0.5$

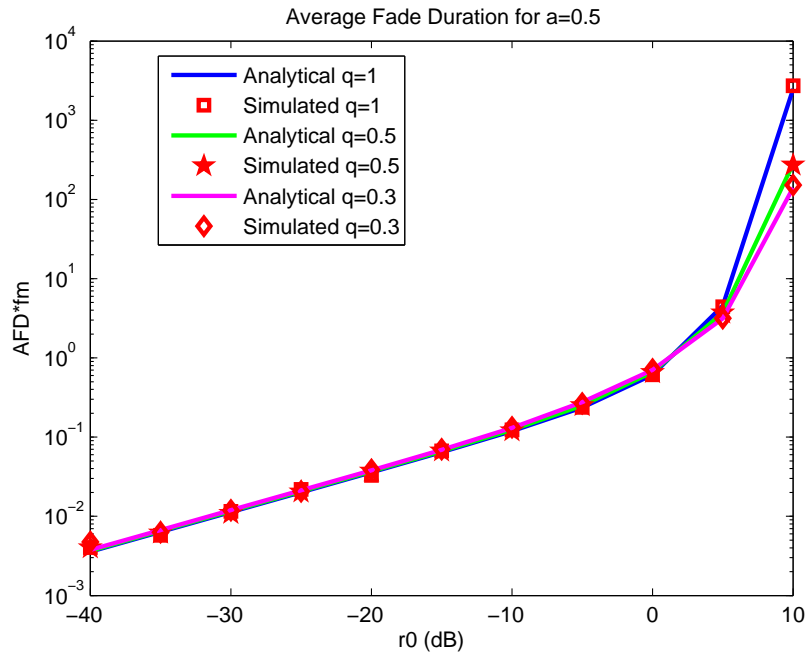


Figure 2.8: Average Fade Duration for $a=0.5$

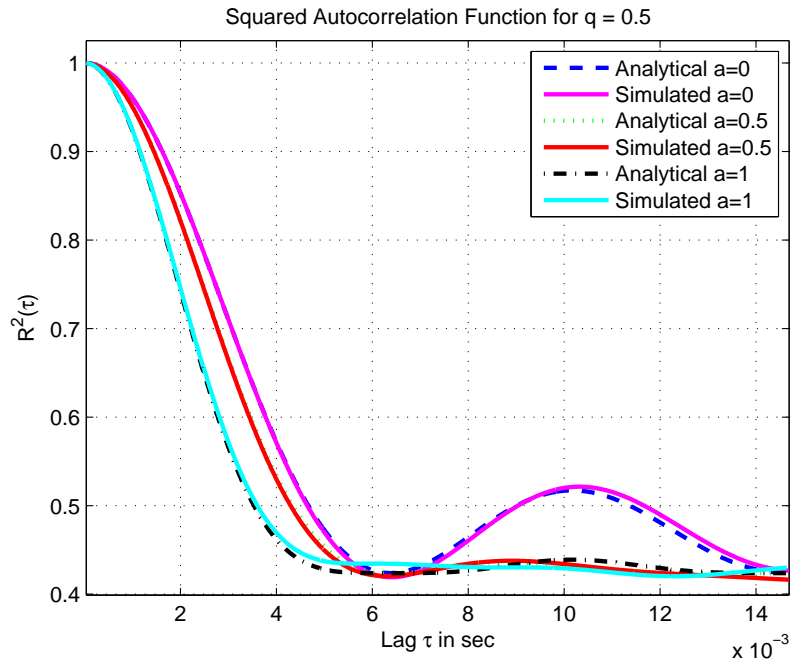


Figure 2.9: Squared Time Autocorrelation Function for $q=0.5$

The MSE between $R_\mu(\Delta t)$ and $\hat{R}_\mu(\Delta t)$ the theoretical and estimated time autocorrelation functions respectively, is defined as

$$MSE = E[(R_\mu(\Delta t) - \hat{R}_\mu(\Delta t))^2] \quad (2.40)$$

$R_\mu(\Delta t)$ is obtained from (2.20) and $\hat{R}_\mu(\Delta t)$ is obtained in MATLAB by estimating the autocorrelation of the channel coefficients obtained by simulator. MSE is plotted in Figure 2.10 as a function of number of frequency sample points N_f . The figure is obtained for $q = 0.5$, $a = 0.5$ and different values of N_f in the range $128 - 8192$ ($N_f = 2^k$ for integer values of k). It is evident from the plot that the MSE decreases when the number of sample points are increased.

2.4 Summary

The second order statistical properties for V2V Nakagami-Hoyt channels under isotropic scattering have been studied. The expressions for space time correlation function, power spectral density, level crossing rates, average duration of fade and squared time autocorrelation function are obtained. The Nakagami-Hoyt V2V simulator is developed to verify the obtained theoretical expressions. A close match between the theoretical and simulated data validates the model.

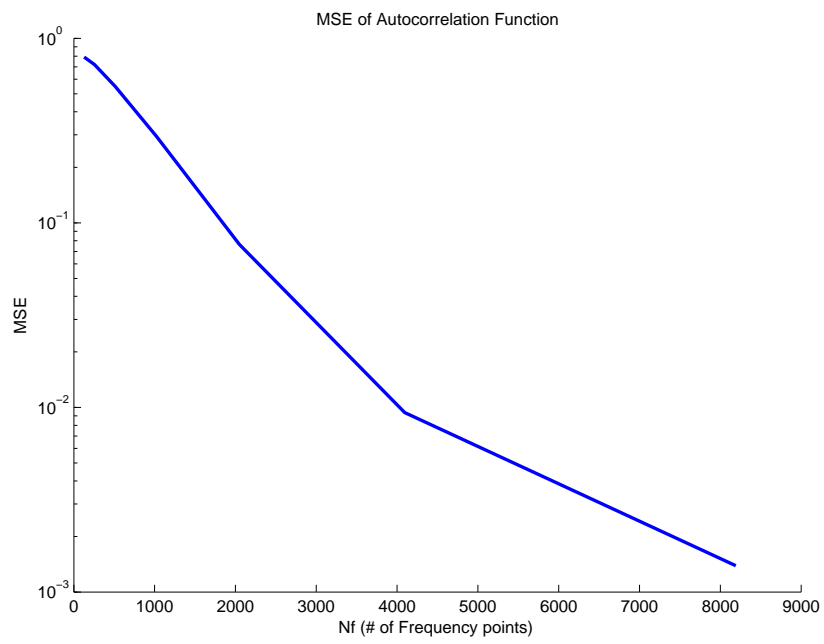


Figure 2.10: Mean Square Error of Autocorrelation Function

CHAPTER 3

V2V HOYT CHANNEL MODEL UNDER NON-ISOTROPIC SCATTERING

In this Chapter, the second order statistics of Hoyt fading channel are derived. These include spatial-time correlation function, time autocorrelation function, power spectral density, squared time autocorrelation function, level crossing rate and average duration of fade. A MATLAB based simulator similar to the one described in the previous Chapter, is developed to validate these properties. It is assumed that the channel is narrow-band, the receiver and transmitter are moving with velocities V_1 and V_2 respectively and the scattering is non-isotropic (i.e, AoA and AoD assumes nonuniform distribution). Finally, MSE between the estimated and theoretical time autocorrelation function is also obtained as a function of number of frequency points of the simulator.

A Hoyt process, $\zeta(t)$, is defined in Chapter 2 by the modulus of the complex Gaussian random process $\mu(t)$,

$$\zeta(t) = |\mu(t)| = \sqrt{|\mu_1(t)|^2 + |\mu_2(t)|^2} \quad (3.1)$$

The baseband equivalent channel components are given by (2.5) and (2.6). Assume that α_{1n} and α_{2n} are non-uniformly distributed having Von Mises PDF described in [51].

$$p_\alpha(\alpha) = \frac{\exp[\kappa \cos(\alpha - \nu)]}{2\pi I_0(\kappa)}, \kappa > 0 \quad (3.2)$$

where ν is the mean direction of the AoD or AoA and κ is the concentration parameter that controls the width of the scatterers.

3.1 Second Order Statistics

In this section, the space time correlation function, power spectral density, level crossing rate and the average duration of fade of the Nakagami-Hoyt V2V fading process under non-isotropic condition are derived.

3.1.1 Spatial Time Correlation Function

A more general case, where $\sigma_1 \neq \sigma_2$ is considered in derivation of spatial time correlation function of Nakagami-Hoyt V2V channel.

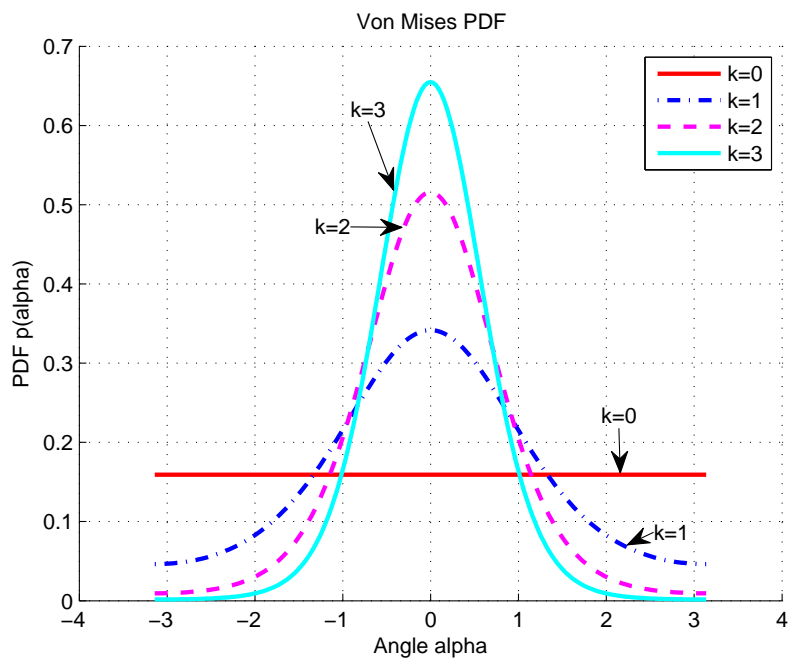


Figure 3.1: Von Mises PDF Showing Non-Isotropic Scattering

The spatial time correlation function of the envelope is given by [74]

$$R(x_1, x_2, t_1, t_2) = \frac{1}{2} E[\mu_{x_2}(t_2) \mu_{x_1}^*(t_1)] \quad (3.3)$$

where $\mu_{x_1}(t_1)$ and $\mu_{x_2}(t_2)$ are the complex envelope received at position x_1 and x_2 at time t_1 and t_2 respectively as given by (2.15) and (2.16) respectively,

Therefore, after algebraic manipulations,

$$\begin{aligned} R(x_1, x_2, t_1, t_2) = & \frac{1}{2} E \left[\sum_{i=1}^{N_p} \sum_{j=1}^{N_p} r_i r_j \right. \\ & \left. \{ \cos[(\omega_{1i} + \omega_{2i})(t_1 + \Delta t) + \phi_i + \psi_i] \right. \\ & \left. \cos[(\omega_{1j} + \omega_{2j})t_1 + \phi_j] \right. \\ & + \frac{1}{q^2} \sin[(\omega_{1i} + \omega_{2i})(t_1 + \Delta t) + \phi_i + \psi_i] \\ & \left. \sin[(\omega_{1j} + \omega_{2j})t_1 + \phi_j] \right. \\ & + j \frac{1}{q} \sin[(\omega_{1i} + \omega_{2i})(t_1 + \Delta t) + \phi_i + \psi_i] \\ & \left. \cos[(\omega_{1j} + \omega_{2j})t_1 + \phi_j] \right. \\ & \left. - j \frac{1}{q} \cos[(\omega_{1i} + \omega_{2i})(t_1 + \Delta t) + \phi_i + \psi_i] \right. \\ & \left. \sin[(\omega_{1j} + \omega_{2j})t_1 + \phi_j] \} \right] \end{aligned}$$

Assuming ϕ_i , α_{1i} , α_{2i} and r_i are mutually independent. Also, assume that α_{1i} and α_{2i} have same distributions for all i . Since ϕ_i is assumed to be uniformly distributed, therefore $E[e^{j(\phi_i - \phi_j)}] = 0$ for all $i \neq j$. Also, using $i = j$, $E[e^{j(\phi_i - \phi_j)}] =$

1 we get,

$$\begin{aligned}
R(\Delta x, \Delta t) &= \frac{1}{2} E \left[\sum_{i=1}^{N_p} r_i^2 \right. \\
&\quad \left. \left\{ \left(1 + \frac{1}{q^2} \right) \cos[(\omega_{1i} + \omega_{2i})\Delta t + \psi_i] \right. \right. \\
&\quad \left. \left. + j \frac{2}{q} \sin[(\omega_{1i} + \omega_{2i})\Delta t + \psi_i] \right\} \right]
\end{aligned}$$

Using formula given in [70] for Von Mises distribution of α_i ,

$$\begin{aligned}
E[e^{j\omega_1 \Delta t + \frac{2\pi}{\lambda} \Delta x \cos \alpha_1}] &= \frac{1}{2\pi I_0(\kappa_1)} \int_{-\pi}^{\pi} e^{\kappa_1 \cos(\alpha_1 - \nu_1)} e^{j(\omega_1 \Delta t + \frac{2\pi}{\lambda} \Delta x \cos \alpha_1)} d\alpha_1 \\
&= \frac{I_0(\sqrt{\kappa_1^2 + (\omega_1 \Delta t + \frac{2\pi}{\lambda} \Delta x)^2} + j\kappa_1(\omega_1 \Delta t + \frac{2\pi}{\lambda} \Delta x) \cos \nu_1)}{I_0(\kappa_1)}
\end{aligned}$$

$$\begin{aligned}
E[e^{j\omega_2 \Delta t}] &= \frac{1}{2\pi I_0(\kappa_2)} \int_{-\pi}^{\pi} e^{\kappa_2 \cos(\alpha_2 - \nu_2) + j(\omega_2 \Delta t)} d\alpha_2 \\
&= \frac{I_0(\sqrt{\kappa_2^2 + \omega_2^2 \Delta t^2} + j2\kappa_2 \omega_2 \Delta t \cos \nu_2)}{I_0(\kappa_2)}
\end{aligned}$$

Hence after substituting $\omega_i = KV_i$ and further simplification,

$$\begin{aligned}
R(\Delta x, \Delta t) &= \sum_{n=0}^1 \frac{(1 + q \cos(n\pi))^2}{4q^2} \sigma_1^2 \\
&\quad \prod_{i=1}^2 \frac{I_0(\sqrt{\kappa_i^2 - K^2 M_i^2} + j2\kappa_i K M_i \cos \nu_i \cos(n\pi))}{I_0(\kappa_i)} \tag{3.4}
\end{aligned}$$

where,

$$M_i(\Delta x, \Delta t) = V_i \Delta t + (2 - i) \Delta x$$

The time correlation function is obtained by setting $\Delta x = 0$ in (3.4)

$$R_\mu(\Delta t) = R(0, \Delta t) = \sum_{n=0}^1 \frac{(1 + q \cos(n\pi))^2}{4q^2} \sigma_1^2 \prod_{i=1}^2 \frac{I_0(\sqrt{\kappa_i^2 - K^2(V_i \Delta t)^2 + j2\kappa_i K V_i \Delta t \cos \nu_i \cos(n\pi)})}{I_0(\kappa_i)} \quad (3.5)$$

For a more specific case (isotropic scattering), substituting $\kappa_i = 0$ and $\nu_i = 0$ in (3.4) and simplifying we obtain (2.18). It can be shown that for $q = 1$, the space time correlation function for V2V Rayleigh fading channel is obtained which matches with the result of [114].

3.1.2 Power Spectral Density

The power spectral density $S(f)$ of the WSS process is obtained by taking the Fourier transform of the time autocorrelation function $R_\mu(\Delta t)$.

$$S(f) = \int_{-\infty}^{\infty} R_\mu(\Delta t) e^{-j2\pi f \Delta t} d\Delta t \quad (3.6)$$

For non-isotropic scattering ($\kappa_i \neq 0$, $\nu_i \neq 0$), the integral is evaluated numerically using the Fourier transform of the time autocorrelation function (3.5).

For isotropic scattering, the power spectral density is obtained as (2.26)

3.1.3 Level Crossing Rate and Average Duration of Fade

The level crossing rate of the process $\zeta(t)$ is obtained by solving the following integral

$$N_\zeta(r) = \int_0^\infty \dot{z} p_{\zeta\dot{\zeta}}(r, \dot{z}) d\dot{z} \quad (3.7)$$

where $p_{\zeta\dot{\zeta}}$ is the joint PDF of $\zeta(t)$ and its time derivative $\dot{\zeta}(r)$. From [25], LCR for stationary to mobile Hoyt channel is given by

$$\begin{aligned} N_\zeta(r) &= \frac{r}{(2\pi)^{3/2} \sigma_1 \sigma_2} \\ &\times \int_0^{2\pi} e^{\left[-\frac{r^2}{2\sigma_1^2 \sigma_2^2} (\sigma_2^2 \cos^2(\theta) + \sigma_1^2 \sin^2(\theta))\right]} \\ &\times \sqrt{\beta_1 \cos^2(\theta) + \beta_2 \sin^2(\theta)} d\theta \end{aligned} \quad (3.8)$$

The expression will remain the same for V2V Nakagami-Hoyt channel except the values of β_1 and β_2 . These can be found using the relationship $\beta_i = -\ddot{R}_{ii}(0)$.

$$R_{ii}(\Delta t) = E[\mu_i(t + \Delta t)\mu_i(t)] \quad i = 1, 2$$

$$\begin{aligned} R_{11}(\Delta t) &= \sigma_1^2 \\ &\sum_{n=0}^1 \prod_{i=1}^2 \frac{I_0(\sqrt{\kappa_i^2 - (KV_i \Delta t)^2 + j2\kappa_i KV_i \Delta t \cos \nu_i \cos(n\pi)})}{I_0(\kappa_i)} \end{aligned}$$

Differentiating twice and substituting $\Delta t = 0$ yields,

$$\begin{aligned}
\beta_1 &= -\ddot{R}_{11}(0) \\
&= \sigma_1^2 K^2 V_1^2 \left[2a^2 \cos \nu_1 \cos \nu_2 \frac{I_1(\kappa_1) I_1(\kappa_2)}{I_0(\kappa_1) I_0(\kappa_2)} \right. \\
&\quad \left. - \frac{I_1(\kappa_1) \cos 2\nu_1}{\kappa_1 I_0(\kappa_1)} - a^2 \frac{I_1(\kappa_2) \cos 2\nu_2}{\kappa_2 I_0(\kappa_2)} + \cos^2 \nu_1 + a^2 \cos^2 \nu_2 \right]
\end{aligned}$$

Provided $\kappa_1, \kappa_2 \neq 0$. Similarly, we get $\beta_2 = \beta_1/q^2$.

For the case of Isotropic scattering ($\kappa_1 = \kappa_2 = \nu_1 = \nu_2 = 0$), differentiating (2.20) with respect to Δt twice and substituting $\Delta t = 0$, we get

$$\beta_1 = -\ddot{R}_{11}(0) = (\sqrt{2\pi} \sigma_1 f_{m1})^2 (1 + a^2)$$

Also, substituting $\beta_2 = \beta_1/q^2$ and $r_0 = r/R_{rms}$ the LCR is obtained as

$$\begin{aligned}
N_\zeta(r_0) &= \frac{r_0 \sqrt{\beta_1 (q^2 + 1)}}{(2\pi)^{3/2} q \sigma_1} \\
&\times \int_0^{2\pi} e^{\left[-\frac{r_0^2 (q^2 + 1)}{2q^2} (\cos^2(\theta) + q^2 \sin^2(\theta)) \right]} \\
&\times \sqrt{q^2 \cos^2(\theta) + \sin^2(\theta)} d\theta \tag{3.9}
\end{aligned}$$

For isotropic scattering, substituting the values of $\beta_1 = (\sqrt{2\pi} \sigma_1 f_{m1})^2 (1 + a^2)$, the

expression becomes,

$$\begin{aligned}
N_{\zeta}(r_0) &= \frac{\sqrt{(1+a^2)(q^2+1)}f_{m1}r_0}{2q\sqrt{\pi}} \\
&\times \int_0^{2\pi} e^{\left[-\frac{r_0^2(q^2+1)}{2q^2}(\cos^2(\theta)+q^2\sin^2(\theta))\right]} \\
&\times \sqrt{q^2\cos^2(\theta)+\sin^2(\theta)}d\theta \tag{3.10}
\end{aligned}$$

It is easy to show that by substituting $a = 0$ and $q = 1$ the above equation reduces to the expression for Base to Mobile Rayleigh LCR given in [75].

The average duration of fade of a signal is defined as average duration of time for which the signal r spends below a specified threshold R_0 . It is given by (2.33) and obtained by substituting (3.10) and (2.34) in (2.33).

3.1.4 Squared Time Autocorrelation Function

The squared time autocorrelation function is obtained using,

$$R_{\mu^2}(\Delta t) = E[|\mu(t)|^2|\mu(t + \Delta t)|^2] \tag{3.11}$$

$$R_{\mu^2}(\Delta t) = E[[\mu_1^2(t) + \mu_2^2(t)][\mu_1^2(t + \Delta t) + \mu_2^2(t + \Delta t)]] \tag{3.12}$$

$$\begin{aligned}
R_{\mu^2}(\Delta t) &= E[\mu_1^2(t)\mu_1^2(t + \Delta t)] + E[\mu_2^2(t)\mu_2^2(t + \Delta t)] \\
&+ E[\mu_1^2(t)\mu_2^2(t + \Delta t)] + E[\mu_2^2(t)\mu_1^2(t + \Delta t)] \tag{3.13}
\end{aligned}$$

For zero mean Gaussian random variable we have from [79],

$$\begin{aligned} E[\mu_1^2(t)\mu_1^2(t + \Delta t)] &= E[\mu_1^2(t)]E[\mu_1^2(t + \Delta t)] + 2E^2[\mu_1(t)\mu_1(t + \Delta t)] \\ &= \sigma_1^4 + 2R_{11}^2(\Delta t) \end{aligned}$$

Similarly,

$$\begin{aligned} E[\mu_2^2(t)\mu_2^2(t - \Delta t)] &= \sigma_2^4 + 2R_{22}^2(\Delta t) \\ E[\mu_1^2(t)\mu_2^2(t - \Delta t)] &= \sigma_1^2\sigma_2^2 + 2R_{12}^2(\Delta t) \end{aligned}$$

Hence substituting in (3.13) yields,

$$R_{\mu^2}(\Delta t) = \sigma_1^4 \frac{(1+q^2)^2}{q^4} + 2[R_{11}^2(\Delta t) + R_{22}^2(\Delta t) + 2R_{12}^2(\Delta t)]$$

where,

$$\begin{aligned} R_{12}(\Delta t) &= \frac{1}{q} \sigma_1^2 \left[\sum_{n=0}^1 \cos(n\pi) \right. \\ &\times \left. \prod_{i=1}^2 \frac{I_0(\sqrt{\kappa_i^2 - (KV_i\Delta t)^2 + j2\kappa_i KV_i \Delta t \cos \nu_i} \cos(n\pi))}{I_0(\kappa_i)} \right] \end{aligned}$$

$$\begin{aligned} R_{\mu^2}(\Delta t) &= \sigma_1^4 \frac{(1+q^2)^2}{q^4} \\ &+ 2[R_{11}^2(\Delta t) + R_{22}^2(\Delta t) + 2R_{12}^2(\Delta t)] \end{aligned} \quad (3.14)$$

where R_{11} and R_{22} are the autocorrelation of the in-phase and quadrature components respectively and R_{12} is cross-correlation between them.

3.2 Simulation and Results

A MATLAB based simulator similar to the one described in Chapter 2 is developed. The power spectral density and time autocorrelation functions are replaced with the newly derived one. The block diagram of the proposed simulator is the same as shown in Figure. 2.1. The simulation is run with the following parameters, carrier frequency ($f = 900\text{MHz}$), velocity of receiver $V_1 = 72\text{km/hr}$ which means $f_{m1} = 60\text{Hz}$, three different values of $q = 1, 0.5, 0.3$, three different values of $a = 1, 0.5, 0$ and $N_f = 8192$.

The simulator sample output for $q = 0.5$, $a = 0.5$ is shown in Figure 3.2. It shows the normalized envelope time variation in dB .

The amplitude and phase PDFs plots are shown in Figure 3.3 and 3.4, respectively. The corresponding theoretical output of (2.8) and (2.9), respectively, were also plotted for comparison. The plots are the same as those obtained in the case of isotropic scattering as envelope and phase PDF expressions are independent of AoA and AoD distributions.

The power spectral density plots for $\kappa = (0, 1, 2, 3)$ are shown in Figure 3.5. No closed form for the power spectral density exists. The plots are obtained by taking Fourier transform of normalized time autocorrelation function in MATLAB. The plots for other values of q are the scaled version and are not shown here. It

has been shown that plot is symmetric for $\kappa = 0$ indicating isotropic scattering whereas $\kappa \neq 0$ results in asymmetric PSD (non-isotropic scattering).

The autocorrelation plots for $q = 0.5$ with 4 different values of $\kappa = (0, 1, 2, 3)$ are shown in Figure 3.6. The normalized autocorrelation functions plots have been shown in Figure 3.7. The plots for $a = 1, 0.5, 0$ are compared with the theoretical expression of (2.20) for $q = 0.5$. Since the real and imaginary components are Gaussian, it can be found from the plots that the normalized autocorrelation functions are still Bessel but with different shape than the one shown in [115]. Also the plots are function of κ and ν . The difference between the theoretical and simulated output can be reduced by increasing the number of frequency points N_f of the simulator.

The normalized squared autocorrelation plots of real part for $q = 0.5$, $\kappa = 3$, $a = 0.5$ is shown in Figure 3.8. The plot is compared with the theoretical derived expression. There is some difference between the theoretical and simulated output which can be reduced by increasing the number of frequency points N_f of the simulator. This will result in increasing the computational complexity of the simulator.

The level crossing rates and average duration of fades for $q = (1, 0.5, 0.3)$ are plotted in Figure 3.9-3.14 for three different values of $a = (1, 0.5, 0)$. The curves are matched with their theoretical expressions given by (3.10) and (2.33). $q = 1$ shows the Rayleigh envelop whereas $a = 0$ indicates base to mobile communication plots for LCR and ADF [10].

The MSE of the time autocorrelation function is given by (2.40). Figure 3.15 shows the mean square error of time autocorrelation function as a function of number of frequency sample points N_f . The figure is obtained for $q = 0.5$, $a = 0.5$, $\kappa = 3$ and varying N_f in power of 2 in the range $2048 - 32768$ ($N_f = 2^k$ for integer values of k). It is evident from the curve that the MSE reduces when the number of frequency points are increased. Hence more accurate simulator is obtained at the cost of increasing the complexity of simulator.

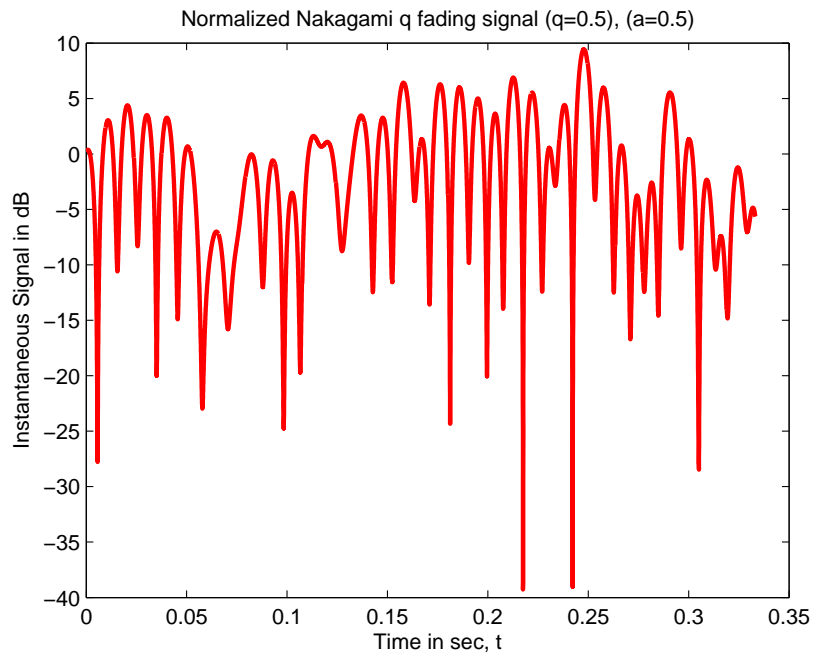


Figure 3.2: Output of the Hoyt Simulator

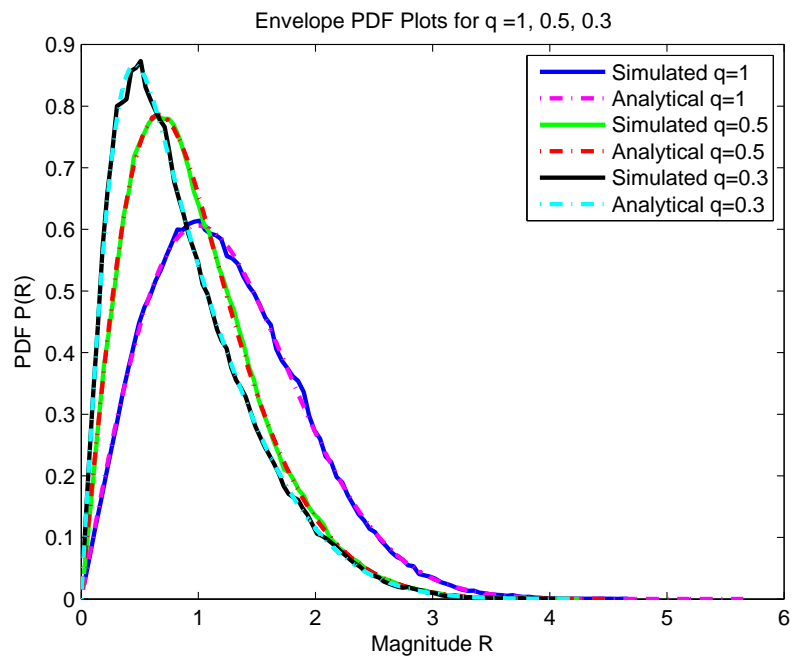


Figure 3.3: Hoyt Amplitude PDF Plot

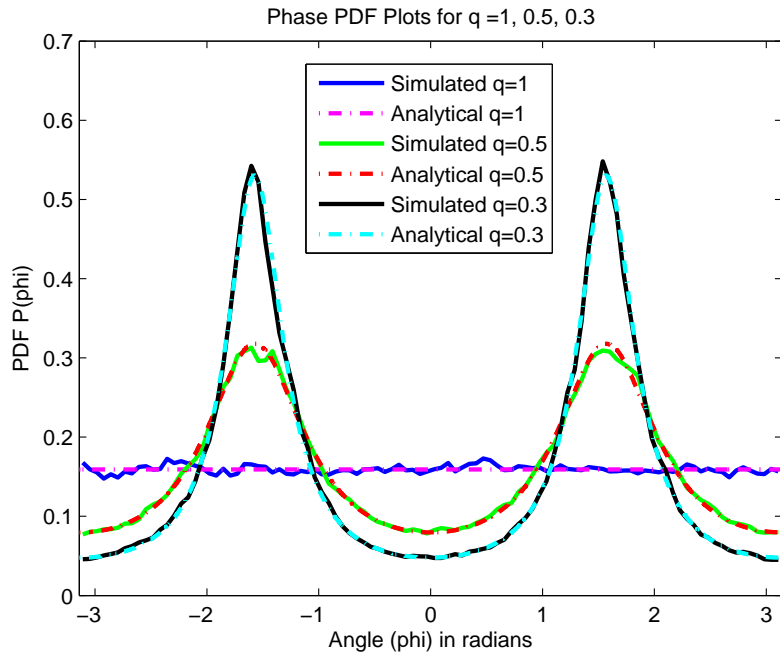


Figure 3.4: Hoyt Phase PDF Plot

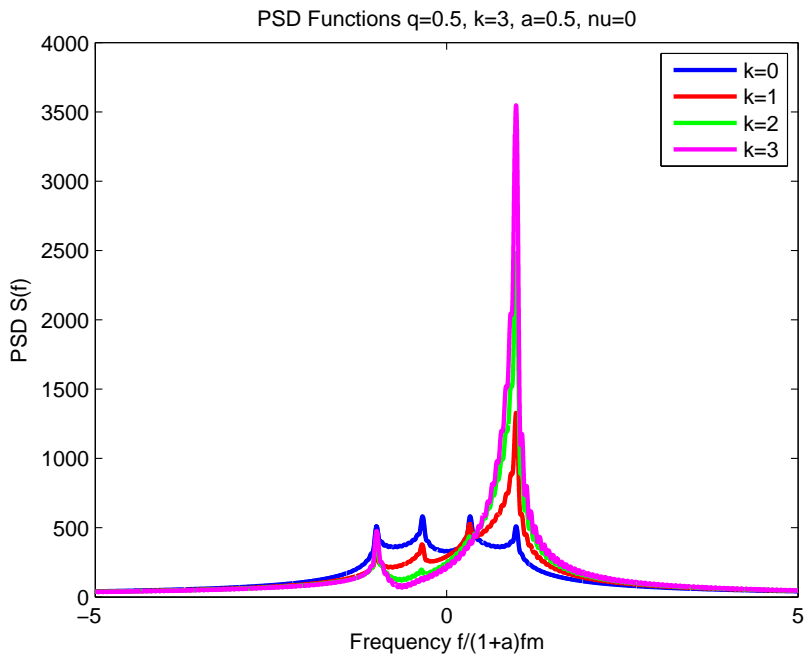


Figure 3.5: PSD Plot for $q=.5$

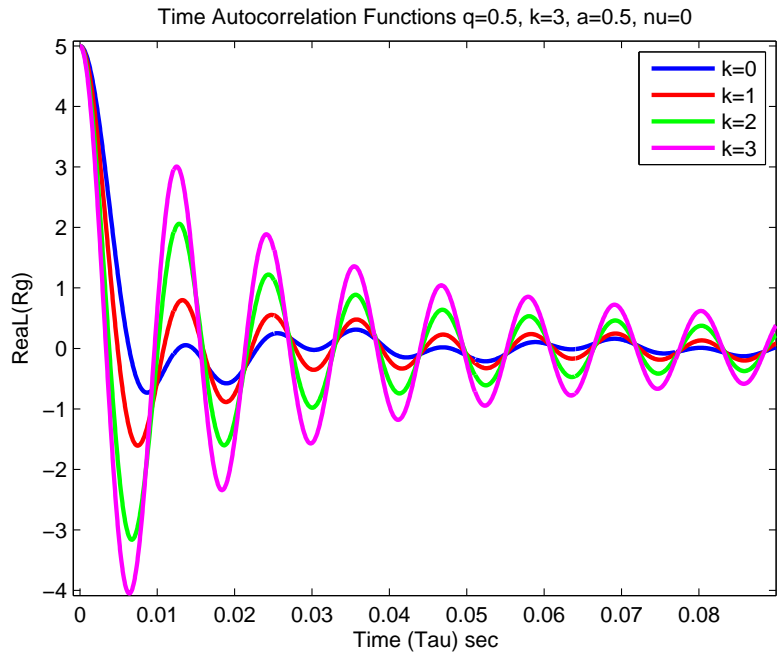


Figure 3.6: Autocorrelation Function of Real Part of Envelop

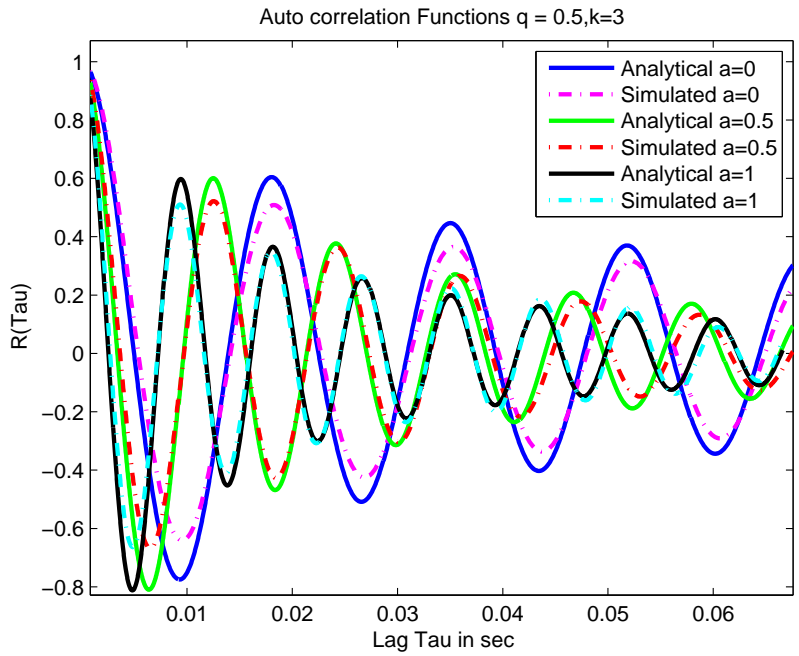


Figure 3.7: Autocorrelation Function of Real Part of Envelop for $q=0.5, k=3$

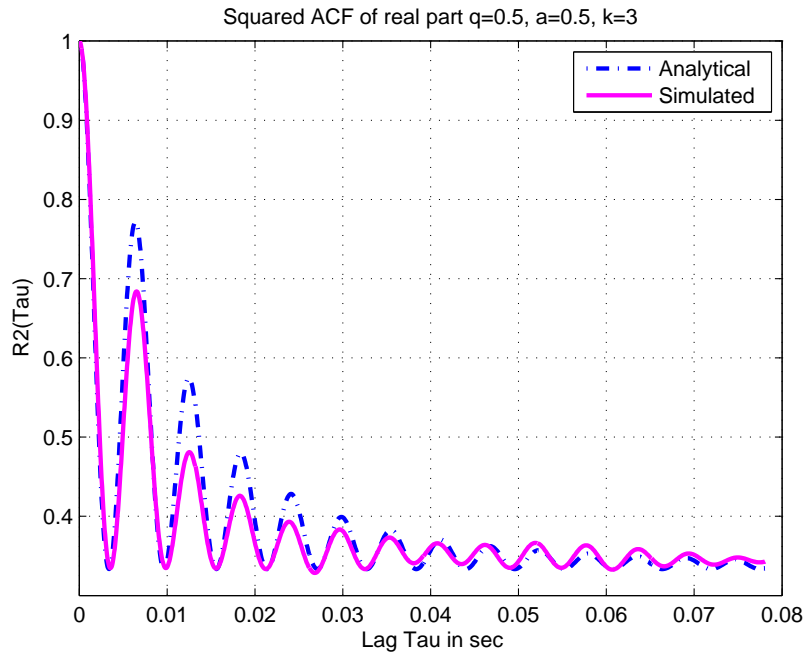


Figure 3.8: Squared Autocorrelation Function of Real Part for $q=0.5, k=3$

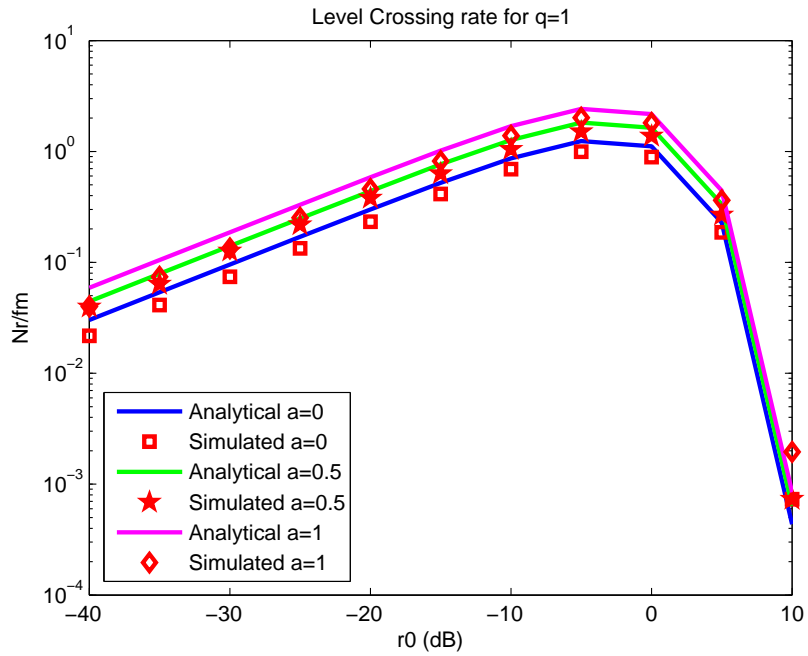


Figure 3.9: Level Crossing Rates for $q=1$

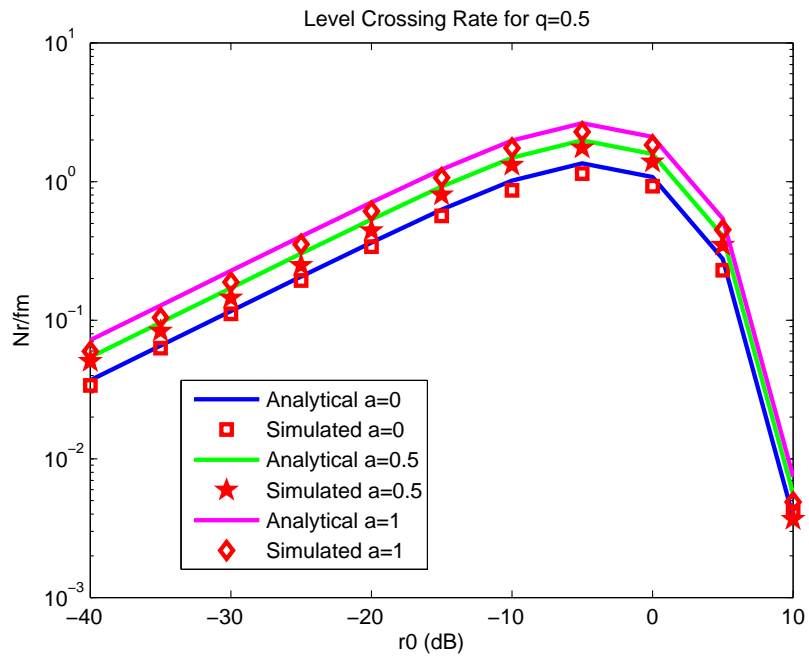


Figure 3.10: Level Crossing Rates for $q=0.5$

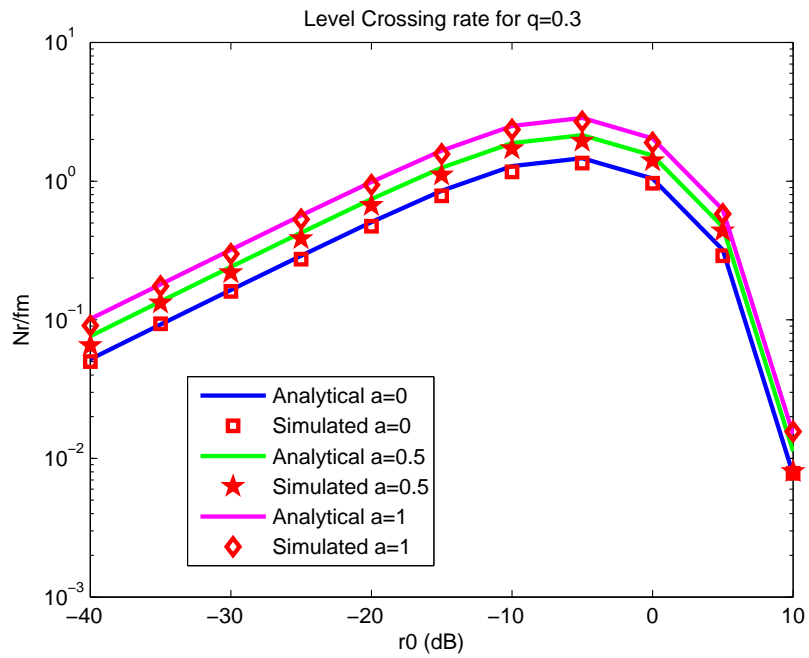


Figure 3.11: Level Crossing Rates for $q=0.3$

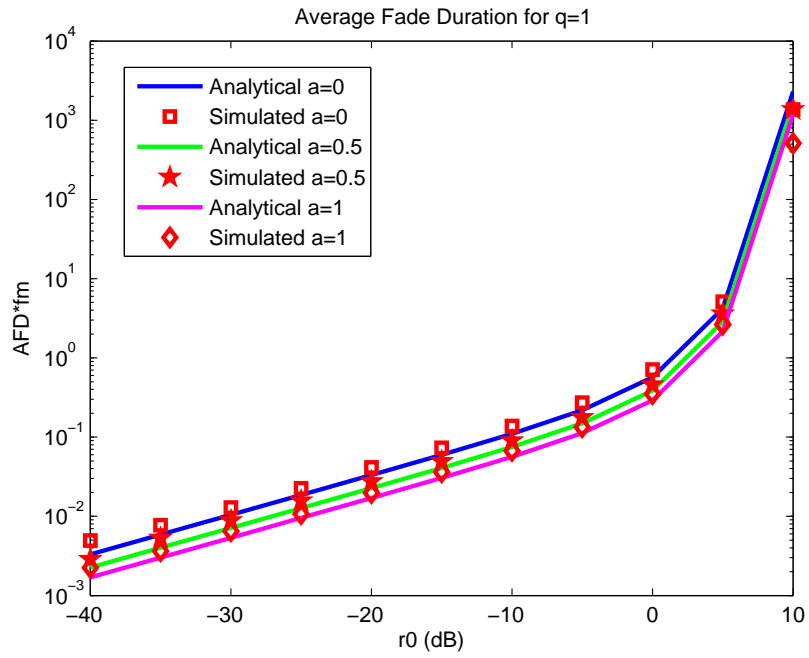


Figure 3.12: Average Duration of Fade for $q=1$

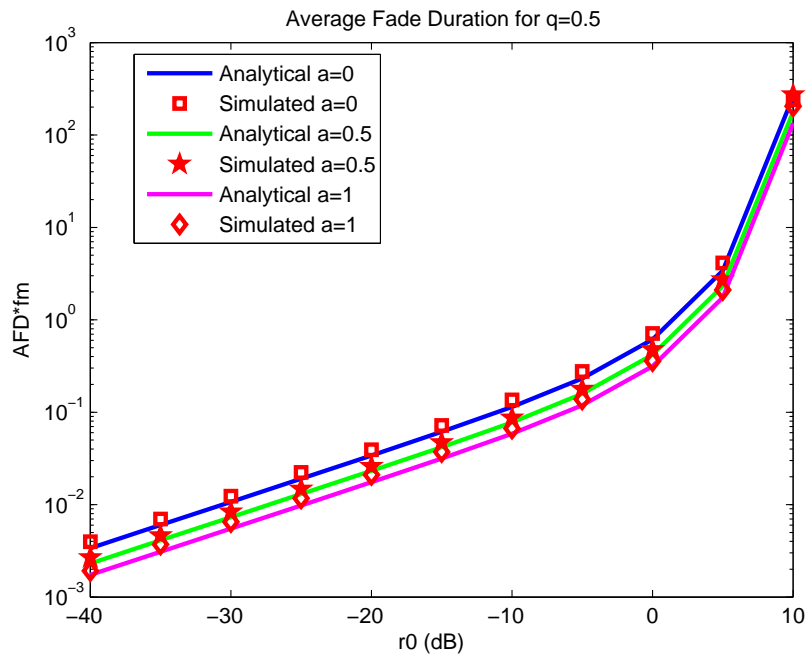


Figure 3.13: Average Duration of Fade for $q=0.5$

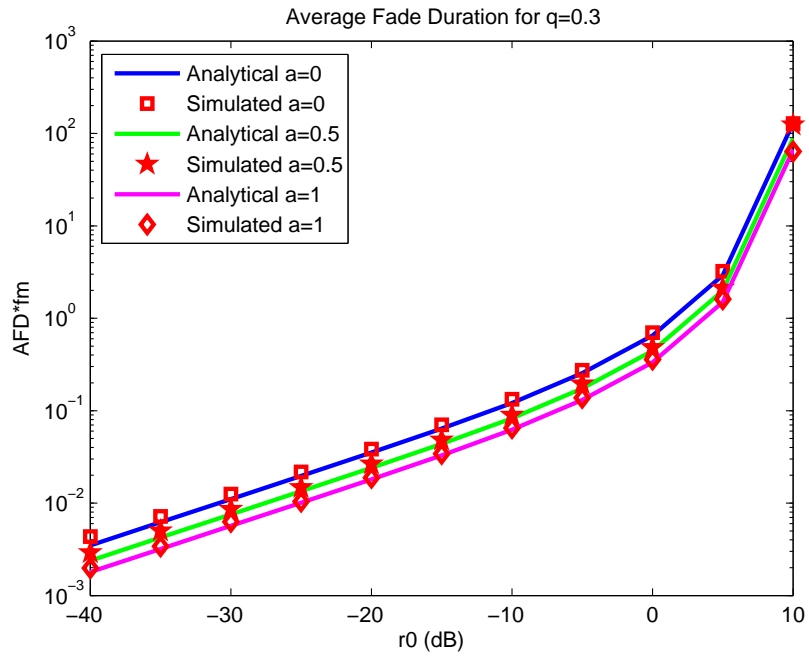


Figure 3.14: Average Duration of Fade for $q=0.3$

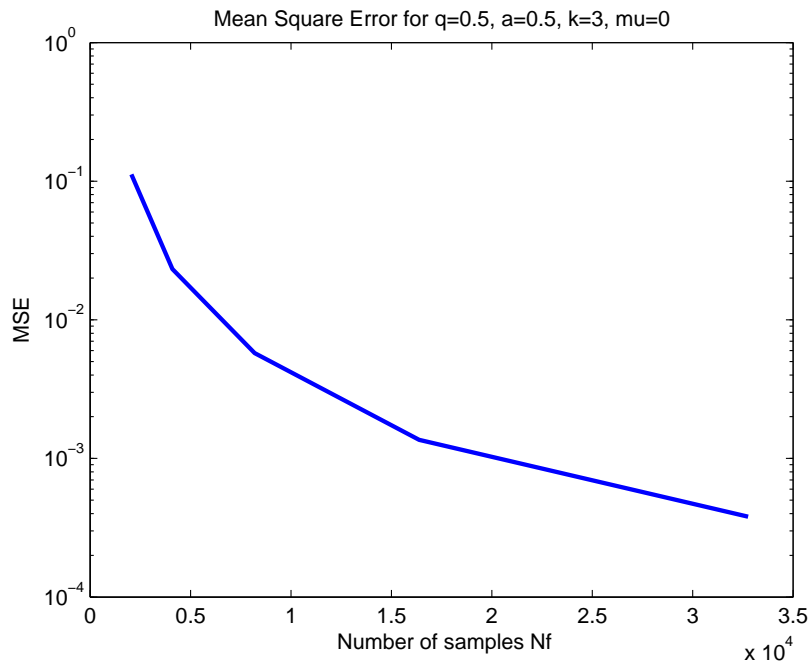


Figure 3.15: Mean Square Error of Autocorrelation Function

3.3 Summary

The second order statistical properties for V2V Nakagami-Hoyt channels under the non-isotropic scattering conditions at both the transmitter and receiver, are developed. These include expressions for space time correlation function, power spectral density, squared time autocorrelation, level crossing rates and average duration of fade. The Nakagami-Hoyt V2V simulator is also developed to verify the above mentioned theoretical expressions. It is found that the theoretical results match closely with the simulated data verifying the validity of the model. MSE between the theoretical and estimated time autocorrelation function is also computed and it is observed that MSE reduces with increase in number of frequency points.

CHAPTER 4

V2V HOYT CHANNEL MODEL WITH DIFFUSED LINE OF SIGHT

4.1 Introduction

In V2V communications the line of sight (LoS) may not always be present and it may be obstructed which results in a diffused LoS component perhaps due to shadowing. Previous V2V research is restricted only to Rayleigh models and does not cover the generic cases when LoS is present.

Hence, a generalized V2V model is required that covers the V2V Rayleigh and Ricean models as special cases. In this Chapter a novel V2V generalized channel model is proposed which combines Nakagami Hoyt and lognormally distributed diffused LoS. The first and second order statistics of the proposed model are

derived in this Chapter. These include amplitude and phase probability density function, spatial time correlation function, power spectral density, level crossing rate, average fade durations, squared time autocorrelation function, and mean square error of time autocorrelation function have been derived. An IFFT based simulator is also developed for the proposed channel model.

4.2 The Proposed Channel Model

The proposed channel model $H(t)$ is a generalized model that can be used in rural environment. It considers, the sum of diffused LoS component $\rho(t)$ and Nakagami-Hoyt $\mu(t)$ component under the assumptions that both transmitter and receiver are in motion. The proposed model covers as special cases

- The base to vehicle (transmitter stationary while vehicle moving) model;
- Nakagami-Hoyt model when no LoS component is present;
- Rice model when LoS component is present and variances of the quadrature components are equal;
- Rayleigh model when no LoS component is present and variances of the quadrature components are equal.

$$H(t) = \rho(t) + \mu(t) \tag{4.1}$$

where $\rho(t)$ is lognormally distributed LoS component and $\mu(t)$ is Hoyt distributed indirect NLoS component. They are given by,

$$\begin{aligned}\rho(t) &= Ae^{z(t)} \\ \mu(t) &= \mu_1(t) + j\mu_2(t)\end{aligned}$$

where $\mu_1(t)$, $\mu_2(t)$ and $z(t)$ are the independent Gaussian random processes with zero mean and variances σ_1^2 , σ_2^2 and σ_3^2 , respectively, and A is the direct LoS component.

4.3 First Order Statistics

The probability density function of the Rice Hoyt envelope $X = \sqrt{(A + \mu_1)^2 + \mu_2^2}$ and phase $\Theta = \arctan \frac{\mu_2(t)}{A + \mu_1(t)}$ are given by [43]

$$\begin{aligned}p_X(x|A) &= \frac{x}{2\pi\sigma_1\sigma_2} \exp \left[-\frac{A^2}{2\sigma_1^2} - \frac{x^2}{4} \left(\frac{1}{\sigma_1^2} + \frac{1}{\sigma_2^2} \right) \right] \\ &\times \int_0^{2\pi} \exp \left[-\frac{x^2}{4} \left(\frac{1}{\sigma_1^2} - \frac{1}{\sigma_2^2} \right) \cos 2\theta \right] \\ &\times \exp \left[\frac{Ax}{\sigma_1^2} \cos \theta \right] d\theta\end{aligned}\tag{4.2}$$

In this Chapter, we briefly describe and review the first and second order statistics of proposed fading channel under the assumptions that the channel is narrow band, the receiver and transmitter are moving with velocities V_1 and V_2 respectively and the isotropic scattering (i.e, omnidirectional antennas have been

used at both end which results in uniform distribution of angle of arrival (AoA) and angle of departure (AoD)).

$$\begin{aligned}
p_{\Theta}(\theta|A) &= \frac{1}{4\pi\sigma_1\sigma_2\sigma_3h_c(\theta)} \\
&\times \exp\left[A^2\left(G^2(\theta) - \frac{1}{\sigma_1^2}\right)\right] \\
&\times \exp(-A^2G^2(\theta) + b\sqrt{\pi}G(\theta)[1 + \phi(AG(\theta))])
\end{aligned} \tag{4.3}$$

Also, $\rho(t)$ is lognormally distributed with PDF

$$p_{\rho}(b) = \frac{1}{\sigma_3 b \sqrt{2\pi}} \exp\left[-\frac{1}{2\sigma_3^2}\left(\log\left(\frac{b}{A}\right)\right)^2\right] \tag{4.4}$$

Hence, using (4.2) and (4.4) and applying total probability theorem, the envelope PDF of the proposed model is given by,

$$\begin{aligned}
p_H(h) &= \int_0^{\infty} p_{H,\rho}(h,b)db = \int_0^{\infty} p_X(h|b)p_{\rho}(b)db \\
p_H(h) &= \frac{h}{(2\pi)^{3/2}\sigma_1\sigma_2\sigma_3} \exp\left[-\frac{h^2}{4}\left(\frac{1}{\sigma_1^2} + \frac{1}{\sigma_2^2}\right)\right] \\
&\times \int_{b=0}^{\infty} \int_{\theta=0}^{2\pi} \frac{1}{b} \exp\left[-\frac{b^2}{2\sigma_1^2} + \frac{bh}{\sigma_1^2} \cos(\theta)\right] \\
&\times \exp\left[-\frac{h^2}{4}\left(\frac{1}{\sigma_1^2} - \frac{1}{\sigma_2^2}\right) \cos(2\theta)\right] \\
&\times \exp\left[-\frac{1}{2\sigma_3^2}\left(\log\frac{b}{A}\right)^2\right] d\theta db, \quad A > 0
\end{aligned} \tag{4.5}$$

Similarly, the PDF of the corresponding phase process $\nu(t) = \arctan \frac{\mu_2(t)}{\rho(t)+\mu_1(t)}$ is

given by

$$\begin{aligned}
p_\nu(\theta) &= \int_{b=0}^{\infty} p_{\Theta,\rho}(\theta, b) db = \int_{b=0}^{\infty} p_{\Theta}(\theta|b) p_{\rho}(b) db \\
p_\nu(\theta) &= \frac{1}{2(2\pi)^{3/2} \sigma_1 \sigma_2 \sigma_3 h_c(\theta)} \\
&\times \int_{b=0}^{\infty} \frac{1}{b} \exp \left[b^2 \left(G^2(\theta) - \frac{1}{\sigma_1^2} \right) - \frac{1}{2\sigma_3^2} \left(\log \frac{b}{A} \right)^2 \right] \\
&\times \left[\exp(-b^2 G^2(\theta)) + b\sqrt{\pi} G(\theta) [1 + \phi(bG(\theta))] \right] db, \quad A > 0
\end{aligned} \tag{4.6}$$

where $\phi(x)$ is an error function defined as

$$\phi(x) = \int_{t=0}^x \frac{2}{\sqrt{\pi}} e^{-t^2} dt$$

and $h_c(\theta)$ and $G(\theta)$ are defined as

$$h_c(\theta) = \sqrt{\frac{\cos^2(\theta)}{2\sigma_1^2} + \frac{\sin^2(\theta)}{2\sigma_2^2}}$$

$$G(\theta) = \frac{\cos(\theta)}{2\sigma_1^2 h_c(\theta)}$$

For $A = 0$, the model will be reduced to the Hoyt model under isotropic scattering as described in Chapter 2. The envelope and phase PDFs of this model are given by (2.8) and (2.9), respectively. Further, when variances are equal i.e. $\sigma_1 = \sigma_2$, the envelope and phase will have Rayleigh (2.10) and Uniform (2.11) PDFs, respectively.

For the zero mean WSS random processes $\mu_1(t)$, $\mu_2(t)$ and $z(t)$, the mean m_H

and RMS R_{rms} values can be easily obtained as

$$\begin{aligned} m_H = E[H(t)] &= E[Ae^{z(t)}] + E[\mu_1(t)] + jE[\mu_2(t)] \\ &= Ae^{\sigma_3^2/2} \end{aligned}$$

$$\begin{aligned} R_{rms} = \sqrt{E[H(t)^2]} &= \sqrt{E[(Ae^{z(t)} + \mu_1(t))^2] + E[\mu_2(t)^2]} \\ &= \sqrt{A^2e^{2\sigma_3^2} + E[\mu_1^2(t)] + E[\mu_2^2(t)]} \\ &= \sqrt{A^2e^{2\sigma_3^2} + (q^2 + 1)\sigma_2^2} \end{aligned}$$

4.4 Second Order Statistics

In this section, we shall derive the spatial time correlation function, power spectral density, level crossing rate, the average duration of fade and squared time autocorrelation function of the Nakagami-Hoyt V2V fading process.

4.4.1 Spatial Time Correlation Function

For the derivation of spatial time correlation function of the proposed model, we follow the technique used in [114]. The reference describes the case for Rayleigh distribution. The results have been obtained for more general case where $\sigma_1 \neq \sigma_2$ and lognormally distributed LoS is present. The spatial time correlation function

of the envelope is given by [74]

$$R_H(x_1, x_2, t_1, t_2) = \frac{1}{2}E[H_{x_2}(t_2)H_{x_1}^*(t_1)] \quad (4.7)$$

where $H_{x_1}(t_1)$ and $H_{x_2}(t_2)$ are the complex envelope received at position x_1 and x_2 at time t_1 and t_2 respectively as given in [114].

The time autocorrelation function of a WSS complex random process is defined as

$$R_H(\Delta t) = \frac{1}{2}E[H(t)H^*(t + \Delta t)]$$

where $H^*(t)$ is the complex conjugate of $H(t)$

$$\begin{aligned} R_H(\Delta t) &= \frac{1}{2}E[\{\rho(t) + \mu_1(t) + j\mu_2(t)\} \\ &\quad \times \{\rho(t + \Delta t) + \mu_1(t + \Delta t) - j\mu_2(t + \Delta t)\}] \\ &= \frac{1}{2}\left[E[\rho(t)\rho(t + \Delta t)] \right. \\ &\quad \left. + E[\mu_1(t)\mu_1(t + \Delta t)] + E[\mu_2(t)\mu_2(t + \Delta t)] \right] \end{aligned} \quad (4.8)$$

$\mu_1(t)$, $\mu_2(t)$ and $z(t)$ are assumed independent and by definition

$$E[\rho(t)\rho(t + \Delta t)] = E[A^2 e^{z(t)+z(t+\Delta t)}]$$

$z(t)$ and $z(t + \Delta t)$ are random variable with zero mean and variance σ_3^2 . Hence

their sum is another random variable with zero mean and variance σ_z^2

$$\begin{aligned}
\sigma_z^2 &= E[\{z(t) + z(t + \Delta t)\}^2] \\
&= E[z^2(t)] + E[z^2(t + \Delta t)] + 2E[z(t)z(t + \Delta t)] \\
&= 2\sigma_3^2 + 2R_z(\Delta t)
\end{aligned}$$

where $R_z(\Delta t)$ is given by

$$R_z(\Delta t) = \sigma_3^2 J_0(2\pi f_{m3} \Delta t)$$

Therefore,

$$\begin{aligned}
E[\rho(t)\rho(t + \Delta t)] &= A^2 e^{\sigma_z^2/2} \\
&= A^2 e^{\sigma_3^2[1+J_0(2\pi f_{m3}\Delta t)]} \tag{4.9}
\end{aligned}$$

Also, from [115], the autocorrelation function for the V2V channel is given by

$$E[\mu_i(t)\mu_i(t + \Delta t)] = \sigma_i^2 J_0(2\pi f_{m1}\Delta t) J_0(2\pi f_{m2}\Delta t) \tag{4.10}$$

Substituting (4.10) and (4.9) in (4.8)

$$\begin{aligned}
R_H(\Delta t) &= \frac{A^2}{2} e^{\sigma_3^2[1+J_0(2\pi f_{m3}\Delta t)]} \\
&+ \frac{q^2 + 1}{2q^2} \sigma_1^2 J_0(2\pi f_{m1}\Delta t) J_0(2\pi f_{m2}\Delta t) \tag{4.11}
\end{aligned}$$

Using this result and the results in [114], the spatial time correlation function for the proposed model is given by

$$\begin{aligned}
R_H(\Delta x, \Delta t) &= \frac{A^2}{2} \exp[\sigma_3^2(1 + J_0(2\pi f_{m3}\Delta t))] \\
&+ \frac{1 + q^2}{2q^2} \sigma_1^2 J_0(KV_2\Delta t) J_0(KV_1\Delta t + K\Delta x) \quad (4.12)
\end{aligned}$$

where, f_{m3} is the LoS component maximum Doppler. Generally, due to the slow variation of LoS component $f_{m3} \ll f_{m1}, f_{m2}$. $R_H(\Delta x, \Delta t)$ is the correlation functions of two signal envelopes obtained at two locations Δx apart, and at two time instant Δt apart.

It can be shown that for $q = 1$ and $A = 0$, the spatial time correlation function for V2V Rayleigh fading channel reduces to (2.18) which also matches with the result of [114].

The spatial correlation function is obtained by setting $\Delta t = 0$ in (4.12).

$$R_H(\Delta x) = R_H(\Delta x, 0) = A^2 e^{\sigma_3^2} + \frac{1 + q^2}{2q^2} \sigma_1^2 J_0(K\Delta x) \quad (4.13)$$

For Rayleigh fading ($A=0$ and $q=1$) case, (4.11) reduces to (2.22) whereas (4.13) reduces to (2.23).

4.4.2 Power Spectral Density

The power spectral density $S(f)$ of the the proposed channel model (which is wide sense stationary process) is obtained by taking the Fourier Transform of

time autocorrelation function.

$$\begin{aligned}
S_H(f) &= \int_{-\infty}^{\infty} R_H(\Delta t) e^{-j2\pi f \Delta t} d\Delta t \\
&= S_\rho(f) + S_\mu(f)
\end{aligned} \tag{4.14}$$

where,

$$S_\rho(f) = A^2 e^{\sigma_3^2} \int_{-\infty}^{\infty} e^{\sigma_3^2 J_0(2\pi f_{m3} \Delta t)} e^{-j2\pi f \Delta t} d\Delta t \tag{4.15}$$

This equation has closed form approximation only for the small values of σ_3 ($\sigma_3 < 0.3$). Under such condition, using Taylor's series approximation and ignoring the faster converging terms

$$S_\rho(f) = A^2 e^{\sigma_3^2} \int_{-\infty}^{\infty} [1 + \sigma_3^2 J_0(2\pi f_{m3} \Delta t)] e^{-j2\pi f \Delta t} d\Delta t \tag{4.16}$$

which has a closed form solution in [76]

$$S_\rho(f) = A^2 e^{\sigma_3^2} \left[\delta(f) + \sigma_3^2 f_{m3} \frac{\text{rect}(\pi f / f_{m3})}{\sqrt{f_{m3}^2 - 4\pi^2 f^2}} \right] \quad |f| < \frac{f_{m3}}{2\pi} \tag{4.17}$$

where,

$$\text{rect}(t/T) = \begin{cases} 1, & t \leq |T| \\ 0, & \text{otherwise} \end{cases} \tag{4.18}$$

Also the second term $S_\mu(f)$ is given by

$$S_\mu(f) = \frac{1+q^2}{2q^2} \sigma_1^2 \int_{-\infty}^{\infty} J_0(KV_2\Delta t) J_0(KV_1\Delta t) e^{-j2\pi f\Delta t} d\Delta t \quad (4.19)$$

The solution to this form of integral can be found in [76]. From [114], the reduced form is

$$S_\mu(f) = \frac{1+q^2}{2q^2\pi^2 f_{m1}\sqrt{a}} \sigma_1^2 \times K \left[\frac{(1+a)}{2\sqrt{a}} \sqrt{1 - \left(\frac{f}{(1+a)f_{m1}} \right)^2} \right], \quad |f| < (1+a)f_{m1} \quad (4.20)$$

where $K(\cdot)$ is the elliptical integral function of first kind

Now, for the case $a = 0$, we have $V_2 = 0$. Assuming $A = 0$ (NLoS) (4.17) reduces to 0, the PSD $S_\mu(f)$ is obtained as

$$S_\mu(f) = \frac{1+q^2}{2q^2} \sigma_1^2 \int_{-\infty}^{\infty} J_0(KV_1\Delta t) e^{-j2\pi f\Delta t} d\Delta t \quad (4.21)$$

which is evaluated in [76] and is obtained in Chapter 2 as (2.28).

4.4.3 Level Crossing Rate and Average Duration of Fade

The level crossing rate of the process $H(t)$ is obtained by solving the following integral

$$N_H(r) = \int_{\dot{z}=0}^{\infty} \dot{z} p_{HH}(r, \dot{z}) d\dot{z} \quad (4.22)$$

where $p_{H\dot{H}}$ is the joint PDF of $H(t)$ and its time derivative $\dot{H}(t)$. This obtained from the Joint PDF $p_{H\dot{H}\Theta\dot{\Theta}}(r, \dot{r}, \theta, \dot{\theta})$.

$$p_{H\dot{H}}(r, \dot{r}) = \int_{\theta=0}^{2\pi} \int_{-\infty}^{\infty} p_{H\dot{H}\Theta\dot{\Theta}}(r, \dot{r}, \theta, \dot{\theta}) d\theta d\dot{\theta} \quad (4.23)$$

Again, using the total probability theorem, $p_{H\dot{H}\Theta\dot{\Theta}}(r, \dot{r}, \theta, \dot{\theta})$ is obtained as

$$p_{H\dot{H}\Theta\dot{\Theta}}(r, \dot{r}, \theta, \dot{\theta}) = \int_{b=0}^{\infty} p_{H\dot{H}\Theta\dot{\Theta}}(r, \dot{r}, \theta, \dot{\theta}|b) \cdot p(b) db \quad (4.24)$$

where $p_{H\dot{H}\Theta\dot{\Theta}}(r, \dot{r}, \theta, \dot{\theta}|b)$ is the Joint PDF of Rice Hoyt Process obtained from [80].

Hence, after some algebraic manipulations and simplifications, LCR is obtained as

$$\begin{aligned} N_H(r) &= \frac{r}{4\pi\sigma_1\sigma_2\sigma_3} \\ &\times \int_{b=0}^{\infty} \int_{\theta=0}^{2\pi} \exp \left[-\frac{(r \cos(\theta) - b)^2}{2\sigma_1^2} - \frac{(r \sin(\theta))^2}{2\sigma_2^2} \right] \\ &\times \exp \left[-\frac{1}{2\sigma_3^2} \left(\log \frac{b}{A} \right)^2 \right] \\ &\times \frac{\sqrt{\beta_1 \cos^2(\theta) + \beta_2 \sin^2(\theta)}}{b} d\theta db \end{aligned} \quad (4.25)$$

where, $\beta_i = -\ddot{R}_{\mu_i}(0)$. We obtain $\beta_1 = (\sqrt{2}\pi\sigma_1 f_{m1})^2(1 + a^2)$ and $\beta_2 = \beta_1/q^2$.

Further, defining $r_0 = r/r_{rms}$ as normalized amplitude, the LCR is obtained

as

$$\begin{aligned}
N_H(r_0) &= \frac{\sqrt{(1+a^2)(q^2+1)}f_{m1}r_0}{2\sqrt{2}\pi q\sigma_3} \\
&\times \int_{b=0}^{\infty} \int_{\theta=0}^{2\pi} \exp\left[-\frac{(r_0\sqrt{1+q^2}\sigma_2\cos(\theta)-b)^2}{2q^2\sigma_2^2}\right] \\
&\times \exp\left[-\frac{(r_0\sqrt{1+q^2}\sigma_2\sin(\theta))^2}{2\sigma_2^2}\right] \\
&\times \exp\left[-\frac{1}{2\sigma_3^2}\left(\log\frac{b}{A}\right)^2\right] \\
&\times \frac{\sqrt{q^2\cos^2(\theta)+\sin^2(\theta)}}{b}d\theta db
\end{aligned} \tag{4.26}$$

The average duration of fade of a signal is defined as average duration of time for which the signal r_0 spends below a specified threshold R_0 . It is given by [81]

$$\bar{\tau} = \frac{P(r_0 < R_0)}{N_H(r_0)} \tag{4.27}$$

where $P(r_0 < R_0)$ is the Cumulative Density Function obtained by

$$P(r_0 < R_0) = \int_0^{R_0} p_H(x)dx \tag{4.28}$$

This is obtained by integrating (4.2). Hence substituting (4.26) and (4.28) in (4.27), ADF can be directly obtained.

4.4.4 Squared Time Autocorrelation Function

The squared time autocorrelation function for the proposed channel is derived as

$$\begin{aligned}
R_{H^2}(\Delta t) &= E[|H(t)|^2 |H(t + \Delta t)|^2] \\
&= E[\{Ae^{z(t)} + \mu_1(t)\}^2 + \mu_2^2(t)] \\
&\times [\{Ae^{z(t+\Delta t)} + \mu_1(t + \Delta t)\}^2 + \mu_2^2(t + \Delta t)] \\
&= E[A^4 e^{2z(t)+2z(t+\Delta t)} + 2A^3 e^{2z(t)+z(t+\Delta t)} \\
&+ A^2 \mu_1^2(t + \Delta t) e^{2z(t)} + A^2 \mu_2^2(t + \Delta t) e^{2z(t)} \\
&+ 2A^3 e^{z(t)+2z(t+\Delta t)} + 2A\mu_1(t)\mu_1^2(t + \Delta t) e^{z(t)} \\
&+ 4A^2 \mu_1(t)\mu_1(t + \Delta t) e^{z(t)+z(t+\Delta t)} \\
&+ 2Ae^{z(t)}\mu_1(t)\mu_2^2(t + \Delta t) \\
&+ A^2 \mu_1^2(t) e^{2z(t+\Delta t)} + 2A\mu_1^2(t)\mu_1(t + \Delta t) e^{z(t+\Delta t)} \\
&+ \mu_1^2(t)\mu_1^2(t + \Delta t) + \mu_2^2(t)\mu_2^2(t + \Delta t) \\
&+ \mu_1^2(t)\mu_2^2(t + \Delta t) + \mu_2^2(t)\mu_1^2(t + \Delta t) \\
&+ A^2 \mu_2^2(t) e^{2z(t+\Delta t)} + 2A\mu_1(t + \Delta t)\mu_2^2(t) e^{z(t)}] \quad (4.29)
\end{aligned}$$

All the Gaussian processes are assumed zero mean i.e $E[\mu_i(t)] = E[\mu_i(t + \Delta t)] = E[z(t)] = E[z(t + \Delta t)] = 0$. Also, for lognormal process $\rho(t)$ having zero mean Gaussian $z(t)$, we have,

$$E[\rho(t)] = E[Ae^{z(t)}] = Ae^{\sigma_3^2/2} \quad (4.30)$$

$$\begin{aligned}
E[\rho^2(t)\rho^2(t + \Delta t)] &= E[A^4 e^{2z(t)+2z(t+\Delta t)}] \\
&= A^4 e^{4\sigma_3^2[1+J_0(w_{m3}\Delta t)]}
\end{aligned} \tag{4.31}$$

Since $\mu_1(t)$ and $\mu_2(t)$ are independent. therefore

$$E[\mu_1^2(t)\mu_2^2(t)] = E[\mu_1^2(t)]E[\mu_2^2(t)] = \sigma_1^2\sigma_2^2 \tag{4.32}$$

Also, we have for $i = 1, 2$

$$\begin{aligned}
E[\mu_i^2(t)\mu_i^2(t + \Delta t)] &= E[\mu_i^2(t)]E[\mu_i^2(t + \Delta t)] \\
&+ 2\{E[\mu_i(t)\mu_i(t + \Delta t)]\}^2 \\
&= \sigma_i^4[1 + 2J_0^2(w_{m1}\Delta t)J_0^2(w_{m2}\Delta t)]
\end{aligned} \tag{4.33}$$

Also, since $\rho(t)$ and $\mu_i(t)$ are independent, therefore

$$E[Ae^{z(t)}\mu_i(t + \Delta t)] = AE[e^{z(t)}]E[\mu_i(t + \Delta t)] = 0 \tag{4.34}$$

$$\begin{aligned}
E[A^2 e^{2z(t)}\mu_i^2(t + \Delta t)] &= A^2 E[e^{2z(t)}]E[\mu_i^2(t + \Delta t)] \\
&= A^2 \sigma_i^2 e^{2\sigma_3^2}
\end{aligned} \tag{4.35}$$

Substituting (4.30)-(4.35)in (4.29) will result in

$$\begin{aligned}
R_{H^2}(\Delta t) &= A^4 e^{4\sigma_3^2(1+J_0(w_{m3}\Delta t))} \\
&+ 2\sigma_1^2\sigma_2^2 + 2A^2(\sigma_1^2 + \sigma_2^2)e^{2\sigma_3^2} \\
&+ 2A^2\sigma_1^2 J_0(w_{m1}\Delta t)J_0(w_{m2}\Delta t)e^{\sigma_3^2(1+J_0(w_{m3}\Delta t))} \\
&+ (\sigma_1^4 + \sigma_2^4)(1 + 2J_0^2(w_{m1}\Delta t)J_0^2(w_{m2}\Delta t))
\end{aligned}$$

where, $w_{mi} = 2\pi f_{mi}$, for $i = 1, 2$ is angular frequency in radians per second.

4.5 Simulation and Results

The MATLAB based simulator developed here is an IFFT based simulator. The block diagram of the proposed simulator is shown in Figure 4.1. The simulation is run with the following parameters, carrier frequency ($f = 900\text{MHz}$), velocity of receiver $V_1 = 72\text{km/hr}$ which means $f_{m1} = 60\text{Hz}$, three different values of $q = 1, 0.5, 0.3$, three different values of $a = 1, 0.5, 0$ and $N_f = 8192$. For the LoS component, we set $A = 1$ and $\sigma_3 = 0.3$. The simulator sample output for $q = 0.5$, $a = 0.5$ is shown in Figure 4.2. The normalized envelope time variation is plotted.

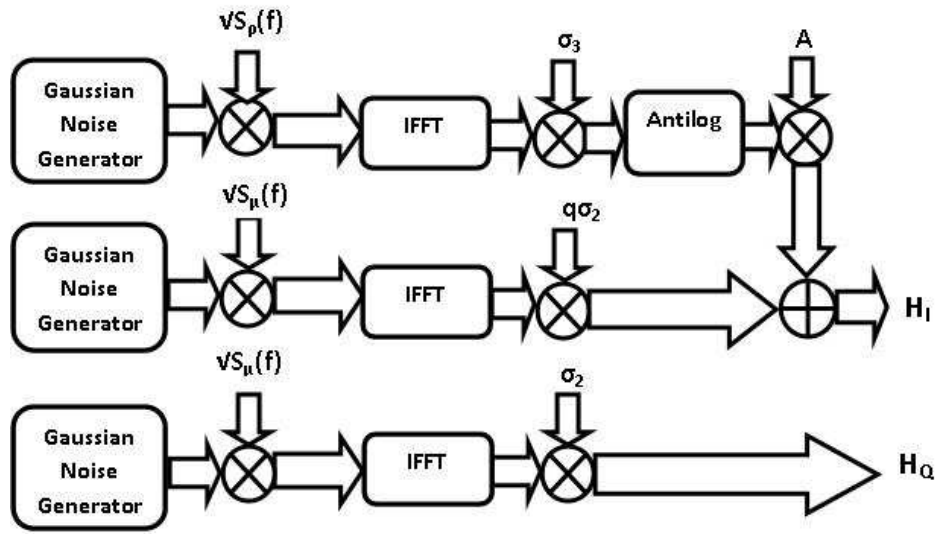


Figure 4.1: Block Diagram of the Simulator Using Proposed Model

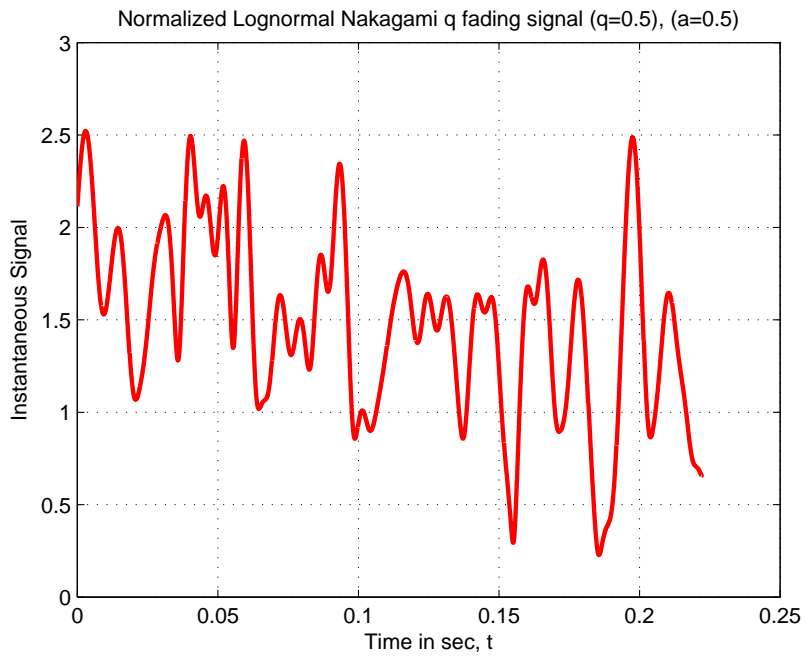


Figure 4.2: Envelope Output of the Simulator

The amplitude and phase PDFs plots are shown in Figure 4.3 and Figure 4.4 respectively. The corresponding theoretical output of (4.2) and (4.3) respectively are also plotted for comparison. For $q = 1$, the plots show envelope and phase of Rice with diffused LoS.

The power spectral density plots for $a = 1, 0.5, 0$ are shown in Figure 4.5 for $q = 0.5$. The plots for other values of q are the scaled version of this and has not been shown here. It is evident from the plot that $S(f)$ has peaks at $f = \pm(f_{m1} - f_{m2})$ due to the characteristics of elliptical integral function K . Other than that zero frequency (LoS component) is also shown.

The normalized autocorrelation functions plots have been shown in Figure 4.6. The plots for $a = 1, 0.5, 0$ are compared with the theoretical expression of (4.11) for $q = 0.5$. For $a = 0$, the plot is a Bessel function showing B2V communication.

The level crossing rates and average duration of fades for $q = 1, 0.5, 0.3$ are plotted in Figure 4.7 and Figure 4.8 respectively of $a = 0.5$. The curves are matched with their theoretical expressions given by (4.26) and (4.27). For $q = 0.3$, there exists some dissimilarities for the lower values of ρ . These can be overcome by increasing the number of frequency points N_f and number of samples M which will result in increasing simulator computational complexity.

The normalized squared time autocorrelation function plot is shown in Figure 4.9. The plot for $q = 0.5$ is compared with the theoretical expression of (4.36) for $a = 0.5$

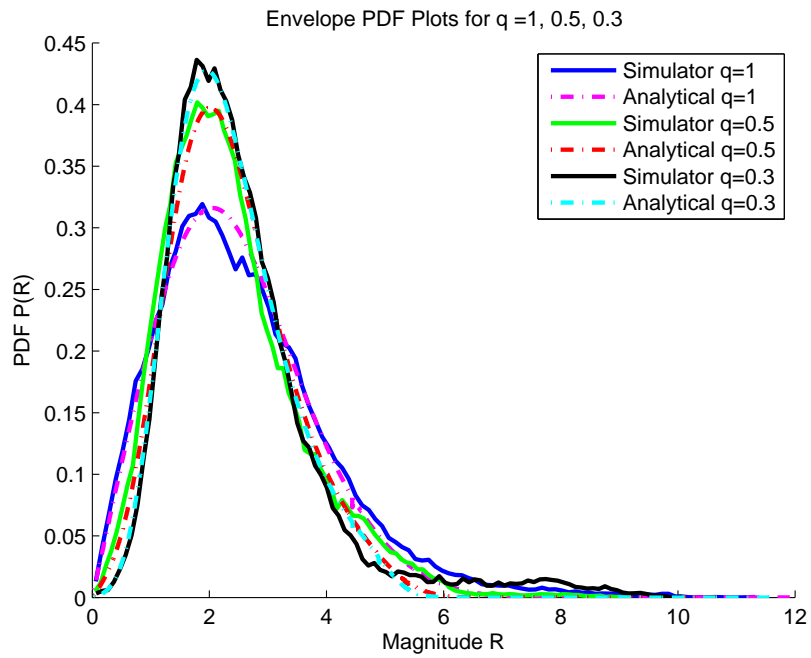


Figure 4.3: Envelope PDF Plot

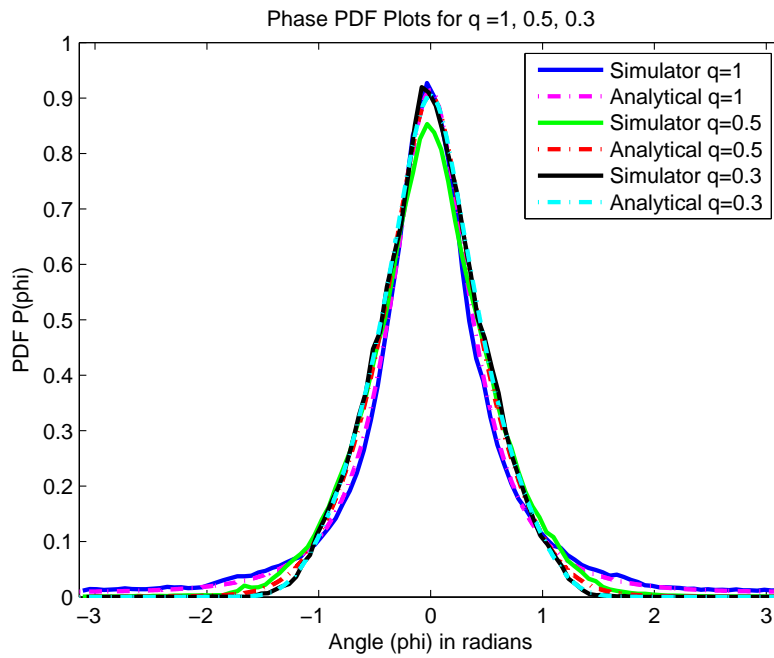


Figure 4.4: Phase PDF Plot

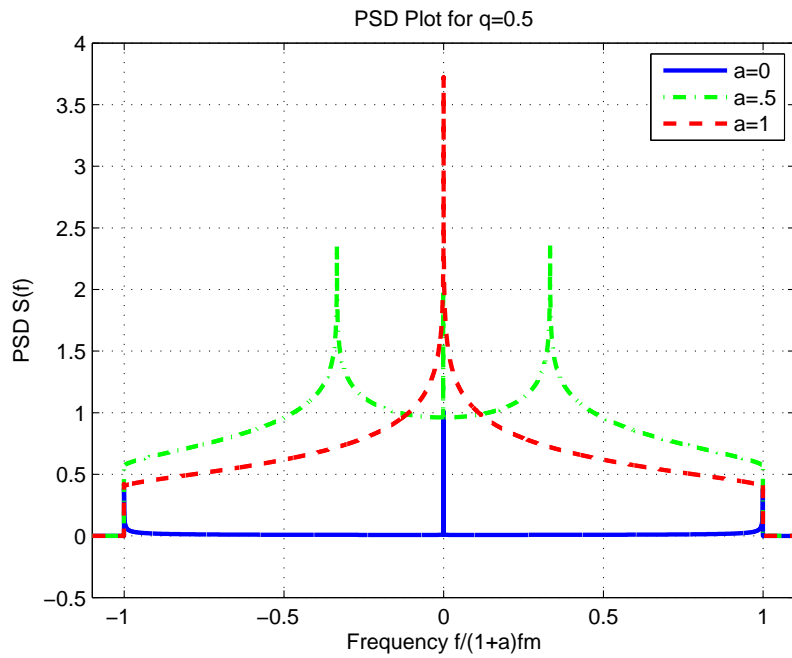


Figure 4.5: PSD Plot for q=0.5

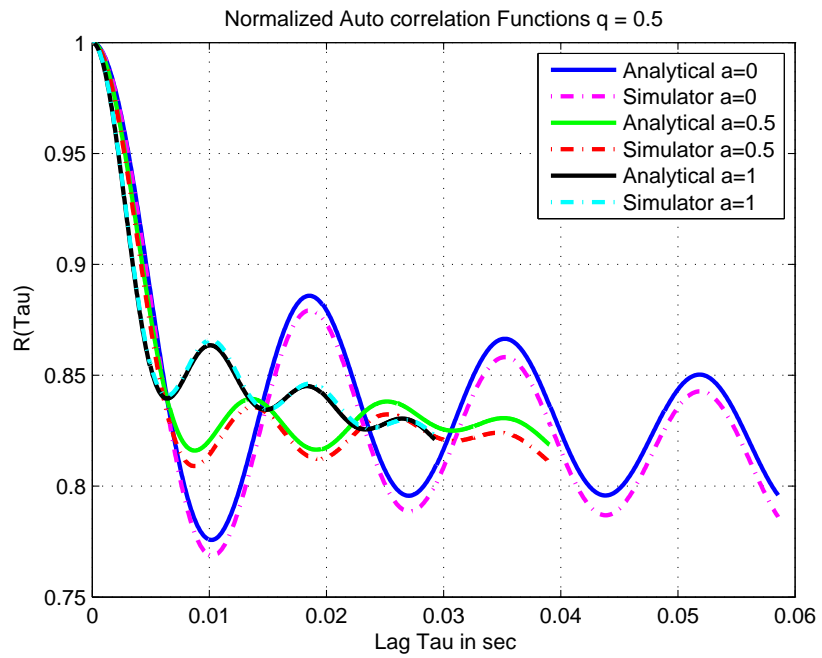


Figure 4.6: Autocorrelation Function of Real Part of Envelope

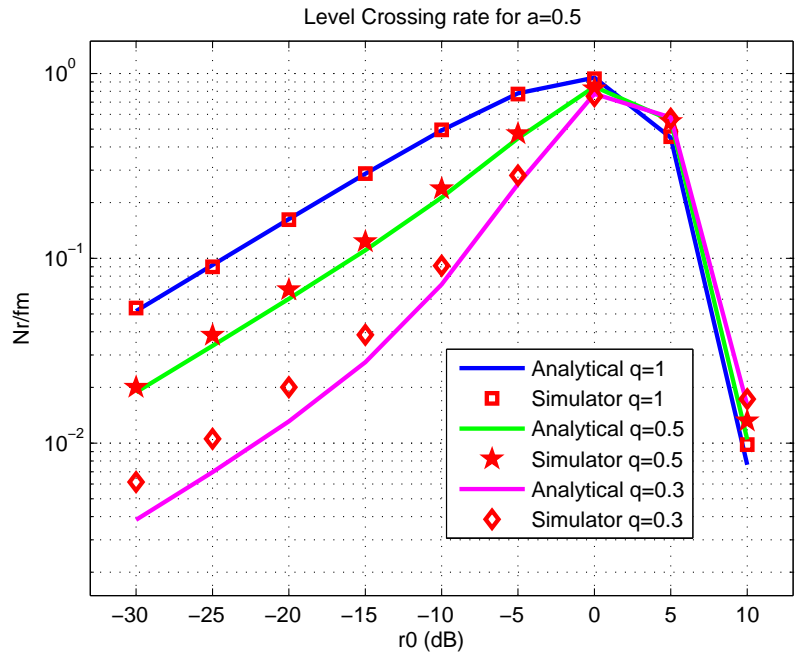


Figure 4.7: Level Crossing Rate for a=0.5

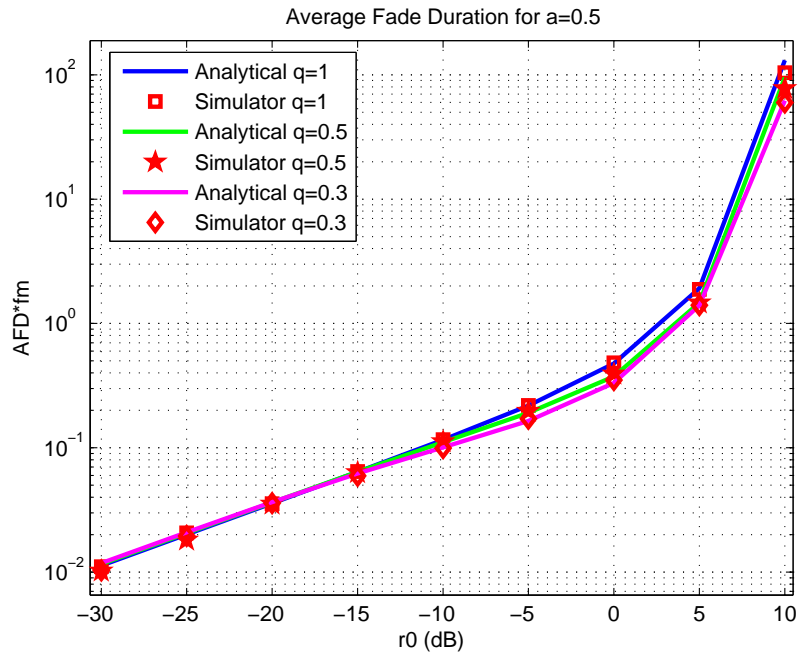


Figure 4.8: Average Fade Duration for a=0.5

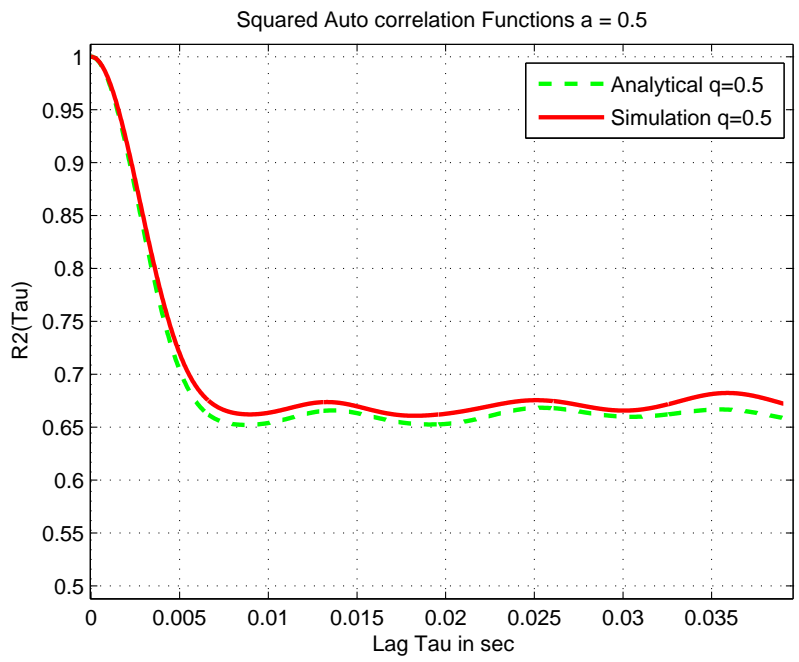


Figure 4.9: Normalized Squared Autocorrelation Function of envelope $q = 0.5$

The Mean Square Error of the time autocorrelation function is given by

$$MSE = E[(R_H(\Delta t) - \hat{R}_H(\Delta t))^2] \quad (4.36)$$

Where $R_H\Delta t$ and $\hat{R}_H\Delta t$ are the theoretical and estimated autocorrelation functions respectively. Figure 4.10 shows the Mean square error of time autocorrelation function as a function of number of frequency sample points N_f . The figure is obtained for $q = 0.5$, $a = 0.5$ and varying N_f in the range 128 – 8192 ($N_f = 2^k$ for integer values of k) for integer values of k . It is evident from the curve that the MSE reduces when the number of sample points are increased. Hence more accurate simulator is obtained at the cost of increasing the simulator complexity.

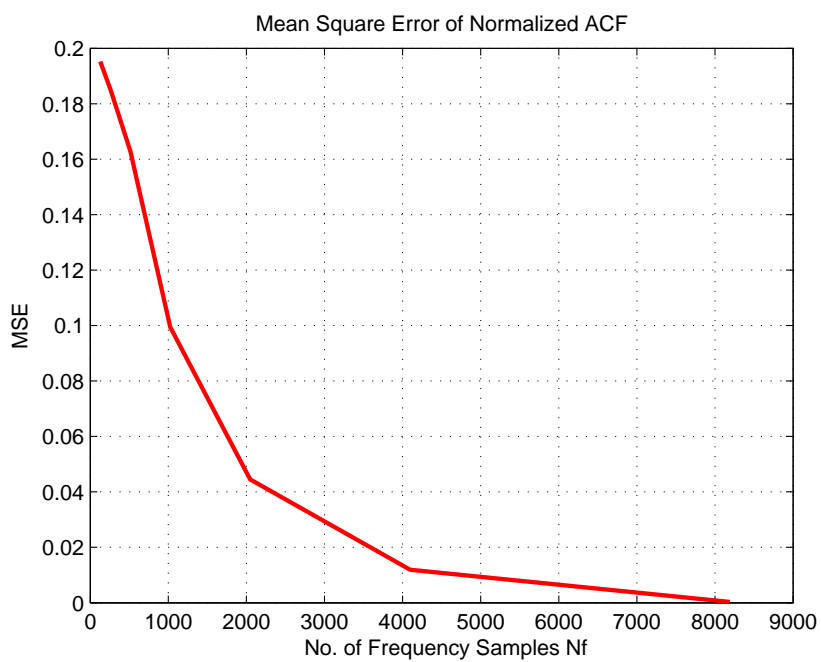


Figure 4.10: Mean Square Error of Autocorrelation Function

4.6 Summary

The statistical properties for V2V Nakagami-Hoyt channel with diffused LoS component, assuming omnidirectional antennas at both the transmitter and receiver, have been derived. These include expressions for envelope and phase PDFs, mean and RMS values, space time correlation function, time autocorrelation function, power spectral density, level crossing rates, average duration of fade and squared time autocorrelation function. A V2V simulator is developed to verify the theoretical derived expressions. MSE between the theoretical and estimated time autocorrelation function is also computed and it is observed that MSE reduces with increase in number of frequency points. It is shown that the analytical and simulated results corroborate.

CHAPTER 5

CHANNEL EMULATOR DESCRIPTION

This Chapter describes the design and implementation of a DSP based wide-band channel emulator. The emulator implementation uses a floating point (TMS320C6713) and a fixed point (TMS320C6416) DSPs. The emulator has 8 taps and baseband bandwidth of 20 MHz. It has flexibility to generate several channel models under varied environmental conditions. To validate the functionality of the emulator, the baseband data is applied to the emulator input and its output is statistically analyzed and the results are compared with those derived analytically. The statistical properties include envelope and phase PDFs of the generated channel coefficients, LCR and ADF of the envelope. BPSK bit error rate (BER) plot is also generated and compared with the analytical plot.

5.1 Design Philosophy

In the design of efficient real time systems, all available system resources are optimized towards minimizing the cost and maximizing the productivity. To acquire data at high rate, it is difficult to directly interface the DSPs with high speed ADCs and DACs due to I/O bandwidth limitations. The best solution is to use FPGA for I/O interfacing. Therefore, Microline ORS114 daughter board was used for this purpose. The board consists of a Vertex-2 FPGA, multiple channel ADC and DAC, FIFO memory and control circuitry used to synchronize the data input-output events with DSP. The board is mounted over the peripheral expansion of TMS320C6416 fixed point DSP Starter Kit (DSK) which performs the TDL filtering. An optimal TDL filtering is implemented for filtering operation at high data rates. This require high clock rate fixed point processor. Hence for that purpose TMS320C6416 processor with 1 GHz clock was selected. The generation of channel filter coefficient depends on the channel variation or the transmitter and receiver velocities that produce Doppler frequencies. This channel variations are normally much slower than the baseband data rate. Therefore, for generation of the channel coefficients with high precision a processor operating at relatively lower clock rate is adequate, therefore a TMS320C6713 32 bit floating point processor is used.

Several papers regarding V2V channel characterizations are considered, these include [121], [122], [123] and [125]. The outcome of these papers are added in the emulator design to run it in the realistic scenarios. Following are the findings,

- More than 99% of the PDP energy is in 8 taps. Hence the maximum number of selected emulator taps is 8.
- RMS Delay spread ranges from 1.8 μ sec to 0.3 ns.
- For urban environment, maximum Doppler frequency is 400 Hz where as the emulator currently supports up to 480 Hz.
- V2V tap location varies with time. The emulator tap delay line filter implementation supports this time variations.
- The emulator is quite flexible to playback the stored channel measurements when the statistical parameters of the channel are provided.

5.2 Emulator Design Specification

Figure 5.1 shows the overall block diagram of the channel emulator. It consists of two DSKs communicating with each other using the Multiple Channel Buffered Serial Port 0 (MCBSP0). The TMS320C6713 DSK board acts as a Master device. It generates and transmits channel coefficients to the primary TMS320C6416 DSK board which acts as a slave. The system runs according to the following specification:

- TMS320C6416 DSK board having 1 GHz fixed point processor works as a primary board to accept the baseband input and generate output;

- TMS320C6713 DSK board having 225 MHz floating point processor works as a secondary board that will generate channel taps at the required rate;
- Input Baseband data bandwidth 20 MHz (10 MHz each I & Q);
- Maximum number of Taps (channel coefficients) generated $N = 8$;
- Maximum Doppler frequency that can be set = 480 Hz;
- ADC and DAC Buffer size = 1024 Elements (16I + 16Q) = 32 bits;
- ADC and DAC resolution = 14 bits;
- Maximum sampling rate of ADC and DAC = 25 MHz;
- Transfer rate of channel coefficients = 16 KHz (2 KHz per tap);
- Maximum excess delay = 1024 samples which on 25 MHz sampling frequency becomes 41 *usec*.

5.3 Channel Emulator Functionality

In this section, the emulator functionality is discussed. The baseband data is acquired using ORS114 daughter board and processed using TMS320C6416 DSP in real time. The channel coefficients are generated using TMS320C6713 DSP and transferred to the C6416 DSP using MCBSP0 port to be used in real time. The emulator performs the following tasks

5.3.1 Baseband Data Acquisition

The baseband data acquisition uses Signalware's ORS-114 daughter board. This card is designed to facilitate rapid construction of prototypes or small to medium production runs with minimum time-to-market. The peripheral card provides flexible analog input and output for applications with a Texas Instruments (TI) Digital Signal Processors (DSP). It mounts on a card that contains TI TMS320C6xxx DSPs made by ORSYS, Inc. These DSP cards, known as the "micro-line" series, contain the processor, DRAM memory and an expansion interface which allows the peripheral card full access to all of the DSP's resources. The hardware block diagram of ORS114 board is shown in Figure 5.2.

The daughter board has two connectors. 26 pins output connector *J3* and 50 pins input connector *J4*. Both input and output are configured to use differential voltages. One input pin is connected to 2 volts peak to peak centered at 1 volt while the other input pin is tied to constant 1 volt. Each Inphase and Quadrature component is connected as a differential input. On each differential line the output voltage range is 0 to 0.5 volts.

The daughter board is configured to use 2 channels ADC and DAC working at 25 MSPS each and transfers 14 bit data in and out of DSP. The data transfer is done using enhanced direct memory access (EDMA) interface configured with optimal external memory interface (EMIF) setting to read and write data. The pin configuration detail is given in [145].

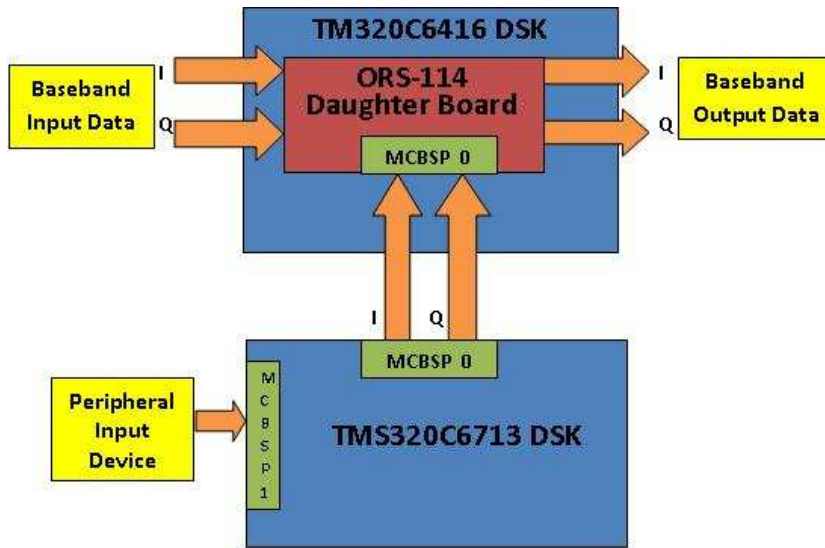


Figure 5.1: Channel Emulator Block Diagram

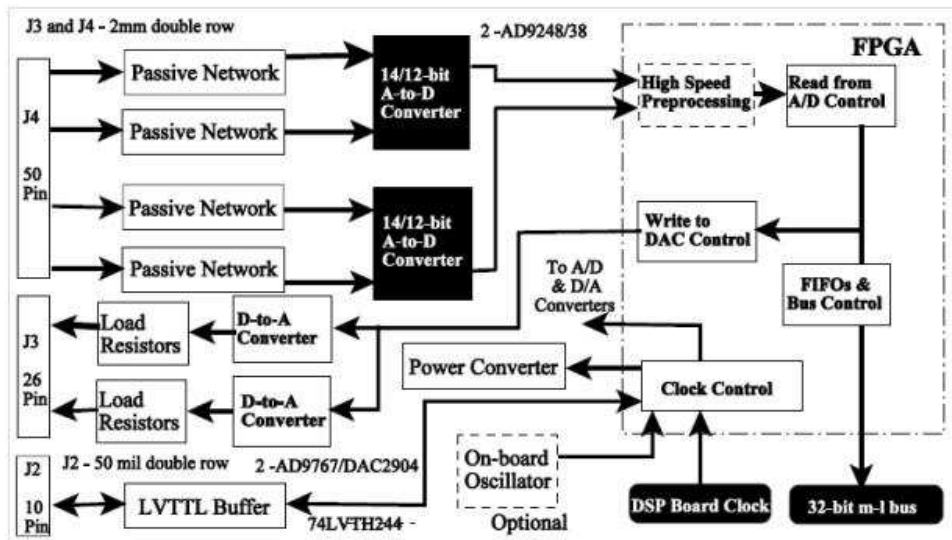


Figure 5.2: ORS-114 Block Diagram [145]

The main benefit of using ORS114 daughter board over other boards that contain only ADC and DAC is that it provides Vertex-2 FPGA for preprocessing of data before placing it in the DSP internal memory. The ADC is connected to the FPGA via parallel digital interface whereas DAC to FPGA interface is serial. The FPGA is connected to the DSP via the parallel micro-line bus which can connect directly to an other FPGA on compact board series.

The location of the FPGA between the DSP and the parallel buses allows it to perform some useful tasks. It allows blocking and FIFO buffering of signals before they are placed in the DSP memory. This can optimize the use of DSP memory and EMIF memory bus bandwidth which is often a limiting factor in DSP applications. The FPGA can provide further input decimation filtering which limits the bandwidth with sharp digital filter edges and reduces the number of samples allowing the application to work with higher total sample rates than the DSP can handle. The FPGA can construct high speed output samples for the DAC based on DSP inputs or the signals coming from the ADC. The FPGA also connects to the external digital I/O connector and to the clock/control lines of the converters. This allows synchronization of the converters either with an external signal, with an on-board oscillator or with DSP signals.

Ping Pong buffering technique described in TI documentations [146] has been used to perform data transfer efficiently between the I/O devices and internal memory (SRAM) of DSP. EDMA engine performs the data transfer between the ping/pong buffers and I/O device alternately and a pingpong flag ensures that

the DSP is processing the buffer that is not being overwritten by the EDMA. Since EDMA runs independently from the CPU, the CPU continues to process the block of data in the ping buffer while the EDMA is writing data on the pong buffers and vice versa. In order to remain synchronized with EDMA and void data loss, it is essential for CPU to finish the processing before the next EDMA interrupt is generated i.e., the data transfer is completed.

After reset, the DSP performs all the necessary initializations. It configures EMIF settings, initializes the Daughter board, configures EDMA channels to start data transfer and waits for the peripheral device to input the channel parameters. For the ADC Sampling time T_s and PING/PONG buffer size N , the data transfer flow is shown in the Figure 5.3 . The timing diagram is shown in Figure 5.4.

5.3.2 Primary Secondary Board Interface

The function of the primary secondary board interface is to obtain the channel coefficients in real time. For this purpose, the Multiple Channel Buffered Serial Port (MCBSP 0) present at the external peripheral interface of the TMS320C6416 DSK board, is used. The port is directly connected with the MCBSP 0 of the secondary board in Master/Slave configuration such that the secondary board that is generating channel coefficients work as Master device since it also generates clock and frame signal for the serial port whereas the primary board acts as a Slave and use these signals to get data. The block diagram of the connection between the two DSPs via MCBSP ports is shown in the Figure 5.5.

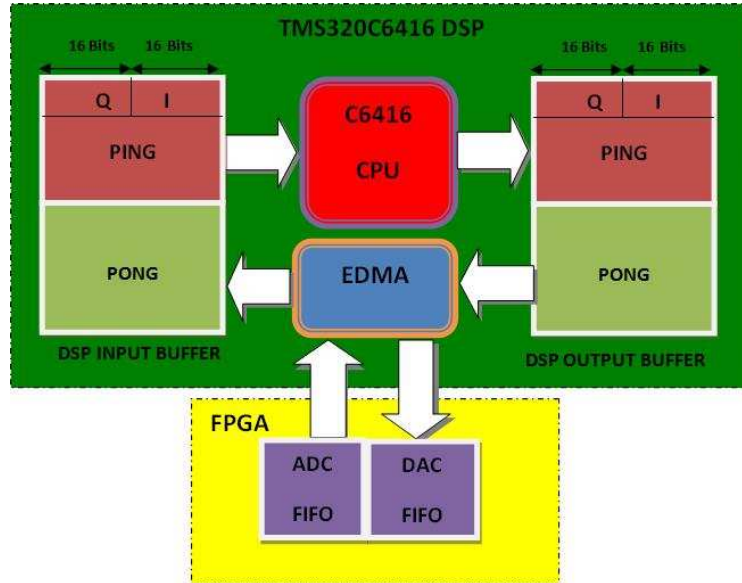


Figure 5.3: Block Diagram Showing Input Output Operations

Time Line →	0	NT_s	$2NT_s$	$3NT_s$
EDMA Transfer	ADC->PING IN	PONG OUT->DAC	ADC->PONG IN	PING OUT->DAC
DSP Processes	IDLE	PING BUFF	IDLE	PONG BUFF

Figure 5.4: Timing Diagram

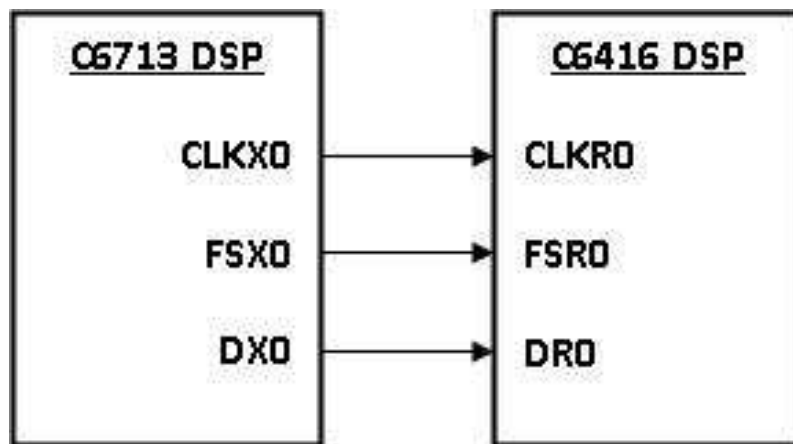


Figure 5.5: MCBSP Connection Between the Two DSPs

After connecting the two DSPs together the next step is to configure the ports so that the data can be transmitted and received successfully. The ports are configured by the setting the appropriate values of the four serial port registers. They are Receive Control Register (RCR), Transmit Control Register (XCR), Sample Rate Generator Register (SRGR), Pin Control Register (PCR).

The details of how to set these registers are given in TI documentation [147]. The values are set so that one frame consisting of 8 channel coefficients (32 bits each) is transmitted in 500 μ sec that results in a transmission rate of 16 KHz per coefficient.

Again, EDMA along with ping pong buffering technique is used to perform this transfer efficiently. At the transmitting end, the EDMA interrupt is generated periodically and at the same time, the CPU generates new channel coefficients. Whereas, at the receiving end, when a complete frame is received an interrupt is generated and the channel coefficients are updated

5.3.3 Tap Delay Line Filtering

Tap delay line filter is the basic block of many digital signal processing applications. It is based on the following equation

$$y[n] = \sum_{k=0}^M x[n-k].h[k] \quad (5.1)$$

where $y[n]$, $x[n]$, $h[n]$ are samples of the output, input and filter coefficient respectively at n th sample instant of a digital system of order M .

As seen from (5.1), in order to obtain an output $y[n]$, a buffer of M previous values (delay line) need to be maintained along with the current sample. Typically, a pointer is set up at the beginning of the sample array (oldest sample) and then manipulated to access the consecutive values.

Whenever a new sample needs to be added to the delay line all the values need to be shifted down. For large values of M (longer delay line), this will cause additional overhead of shifting the large amount of data. The alternate approach is to overwrite the oldest value. This can be implemented by using circular mode for pointer access.

The input data buffer has finite size and has to be accessed circularly as the new samples are continuously overwritten where the previously stored (oldest samples) need to be overwritten so that the buffer memory is reused. When the pointer reaches the last location of the buffer, it needs to wrap back to the beginning of the buffer. This would normally involve some amount of software overhead. When Input buffer addressing is defined as circular, the pointer automatically wraps back to the top whenever the bottom of the buffer is reached. Figure 5.6 illustrates the circular addressing. The input buffer is made circular for that purpose it must be properly aligned in the internal memory. The detail of how to set up the Circular buffer is given in [148].

TDL Filter can be implemented in several ways depending upon the application. Here, the filter is modeled as a frequency selective channel, where the channel taps are assumed as multipath fingers located at multiple of sampling

time T_s . $N = M + 1$ tap time intervals are assumed as τ_i where i varies from 0 to M and $\tau_0 = 0$. The channel model is shown in Figure 5.7. The tap index N_i is related with τ_i as

$$N_i = \left\lfloor \frac{\tau_i}{T_s} + 0.5 \right\rfloor \quad (5.2)$$

where $\lfloor \cdot \rfloor$ indicates the truncation operation. For the buffer size L , the maximum excess delay that can be simulated as

$$\tau_{max} = LT_s \quad (5.3)$$

Using the pipeline approach mentioned in [149] the code has been optimized for $N = 8$ taps. The inner loop was completely unrolled to reduce the loop overhead, the dependency graph was created and the instructions were pipelined to reduce the number of cycles. The optimized code consists of 3 parts. The *prolog*, the *mainloop* and *epilog*.

The prolog consists of initialization of local variables, pushing registers over stack for usage inside the function, loading taps coefficients $h[n]$ from memory into registers and defining input buffer as circular. Defining the input as circular buffer removes the overhead of an additional branch instruction inside the loop. The use of circular buffer prevents the constant test of wrapping. The prolog is to be executed once for L size input buffer. It takes 45 cycles to execute this code.

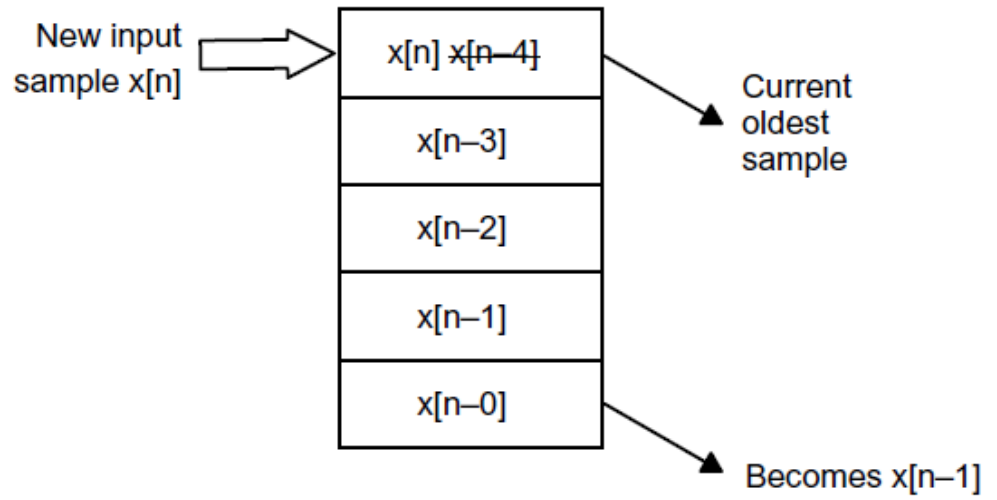


Figure 5.6: Pointer Manipulation Using Circular Addressing

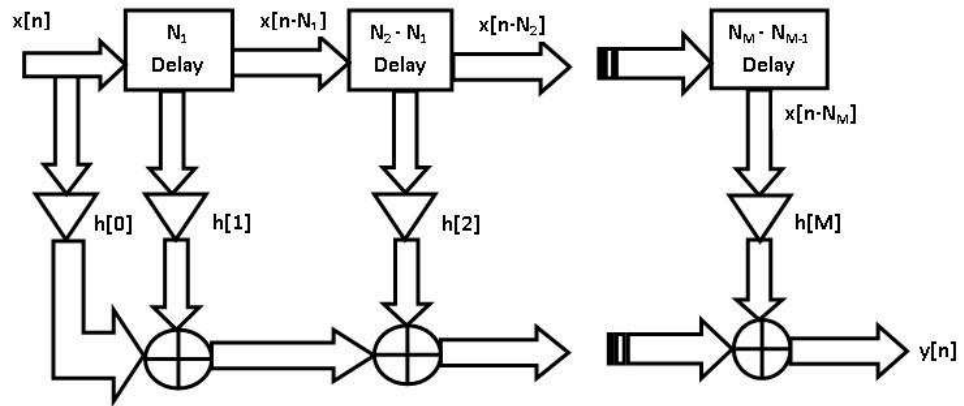


Figure 5.7: Tap Delay Line Filter Model

The main loop is also known as kernel of the program which is executed most of the time. It is optimized and instructions are scheduled to maximize the utilization of the CPU resources. For N taps it is executed $2N$ times per input sample. For 4 taps, the resources allocations are shown in Table 5.1. It is also shown that loading of data from memory and its storage into memory are done at the same time using .D1 and .D2 functional units whereas branching instruction, re-initialization, output storing and counter increments have also been scheduled. *STH* instructions have been used to store the sample output back into the internal memory, *ZERO* to re-initialize the output registers back to zero for the computation of next sample output and *SHR* to bring the output in Q3.13 format.

The epilog consists of the remaining part of the function. This include remaining loop portion, popping data back to the registers and branch out of the function. This part takes 42 cycles to execute.

5.3.4 Channel Gains Generations

The channel coefficients are generated using a floating point TMS320C6713 DSP. Reference [98] describes the efficient method of generating the channel gains. It uses an infinite impulse response (IIR) Doppler filter along with the polyphase interpolator for the generation of correlated Gaussian channel coefficients. The original approach was for flat fading channel Rayleigh channel only. It was modified for the more generalized 8 taps frequency selective Nakagami-Hoyt mobile to mobile fading channel with diffused LoS.

Table 5.1: Four Taps TDL Resources Allocation for Main Loop

Cy. FU	1	2	3	4	5	6	7	8
.M1	MPY	MPYH	MPY	MPYH	MPY	MPYH	MPY	MPYH
.M2	MPYHL	MPYLH	MPYHL	MPYLH	MPYHL	MPYLH	MPYHL	MPYLH
.L1	SUB	ADD	SUB	ADD	SUB	ADD	SUB	ADD
.L2	ADD	ADD	ADD	ADD	ADD	ADD	ADD	ADD
.S1		ADD	B	ZERO	SHR		ADD	
.S2				ZERO	SHR			ADD
.D1	LDW	LDW			LDW	LDW	STH	
.D2					SUB			STH

The block diagram of the channel coefficient generation unit of the single (first) tap is shown in Figure 5.8. The block diagram represents a generalized channel model. By varying the values of parameters (a , q , σ_2 and A) different channel models can be obtained and simulated. These models are shown in the Table 5.2. For $a = 0$, the models are obtained for Base to mobile communication whereas $a > 0$ represents V2V communications.

The Doppler Shaping Filter is implemented as an IIR Filter having the frequency response obtained by taking the square root of $S(f)$ i.e. $\sqrt{S(f)}$. The filter has been designed for the Doppler rate of $F_d T_s = 0.2$. The higher rate is achieved by interpolating the channel coefficients I times using polyphase interpolator. For the Fade Rate ($f_d T_s$) of 0.01, the value of $I = 20$ is used. For the maximum Doppler frequency of 160 Hz the channel sampling rate of 16 KHz is set.

The maximum Doppler frequency is configurable and is set using LCD Keypad interfacing of TMS320C6713 DSK (MCBSP1 port). This can go up to 480 Hz. For a single emulator run, it will remain unchanged. The filter coefficients are computed on the base of normalized Doppler frequency. The algorithm for filter coefficient generation uses fade rate ($f_d T_s$) of 0.01. For 160Hz Doppler the Sampling frequency (Filter coefficient update rate is 16 KHz). This means if the Doppler frequency is increased the sampling frequency will also be increased in the same proportion so as to make the fade rate constant. The increase in sampling frequency means MCBSP0 port data rate will be increased. This rate is software

configurable and can be set by changing the value of Sample Rate Generator Register (SRGR) of the MCBSP0 port. The upper limit depends upon the complexity of the channel coefficient generation algorithm and number of taps. For 8 taps, it is 480 Hz and this can be increased if we further optimize the channel generation code using some optimization techniques (reducing mathematical complexity and efficient use of DSP resources).

The interpolator is implemented as a polyphase filter with a windowed *sinc*(.) function impulse response. The algorithm for channel coefficient generation has been modified in order to consider the generalized cases. Figure 5.9, 5.10, 5.11 show the frequency response of the modified PSD under different values of $a = (0, 0.5, 1)$, $A = 0$, $\sigma_2 > 0$ and $q = 0.5$.

Table 5.2: Various Channel Models for Simulation

	$A = 0$	$A \neq 0$	
		$z(t) = 0$	$z(t) \Rightarrow \text{Gaussian}$
$q = 1$	Rayleigh	Rice	Log-Normal Rice
$0 < q < 1$	Hoyt	Rice Hoyt	Diffused Hoyt
$\sigma_2 = 0$	-	Static	Lognormal

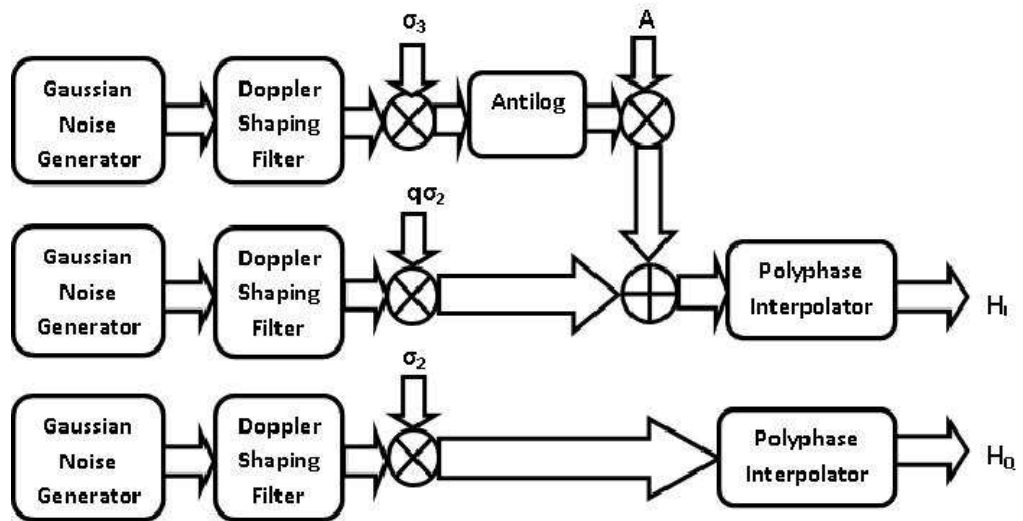


Figure 5.8: Single Tap Generation Using Filter Method

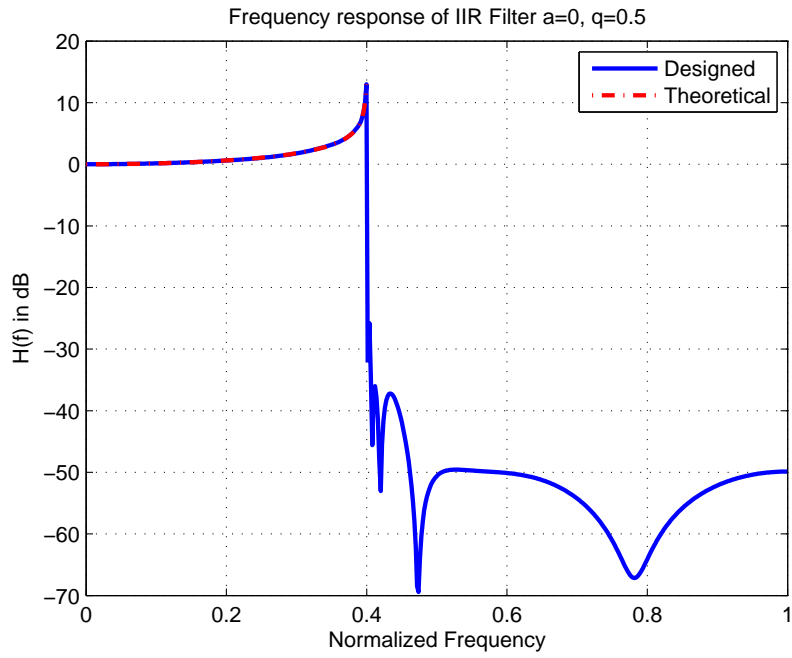


Figure 5.9: Frequency Response of IIR Filter $q=0.5, a=0$

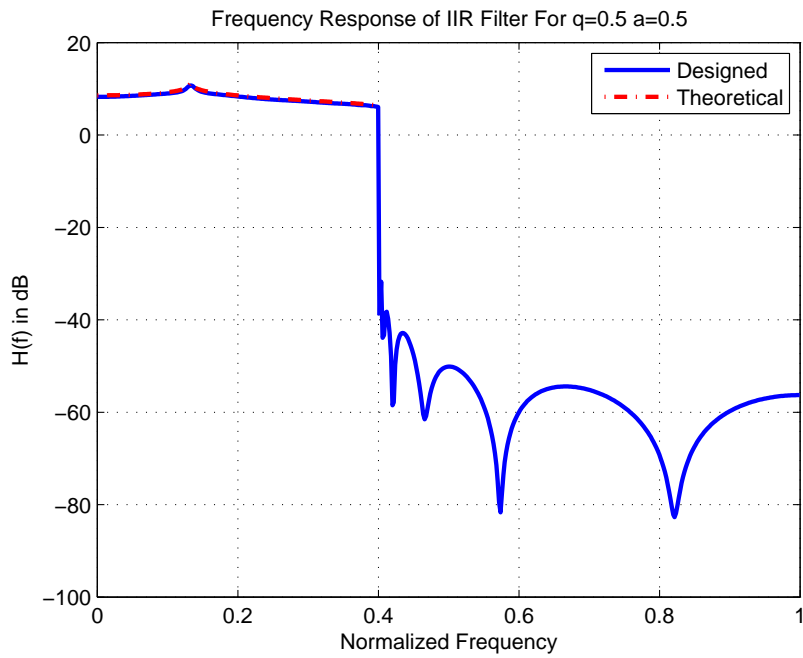


Figure 5.10: Frequency Response of IIR Filter $q=0.5, a=0.5$

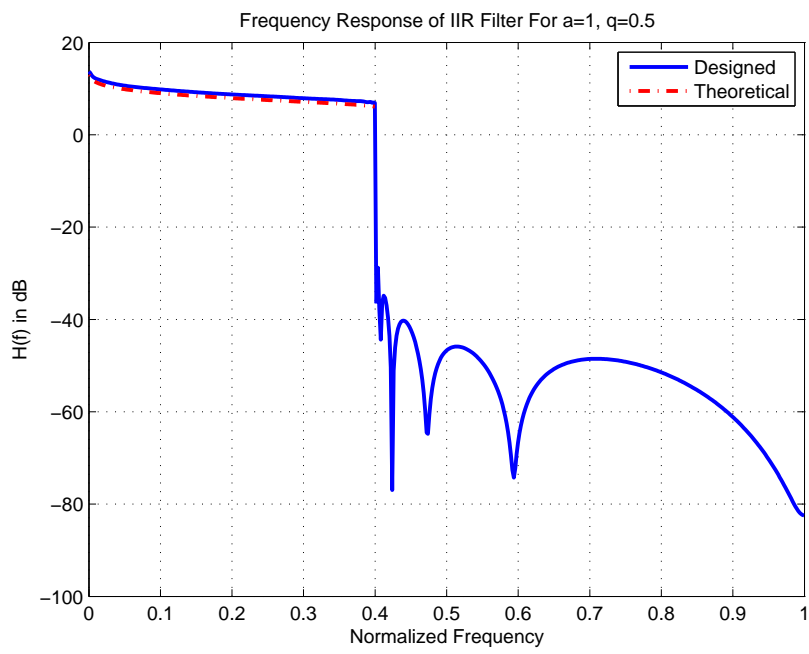


Figure 5.11: Frequency Response of IIR Filter $q=0.5$ $a=1.0$

5.4 Results and Comparison

A TDL filter with N taps is modeled here as a frequency selective multipath channel. Each tap is complex having defined location. The channel is assumed static for one buffer period of time. Both C and assembly functions were executed for $L = 1024$ I/O buffer size, data sampling frequency $F_s = 12.5MHz$ and $N = 8$ taps filter coefficients having values $h = \{1.8362 - 0.5073i, -0.2169 + 0.0915i, -0.1448 + 0.1585i, -0.2169 + 0.0915i, 0.0, 0.0, 0.0, 0.0\}$ with corresponding tap locations at $\{0, 0.5, 1, 1.6, 1.8, 1.9, 2.0, 2.1\} \mu\text{sec}$. The magnitude response $|h|$ of the channel is shown in Figure 5.12.

The sinusoidal input shown in Figure 5.13 is applied on both I & Q channels. The output of both were found exactly match with each other. For fixed point C code, it takes 1460 cycles per sample to generate output whereas the optimized code gives output in 16 cycles per sample. From (5.3), the maximum excess delay τ_{max} the system can have is found to be 81.92 usec.

A comparison has been made with an implementation given in [150] using TMS320C6713 DSP. The comparison is fair in terms of number of CPU cycles as both DSPs have same functional units. The only difference is in terms of number of general purpose registers. It takes $1.95 \mu\text{sec}$ to generate per sample output which on $225MHz$ CPU takes 439 cycles whereas using the proposed optimization method, it takes only 62 cycles which is 7 times faster than the reference approach.

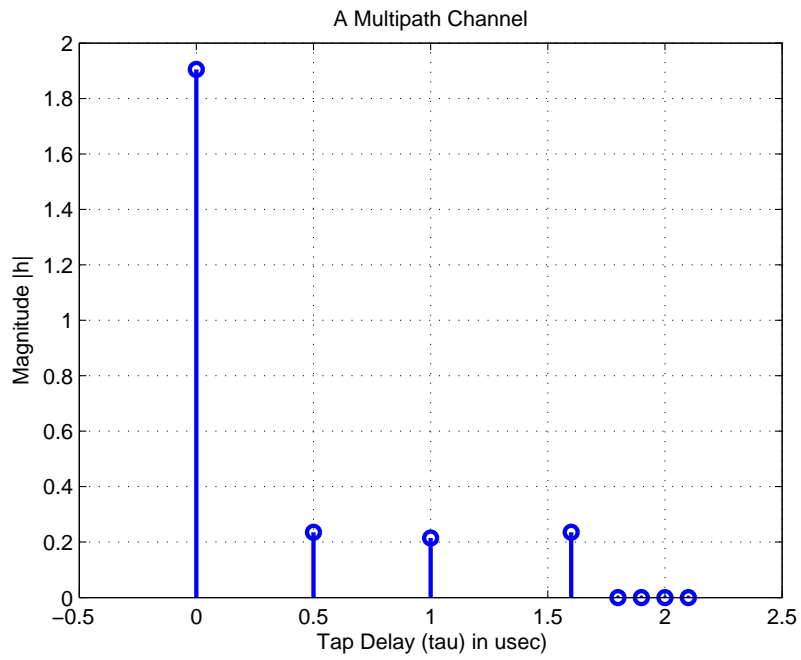


Figure 5.12: Channel Magnitude Impulse Response

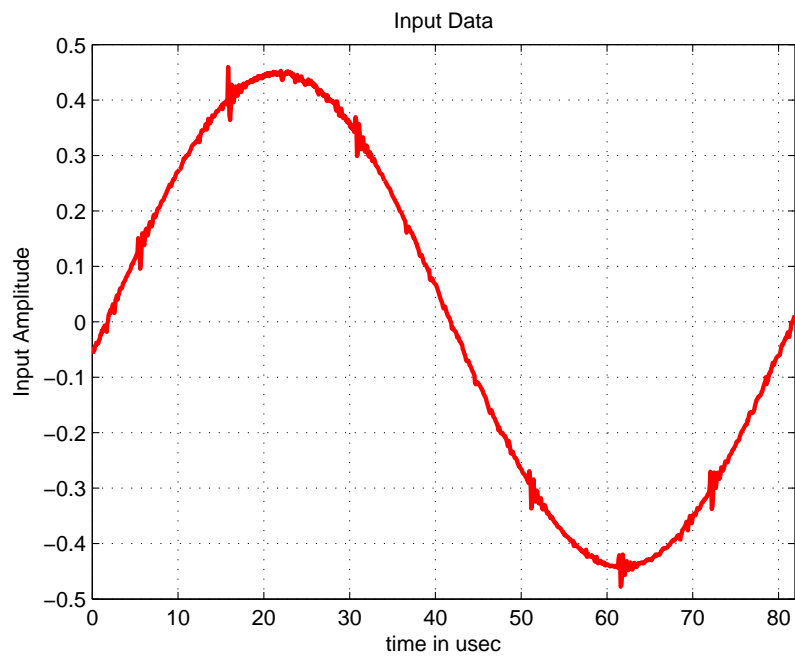


Figure 5.13: Input Data on Both I and Q Channel

A comparison has also been made for a given complex input between the outputs of the MATLAB complex FIR filter code with the fixed point assembly code and are shown in Figure 5.14 (Magnitude plot) and Figure 5.15 (Phase plot). The number of taps assumed are $N = 8$ with buffer size $L = 1024$. For C6416 DSP operating at $1GHz$ (the cycle time of $1ns$), the proposed algorithm will take around $16ns$ per sample. Thus, data with around $60MHz$ sampling frequency can be processed.

In order to verify the channel coefficient generation, the BER analysis of the channel has also been done. The BPSK modulated data is applied to the input of a single tap channel and the output and channel coefficients (400k samples) are stored in the *SDRAM* of TMS320C6416 DSP Board in real time. Since BER analysis is independent of data rate and sampling frequency, hence due to the limited size of *SDRAM* (16 MB), the sampling rate was set to 2 MHz and the input data rate to 200 kbps. The envelope and phase PDF, LCR, ADF and BER plots are shown in the Figure 5.16, 5.17, 5.18, 5.19 and 5.20, respectively. The plots are found to closely match the corresponding theoretical plots. MSE between the theoretical and simulated values of the amplitude, phase PDF, BER curves and LCR are shown in Table 5.3.

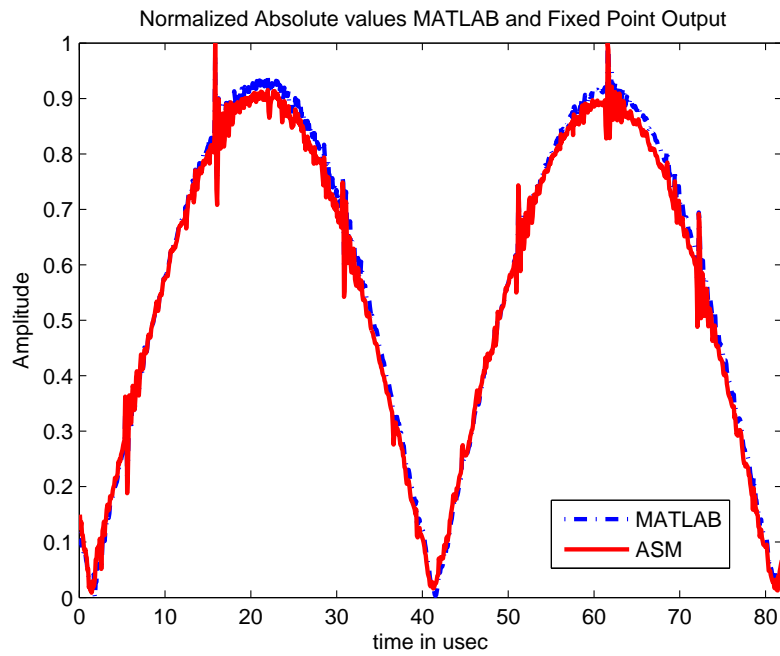


Figure 5.14: TDL Filter Output Magnitude Plot

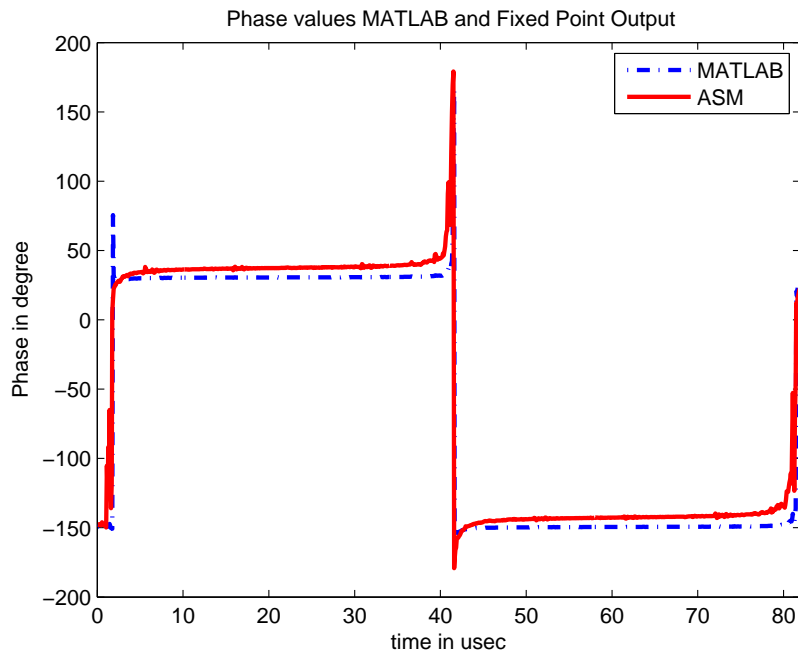


Figure 5.15: TDL Filter Output Phase Plot

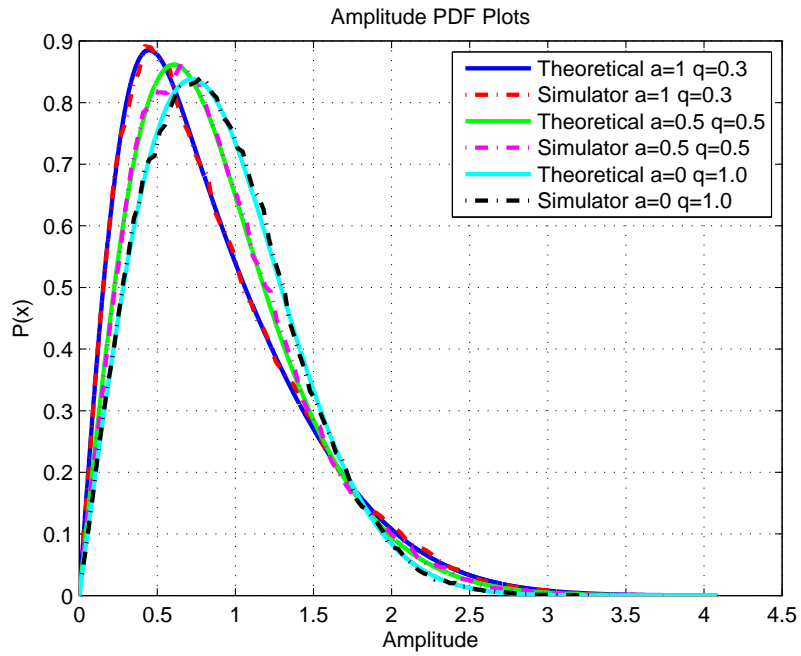


Figure 5.16: PDF Plot for Envelope

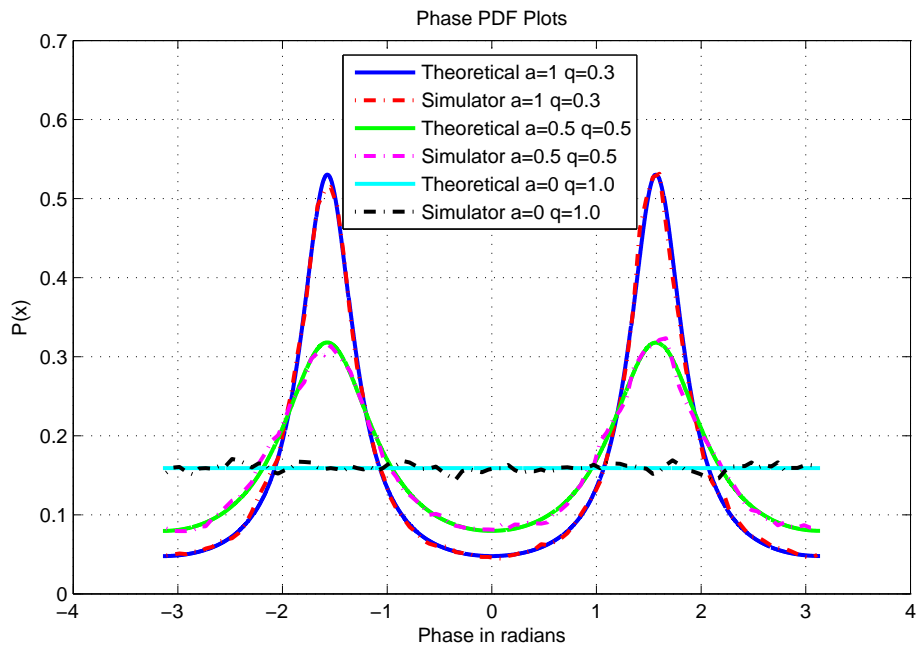


Figure 5.17: PDF Plot for Phase

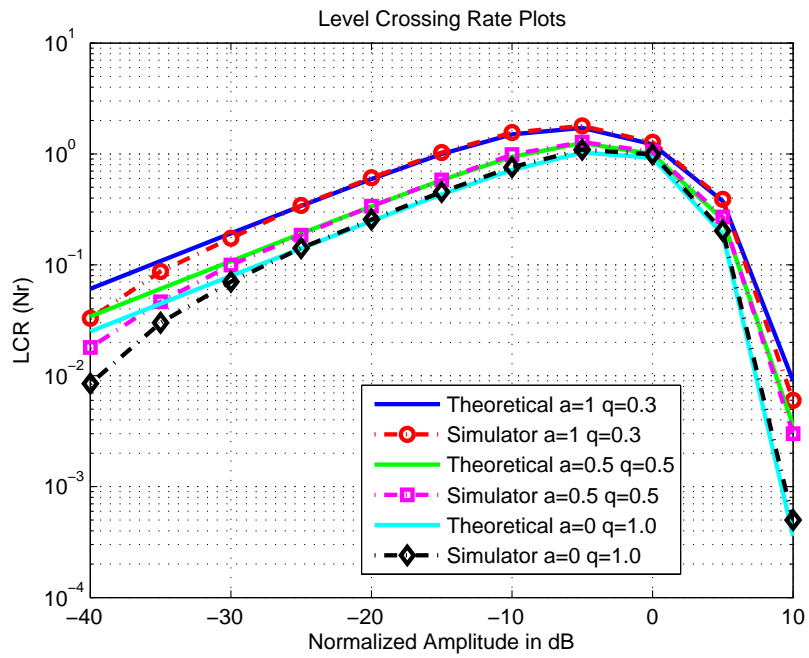


Figure 5.18: PDF Plot for LCR

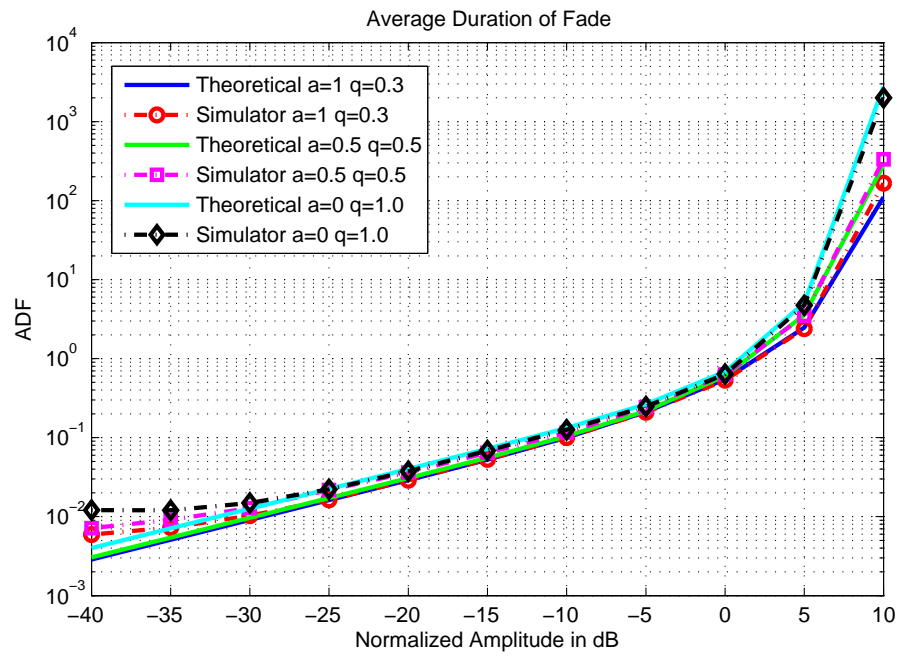


Figure 5.19: PDF Plot for ADF

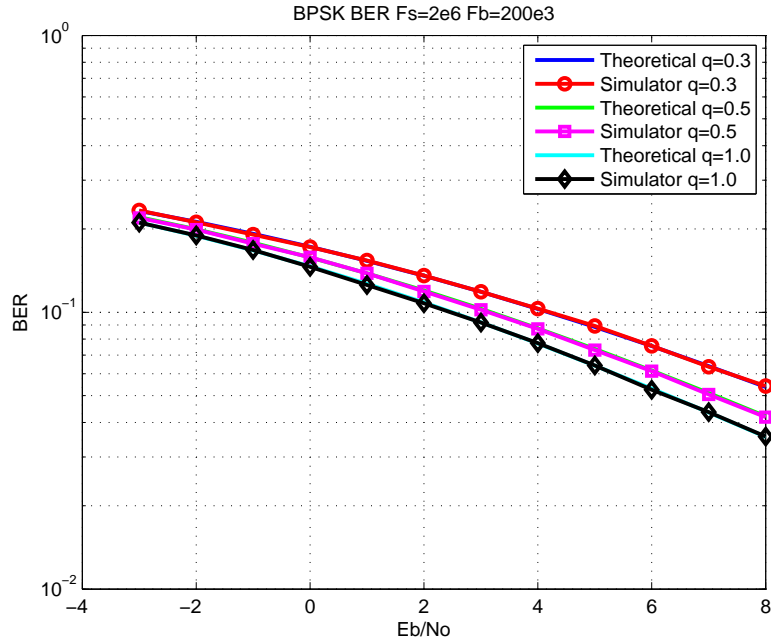


Figure 5.20: BER Plot, BPSK Modulation $q=1$, $q=0.5$, $q=0.3$

Table 5.3: MSE of Various Quantities for $a=0.5$

q	Envelope PDF	Phase PDF	BPSK BER	LCR
0.3	4.240×10^{-5}	4.647×10^{-5}	1.456×10^{-7}	13×10^{-4}
0.5	8.148×10^{-5}	3.371×10^{-5}	4.439×10^{-7}	6×10^{-4}
1.0	6.511×10^{-5}	2.586×10^{-5}	0.775×10^{-7}	11×10^{-4}

5.5 Summary

In this chapter, design and implementation of an efficient real time wideband simulator have been discussed. The emulator has been run in real time with a known input and the output data has been analyzed. The TDL filter has been optimally implemented over TMS320C6416 DSP. The output of the filter has been verified by comparing the emulator output with MATLAB. The pipelined architecture of the processor and the circular buffer have been efficiently utilized. The channel coefficients have been generated and analyzed. The BPSK modulated data has been input and the output has been stored. The bit error rate has been measured and compared with the theoretical data to verify the validity of the channel emulator.

CHAPTER 6

CONCLUSIONS AND FUTURE RECOMMENDATIONS

6.1 Conclusions

This dissertation proposed three channel models and derived their statistical properties for V2V environment. The channel models were validated by developing MATLAB based simulators and comparing the simulator outcome with the derived analytical expressions. Based on these models the dissertation also develops a wideband channel emulator. The main contributions of the dissertation are listed below:

1. Three channel models were proposed and developed. These include V2V Nakagami-Hoyt channel model under isotropic scattering condition, V2V Nakagami Hoyt channel model under non-isotropic scattering condition and V2V Nakagami Hoyt channel model under diffused LOS and Isotropic scat-

tering condition.

2. The statistical properties (spatial time correlation function, power spectral density, level crossing rate, average duration of fade and squared time autocorrelation function) of these models were also derived
3. MATLAB based simulators were developed to validate the derived statistical properties by comparing the theoretical and simulated results. The simulators were based on frequency domain random number generation. Mean square error of the time autocorrelation function was also plotted as a function of number of frequency points of the simulator.
4. A wideband channel emulator was developed on the basis of above models. An efficient Tap Delay Line model was implemented. The known baseband data was input and for known channel coefficients, the output of the simulator was obtained and compared with the MATLAB output. The simulator functionality was also verified by storing the generated channel coefficients, performing the statistical analysis of the stored data and comparing it with the analytical results.

6.2 Future Recommendations

Based on the achieved objective of this work, recommendations for future work are made.

1. An extended generalized model that covers the non-isotropic scattering un-

der diffused LoS environment can be developed.

2. The real time simulator developed currently does not consider the channel model under Non-Isotropic condition. The simulator can be modified to cover this case.
3. The work currently uses SISO channel model and can further be extended to MIMO channel modeling and simulation
4. The simulator currently assumes baseband data input and output. Using appropriate modulator and demodulator hardware it can be extended to passband simulator
5. The simulator has 8 taps and baseband bandwidth of 20 MHz. The number of taps and bandwidth can be increased by selecting appropriate hardware platform like FPGA and optimal algorithm for channel gains generation.
6. The simulator can be modified further to cover other channel models like Weibull and composite models.
7. The simulator takes differential input and generates differential output in a range 0 to 2 volts. Signal interface and conditioning and input output modules are also required to interface with the real world.
8. By optimizing the channel coefficient generation code, the simulator can support the maximum Doppler frequency higher than 1 KHz.

REFERENCES

- [1] Y. Akaiwa, *Introduction to Digital Mobile Communications*, Wiley, New York, 1997
- [2] B. Bing, R. V. Nee, and V. Hayes, *Wireless local area and home networks*, IEEE Commun. Mag., 39(11):63157, Nov. 2001.
- [3] V. K. Garg and J. E. Wilkes, *Wireless and Personal Communications Systems*, Prentice Hall, Upper Saddle River, NJ, 1996
- [4] R. Mangharam, J. Meyers, R. Rajkumar, D. Stancil, J. Parikh, H. Krishnan, C. Kellum, *A multi-hop mobile networking test-bed for telematics*, in Proceedings of Society for Automotive Engineers (SAE) World Congress, Detroit, USA, April 2005.
- [5] J. Dulmage, M. Tsai, M. Fitz, B. Daneshrad, *COTS-based DSRC testbed for rapid algorithm development, implementation, and test*, in Proceedings of WiNTECH, Los Angeles, USA, Sep. 2006.

- [6] T. M. Fernandez Carames, J. A. Garcya Naya, M. Gonzalez-Lopez, and L. Castedo, *FlexVehd: a flexible testbed for vehicular radio interfaces*, in Proceedings of ITST, Phuket, Thailand, Oct. 2008.
- [7] A. Goldsmith, *Wireless Communications*, Stanford University, 2004.
- [8] K. Bullington, *Radio Propagation Variations at VHF and UHF*, Proceedings of the IRE, vol.38, no.1, pp. 27- 32, Jan. 1950
- [9] J. J. Egli, *Radio propagation above 40 MHz over irregular terrain*, Proc. IRE 45, pp. 1383-1391, 1957
- [10] W. C. Jakes, D. O. Reudink, D.O., *Comparison of mobile radio transmission at UHF and X band*, Vehicular Technology, IEEE Transactions on, vol.16, no.1, pp. 10- 14, Oct 1967
- [11] P. M. Trifonov, V. N. Buelko, and V. S. Zotov, *Structure of USW field strength spatial fluctuations in a city*, Trans. Telecomm. Radio Eng. 9, pp. 26-30. 1964
- [12] Y. Okamura, Y. A. kol, *Field Strength and its Variability in VHF and UHF Land-Mobile Radio Service*, Rev. Elec. Comm. Lab. No.9-10, pp. 825 - 873, 1968
- [13] G. L. Turin, F. D. Clapp, T. L. Johnston, S. B. Fine, and D. Lavry, *A statistical model of urban multipath propagation*, IEEE Trans. Veh. Technol., vol. VT-21, p. 19, Feb. 1972.

- [14] D. M. Black, D. O. Reudink, *Some characteristics of mobile radio propagation at 836 MHz in the Philadelphia area*, Vehicular Technology, IEEE Transactions on, vol.21, no.2, pp. 45- 51, May 1972
- [15] D. Cox, *Delay Doppler characteristics of multipath propagation at 910 MHz in a suburban mobile radio environment*, Antennas and Propagation, IEEE Transactions on, vol.20, no.5, pp. 625- 635, Sep 1972
- [16] D. Cox, *Time- and Frequency-Domain Characterizations of Multipath Propagation at 910 MHz in a Suburban Mobile-Radio Environment*, Radio Science, vol. 7, NO. 12, PP. 1069-1077, Dec. 1972
- [17] T. Aulin, *Characteristics of a digital mobile radio channel*, Vehicular Technology, IEEE Transactions on, vol.30, no.2, pp. 45- 53, May 1981
- [18] S. E. Alexander, *Radio propagation within buildings at 900 Mhz*, Electron Lett., vol. 18, no. 21, pp. 913-914, Oct. 14, 1982
- [19] A. A. M. Saleh and R. A. Valenzuela, *A Statisitcal Model for Indoor Multipath propagation*, IEEE Journal on Selected Areas in Communications, vol. sac-5, no. 2 February 1987.
- [20] S. Y. Seidel and T. S. Rappaport, *914 MHz path loss prediction models for wireless communications in multifloored buildings*, IEEE Trans. Antennas Propagation., vol. 40, No.2, pp.207-217, Feb. 1992.

- [21] D. A. Hawbaker and T. S. Rappaport, *Indoor wideband radiowave propagation measurements at 1.3 GHz and 4.0 GHz*, IEE Electronics Letters, Vol.26,No. 1,1990.
- [22] U. Dersch, J. Troger and E. Zollinger, *Multiple Reflections of Radio Waves in a Corridor*, IEEE Trans. on Antenna and Propagation, vol. 42, No.9, pp. 1571- 1574, Sep. 1994.
- [23] F. Babich, G. Lombardi, *Statistical analysis and characterization of the indoor propagation channel*, Communications, IEEE Transactions on, vol.48, no.3, pp.455-464, Mar 2000
- [24] X. Zhao, J. Kivinen, P. Vainikainen, K. Skog, *Propagation Characteristics for Wideband Outdoor Mobile Communications at 5.3 GHz*, IEEE Journal on selected areas in communications, vol.20, No.3, April 2002
- [25] N. Youssef, C. X. Wang, and M. Patzold, *A Study on the Second Order Statistics of Nakagami-Hoyt Mobile Fading Channels*, IEEE transactions on vehicular technology, vol. 54, No. 4, July 2005
- [26] S. O. Rice, *Statistical properties of a sine wave plus random noise*, Bell Syst. J., vol. 27, pp. 109-157, Jan. 1948.
- [27] R. S. Hoyt, *Probability functions for the modulus and angle of the normal complex variate*, Bell Syst. J., vol. 26, pp. 318-359, Apr. 1947.

- [28] M. Nakagami, *The m -distribution - A general formula of intensity distribution of rapid fading*, in *Statistical Methods in Radio Wave Propagation*, W. G. Hoffman, Ed. Oxford, UK: Pergamon Press, 1960, pp. 3-36.
- [29] F. Vatalaro, *Generalized Rice-Lognormal Channel Model for Wireless Communications*, *Electronics Letters*, 31, 22, October 1995, pp. 1899-1900.
- [30] Y. Karasawa and H. Iwai, *Modeling of Signal Envelope Correlation of Line-of-sight Fading with Applications to Frequency Correlation Analysis*, *IEEE Transactions on Communications*, COM-42,6, June 1994, pp. 2201-2203.
- [31] T. T. Tjhung and C. C. Chai, *Fade Statistics in Nakagami-Lognormal Channels*, *IEEE Transactions on Communications*, COM-47,12, December 1999, pp. 1769-1772.
- [32] A. Abdi and M. Kaveh, *K Distribution: An Appropriate Substitute for Rayleigh-lognormal Distribution in Fading-Shadowing Wireless Channels*, *Electronics Letters*, 34, 9, April 1998, pp. 851-852.
- [33] M. A. Taneda, J. Takada, and K. Araki, *A new approach to fading: Weibull model*, in *Proc. IEEE International Symposium on Personal, Indoor, and Mobile Radio Communications*, , pp. 711-715, Osaka, Japan, Sept. 1999.
- [34] F. Hansen and F. I. Meno, *Mobile fading-Rayleigh and lognormal superimposed*, *IEEE Trans. Veh. Technol.*, vol. VT-26, pp. 332-335, Nov. 1977.

- [35] L. Cheng et al., *Mobile Vehicle-to-Vehicle Narrow-Band Channel Measurement and Characterization of the 5.9 GHz Dedicated Short Range Communication (DSRC) Frequency Band*, IEEE JSAC, vol. 25, 2007, pp. 150116.
- [36] Bullington, K. *Radio Propagation Variations at VHF and UHF*, Proceedings of the IRE , vol.38, no.1, pp. 27- 32, Jan. 1950
- [37] <http://www.rajant.com/solutions/military>
- [38] H. Suzuki, *A statistical model of urban multipath propagation*, IEEE Trans. Commun., vol. COM-25, pp. 673-680, 1977.
- [39] F. Vatalaro and G. E. Corazza, *Probability of error and outage in a Rice-lognormal channel for terrestrial and satellite personal communications*, IEEE Trans. Commun., vol. 44, no. 8, pp. 921-924, Aug. 1996.
- [40] H. Mehrina, H. Hashemi, *Mobile Satellite Propagation Channel (part I: A comparative evaluation of current Models)*, Vehicular Technology on communication VTC pp. 2775-2779, 1999.
- [41] C. Loo, *A statistical model for land mobile satellite link*, IEEE Trans. Veh. Technol., vol. VT-34, pp. 122-127, Aug. 1985.
- [42] E. Lutz, D. Cygan, M. Dippold, F. Dolainsky, and W. Papke, *The land mobile satellite communication channel-recording, statistics and channel model*, IEEE Trans. Veh. Technol., vol. 40, pp. 375-385, May 1991.

- [43] I. Jaafar ; N. Youssef, H. Boujemaa, *A generalized Rice channel for modeling mobile satellite link*, Control, Communications and Signal Processing, 2004. First International Symposium on , vol., no., pp. 515- 518, 2004
- [44] N. Youssef, C. Wang, M. Patzold, I. Jaafar, S. Tabbane, *On the statistical properties of generalized Rice multipath fading channels* Vehicular Technology Conference, 2004. VTC 2004-Spring. 2004 IEEE 59th , vol.1, no., pp. 162- 165 Vol.1, 17-19 May 2004
- [45] A. K. Papazafeiropoulos, S .A Kotsopoulos, *An Extended Generalized Rice Model for Wireless Communications*, Vehicular Technology, IEEE Transactions on , vol.59, no.5, pp.2604-2609, Jun 2010
- [46] I. Jaafar, *Statistical Properties of the Combined Generalized Rice-Hoyt Channel Model*, 3rd International Conference: Sciences of Electronic, Technologies of Information and Telecommunications March 27-31, 2005 TUNISIA
- [47] J. C. S. C Filho, M. D. Yacoub, *On the second-order statistics of Nakagami fading simulators*, Communications, IEEE Transactions on, vol.57, no.12, pp.3543-3546, December 2009
- [48] R. K. Mallik, *A New Statistical Model of the Complex Nakagami-m Fading Gain*, Communications, IEEE Transactions on , vol.58, no.9, pp.2611-2620, September 2010
- [49] A. Saleh, R. Valenzuela, *A statistical model for indoor multipath propagation*, IEEE Journal on Selected Areas in Communications 5 (1987) 128.

- [50] COST207, *Digital land mobile radio communications*, final report, Luxembourg, 1989
- [51] A. Abdi, J.A. Barger, and M. Kaveh, *A parametric model for the distribution of the angle of arrival and the associated correlation function and power spectrum at the mobile station*, IEEE Trans. Veh. Technol., vol.51, pp.425-434, May 2002.
- [52] <http://www.spirent.com/Solutions-Directory/SR5500>
- [53] <http://www.elektrobit.com>
- [54] <http://www.azimuthsystems.com/products/ace-channel-emulators>
- [55] T. Okumura, E. Ohmor, K. Fukada, *Field strength and its variability in VHF and UHF land mobile service*, Review Electrical Communication Laboratory (1968) 825873.
- [56] M. Hata, *Empirical formula for propagation loss in land mobile radio service*, Vehicular Technology, IEEE Transactions on , vol.29, no.3, pp. 317- 325, Aug 1980.
- [57] L. R. Maciel, H. L. Bertoni, H. N. Xia, *Unified approach to prediction of propagation over buildings for all ranges of base station antenna height*, Vehicular Technology, IEEE Transactions on , vol.42, no.1, pp.41-45, Feb 1993

- [58] F. Ikegami, S. Yoshida, T. Takeuchi, M. Umehira, *Propagation factors controlling mean field strength on urban streets*, Antennas and Propagation, IEEE Transactions on , vol.32, no.8, pp. 822- 829, Aug 1984.
- [59] H. H. Xia, *An analytical model for predicting path loss in urban and suburban environments*, Personal Indoor and Mobile Radio Communications, 1996. PIMRC'96., Seventh IEEE International Symposium on , vol.1, no., pp.19-23 vol.1, 15-18 Oct 1996
- [60] J. Walfisch, H. Bertoni, *A theoretical model of UHF propagation in urban environment*, IEEE Transactions on Antennas and Propagation, vol. 36 pp. 1788-1796. 1988
- [61] COST231, *Digital mobile radio towards future generation systems*, Final report, 1999.
- [62] M. D. Austin and G. L. Stuber, *Velocity adaptive handoff algorithms for microcellular systems*, IEEE Trans. Veh. Technol., vol. 43, No. 3, pp. 549-561, Aug. 1994.
- [63] A. Abdi, J. A. Barger, and M. Kaveh, *A parametric model for the distribution of the angle of arrival and the associated correlation function and power spectrum at the mobile station*, IEEE Trans. Veh. Technol., vol. 51, no. 3, pp. 425-434, May 2002.

- [64] W. A. T Kotterman, G. F. Pedersen, and K. Olsen, *Diversity properties of multiantenna small handheld terminals*, EURASIP Journal on Applied Signal Processing, vol. 2004, no. 9, pp. 1340-1353, 2004.
- [65] X. Zhao, J. Kivinen, P. Vainikainen, and K. Skog, *Characterization of Doppler Spectra for Mobile Communications at 5.3 GHz*, IEEE Trans. Veh. Technol., vol. 52, no. 1, pp. 14-23, Jan. 2003.
- [66] N. Blaunstein and Y. Ben-Shimol, *Spectral properties of signal fading and Doppler spectra distribution in urban mobile communication links*, Wirel. Commun. Mob. Comput., vol. 6, no. 1, pp. 113-126, Feb. 2006.
- [67] J. Salz and J. H. Winters, *Effect of fading correlation on adaptive arrays in digital mobile radio*, IEEE Trans. Veh. Technol., vol. 43, No. 4, pp. 1049-1057, Nov. 1994
- [68] X. Cheng, C.X. Wang, D. I. Laurenson, and A. V. Vasilakos. *Second Order Statistics of Non-Isotropic Mobile-to-Mobile Ricean Fading Channels*, Communications, 2009. ICC '09. IEEE International Conference on, vol., no., pp.1-5, 14-18 June 2009
- [69] Fayziyev, A.; Patzold, M.; Youssef, N., *On the autocorrelation function of Rice processes for unsymmetrical doppler power spectral densities*, Advanced Technologies for Communications (ATC), 2010 International Conference on, vol., no., pp.118-123, 20-22 Oct. 2010

- [70] Y. R. Zheng, *A non-isotropic model for mobile-to-mobile fading channel simulations*, MILCOM'06 IEEE conference on Military communications, Oct. 2006 Pg. 1-7
- [71] K. Ohtani and H. Omori, *Distribution of burst error lengths in Rayleigh fading radio channels*, *Electron. Lett.*, vol. 16, no. 23, pp. 889-891, 1980.
- [72] K. Ohtani, K. Daikoku, and H. Omori, *Burst error performance encountered in digital land mobile radio channel*, *IEEE Trans. Veh. Technol.*, vol. VT-23, no. 1, pp. 156-160, 1981.
- [73] H. S. Wang and N. Moayeri, *Finite state Markov channel- A useful model for radio communication channels*, *IEEE Trans. Veh. Technol.*, vol. VT-44, no. 1, pp. 163-171, Feb. 1995.
- [74] Schwartz, Bennet, and Stein, *Communication Systems and Techniques*, New York: McGraw-Hill, 1966.
- [75] W. C. Jakes, *Microwave Mobile Communications*, 2nd ed., Piscataway, NJ: IEEE Press, 1993
- [76] Gradshteyn and Ryzhik, *Tables of Integrals, Series and Products*, New York: Academic, 1994.
- [77] T. S. Rappaport, *Wireless communications: Principle and practice*, Printice Hall Communications Engineering and Emerging Technologies series, 2nd Edition, Feb. 1996

- [78] J. G. Proakis, *Digital Communications*, New York: McGraw-Hill, 4th ed., ch. 2, 2001.
- [79] A. Papoulis, S. U. Pillai *Probability, Random Variables and Stochastic Processes*, McGraw-Hill Higher Education, 4th Edition, Feb. 1996
- [80] A. K. Papazafeiropoulos, S .A Kotsopoulos, *An Extended Generalized Rice Model for Wireless Communications*, Vehicular Technology, IEEE Transactions on , vol.59, no.5, pp.2604-2609, Jun 2010
- [81] S. O. Rice, *Mathematical analysis of random noise*, Bell Syst. Tech. J., Jan. 1945
- [82] A. A. Gaston, W. H. Chriss, *A Multipath Fading Simulator for Mobile Radio*, IEEE Transactions On Vehicular Technology, Vol. Vt-22, No. 4, November 1973
- [83] R. C. Fitting, *Wideband troposcatter radio channel simulator*, IEEE Trans. Commun. Technol., vol. COMM-15, no. 4, pp. 565570, Aug. 1975.
- [84] E. L. Caples, K. E. Massad, and T. R. Minor, *A UHF channel simulator for digital mobile radio*, IEEE Trans. Veh. Technol., vol. VT-29, no. 2, pp. 281289, May 1980.
- [85] J. R. Ball, *A real-time fading simulator for mobile radio*, The Radio and Electronic Engineer, Vol. 52, No. 10, pp. 475-478. October 1982

- [86] H. W. Arnold and W. F. Bodtmann, *A hybrid multi-channel hardware simulator for frequency-selective mobile radio paths*, IEEE Trans. Commun., vol. COMM-31, no. 3, pp. 370377, Mar. 1983.
- [87] D. Berthoumieux and J. M. Pertoldi, *Hardware propagation simulator of the frequency selective fading channel at 90 MHz*, in Proc. 2nd Nordic Seminar on Digital Land Mobile Radio Communication, Stockholm, Sweden, Sep. 1986, pp. 331336.
- [88] M. Lecours and F. Marceau, *Design and implementation of channel simulator for wideband mobile radio transmission*, in Proc. Vehicular Technology Conf. (VTC), San Francisco, CA, 1989, pp. 652655.
- [89] R. A. Comroe, *All-digital fading simulator*, in Proc. Nut. Electron. Conf., vol. 32, 1978, pp. 136-139.
- [90] R. A. Goubran, H. M. Hafez and A. U. H. Sheikh, *Real-Time Programmable Land Mobile Channel Simulator*, IEEE, 1986
- [91] Casas, E.; Leung, C., *A simple digital fading simulator for mobile radio*, Vehicular Technology, IEEE Transactions on , vol.39, no.3, pp.205-212, Aug 1990
- [92] J. F. An, A. M. D. Turkmani, J. D. Parsons, *Implementation of a DSP-based frequency non-selective fading simulator*, Radio Receivers and Associated Systems, 1989., Fifth International Conference on, vol., no., pp.20-24, 23-27 Jul 1990

- [93] P. J. Cullen, P. C. Fannin, and A. Garvey, *Real-Time Simulation of Randomly Time-Variant Linear Systems: The Mobile Radio Channel*, IEEE Transactions on Instrumentation and Measurement, VOL. 43, NO. 4, AUGUST 1994
- [94] X. F. CHEN and K. S. CHUNG, *Generation of noise sources for a digital frequency selective fading simulator*, International Symposium on Signal Processing and its Applications, ISSPA, Gold Coast, Australia, 25-30 August, 1996
- [95] A. K. Salkintzis, *Implementation of a digital wide-band mobile channel simulator*, Broadcasting, IEEE Transactions on, vol.45, no.1, pp.122-128, Mar 1999
- [96] J. R. Papenfuss, M. A. Wickert, *Implementation of a real-time, frequency selective, RF channel simulator using a hybrid DSP-FPGA architecture*, Radio and Wireless Conference, 2000. RAWCON 2000. 2000 IEEE, vol., no., pp.135-138, 2000
- [97] S. Fischer, R. Seeger, K. D. Kammeyer, *Implementation of a Real-Time Satellite Channel Simulator for Laboratory and Teaching Purposes*, The Third European DSP Education & Research Conference, Paris, France, vol., no., pp. 20-21, Sep. 2000
- [98] C. Komninakis, *A Fast and Accurate Rayleigh Fading Simulator*, Global Telecommunications Conference, 2003. GLOBECOM '03. IEEE , vol. 6, no., pp. 3306- 3310 1-5 Dec. 2003

- [99] M. Khars, C. Zimmer, *Digital Signal Processing in a Real time Propagation Simulator*, IEEE Transactions on Instrumentation and Measurement, VOL. 55, NO. 1, Feb. 2006
- [100] S. Kandeepan, A. D. S. Jayalath, *Narrow-Band Channel Simulator Based on Statistical Models Implemented on Texas Instruments C6713 DSP and National Instruments PCIE-6259 Hardware*, Communication systems, 2006. ICCS 2006. 10th IEEE Singapore International Conference on, vol., no., pp.1-6, Oct. 2006
- [101] An, J.F.; Vie-Jier Jung; , *Implementation of MIMO Channel Simulator for SUI Channel Model Applications*, Personal, Indoor and Mobile Radio Communications, 2007. PIMRC 2007. IEEE 18th International Symposium on , vol., no., pp.1-5, 3-7 Sept. 2007
- [102] A. Ghazel, E. Boutillon, J. L. Danger, G. Gulak, H. Laamari, *Design and performance analysis of a high speed AWGN communication channel emulator*, Communications, Computers and signal Processing, 2001. PACRIM. 2001 IEEE Pacific Rim Conference on, vol.2, no., pp.374-377 vol.2, 2001
- [103] F. Sattar, M. Mufti, *VLSI architecture of Rayleigh fading simulator based on IIR filter and polyphase interpolator*, Microelectronics, 2004. ICM 2004 Proceedings. The 16th International Conference on, vol., no., pp. 291- 294, 6-8 Dec. 2004

- [104] S. Picol, G. Zaharia, G. El Zein, *Towards the development of a hardware simulator for MIMO radio channels*, Signals, Circuits and Systems, 2005. ISSCS 2005. International Symposium on, vol.1, no., pp. 115- 118 Vol. 1, 14-15 July 2005
- [105] A. Alimohammad, S. F. Fard, B. F. Cockburn, C. Schlegel, *An Improved SOS-Based Fading Channel Emulator*, Vehicular Technology Conference, 2007. VTC-2007 Fall. 2007 IEEE 66th, vol., no., pp.931-935, Sept. 30 2007-Oct. 3 2007
- [106] H. Jeng-Kuang, L. Kuei-Horng, L. Jeng-Da, D. Juinn-Horng, *Fast FPGA prototyping of a multipath fading channel emulator via high-level design*, Communications and Information Technologies, 2007. ISCIT '07. International Symposium on, vol., no., pp.168-171, 17-19 Oct. 2007
- [107] A. Alimohammad, S. F. Fard, B. F. Cockburn, C. Schlegel, *An Accurate and Compact Rayleigh and Rician Fading Channel Simulator*, Vehicular Technology Conference, 2008. VTC Spring 2008. IEEE, vol., no., pp.409-413, 11-14 May 2008
- [108] S. Picol, G. Zaharia, D. Houzet, G. El Zein, *Hardware Simulator for MIMO Radio Channels: Design and Features of the Digital Block*, Vehicular Technology Conference, 2008. VTC 2008-Fall. IEEE 68th, vol., no., pp.1-5, 21-24 Sept. 2008

- [109] Z. Zhan, J. Jiang, P. Zhang, X. Wang, *A generalized hardware implementation of MIMO fading channels*, Communications and Information Technology, 2009. ISCIT 2009. 9th International Symposium on, vol., no., pp.594-597, 28-30 Sept. 2009
- [110] S. F. Fard, A. Alimohammad, B. Cockburn, C. Schlegel, *A single FPGA filter-based multipath fading emulator*, Global Telecommunications Conference, 2009. GLOBECOM 2009. IEEE, vol., no., pp.1-5, Nov. 30 2009-Dec. 4 2009
- [111] S. F. Fard, A. Alimohammad, B. Cockburn, C. Schlegel, *A versatile fading simulator for on-chip verification of MIMO communication systems*, SOC Conference, 2009. SOCC 2009. IEEE International, vol., no., pp.271-274, 9-11 Sept. 2009
- [112] F. Carames, M. Gonzalez-Lopez, L. Castedo, *FPGA-based vehicular channel emulator for evaluation of IEEE 802.11p transceivers*, Intelligent Transport Systems Telecommunications,(ITST), 2009 9th International Conference on, vol., no., pp.592-597, 20-22 Oct. 2009
- [113] K. C. Borries, G. Judd, D. D. Stancil, P. Steenkiste, *FPGA-Based Channel Simulator for a Wireless Network Emulator*, Vehicular Technology Conference, 2009. VTC Spring 2009. IEEE 69th, vol., no., pp.1-5, 26-29 April 2009
- [114] A. S. Akki and F. Haber, *A statistical model for mobile-to-mobile land communication channel*, *IEEE Trans. on Veh. Technol.*, vol. VT-35, no. 1, Feb.

1986.

- [115] A. S. Akki, *Statistical properties of mobile-to-mobile land communication channels*, IEEE Trans. on Veh. Technol., vol. VT-43, no. 4, pp. 826-831, Nov. 1994.
- [116] *Safe and Comfortable Driving Based Upon Inter-Vehicle Communication*, <http://www.cartalk2000.net>, 2001.
- [117] *Car2Car Communication Consortium*, www.car-to-car.org, 2005
- [118] *Project MobiVip*, <http://www-sop.inria.fr/mobivip>, 2005
- [119] A. Paier et al., *First Results from Car-to-Car and Car-to-Infrastructure Radio Channel Measurements at 5.2GHz*, Proc. IEEE Intl. Symp. Personal, Indoor, Mobile Radio Commun., 2007, pp. 15.
- [120] A. Paier et al., *Car-to-Car Radio Channel Measurements at 5 GHz: Pathloss, Power-Delay Profile, and Delay-Doppler Spectrum*, Proc. Intl. Symp. Wireless Commun. Sys., 2007, pp. 22428.
- [121] I. Sen and D. Matolak, *Vehicle-Vehicle Channel Models for the 5-GHz Band*, IEEE Trans. Intell. Trans. Sys., vol. 9, 2008, pp. 23545.
- [122] A. Molisch, F. Tufvesson, J. Karedal, C. Mecklenbrauker, *A survey on vehicle-to-vehicle propagation channels*, *Wireless Communications*, IEEE, vol.16, no.6, pp.12-22, December 2009

- [123] Mecklenbrauker, C.F.; Molisch, A.F.; Karedal, J.; Tufvesson, F.; Paier, A.; Bernado, L.; Zemen, T.; Klemp, O.; Czink, N., *Vehicular Channel Characterization and Its Implications for Wireless System Design and Performance*, Proceedings of the IEEE, vol.99, no.7, pp.1189-1212, July 2011
- [124] FleetNet project Internet on the road, <http://www.et2.tu-harburg.de/fleetnet>, 2000
- [125] D. W. Matolak, I. Sen, X. Wenhui, N. T. Yaskoff, *5 GHZ wireless channel characterization for vehicle to vehicle communications*, Military Communications Conference, 2005. MILCOM 2005. IEEE, vol., no., pp.3016-3022 Vol. 5, 17-20 Oct. 2005
- [126] P. Hoehner, *A statistical discrete-time model for the WSSUS multipath channel*, Vehicular Technology, IEEE Transactions on , vol.41, no.4, pp.461-468, Nov 1992
- [127] P. Dent, G. E. Bottomley, T. Croft, *Jakes fading model revisited*, IEEE Electronics Letters (1993) vol. 29, Issue: 13, Pages: 1162-1163
- [128] M. Patzold, U. Killat, F. Laue, *A deterministic digital simulation model for Suzuki processes with application to a shadowed Rayleigh land mobile radio channel*, Vehicular Technology, IEEE Transactions on, vol.45, no.2, pp.318-331, May 1996

- [129] M. Patzold, U. Killat, F. Laue, and Y. Li, *On the Statistical Properties of Deterministic Simulation Models for Mobile Fading Channels*, Vehicular Technology, IEEE Transactions on, vol. 47, no. 1, February 1998
- [130] M. Patzold, R. Garcia, F. Laue, *Design of high-speed simulation models for mobile fading channels by using table look-up techniques*, Vehicular Technology, IEEE Transactions on, vol.49, no.4, pp.1178-1190, Jul 2000
- [131] M. F. Pop and N. C. Beaulieu *Limitations of sum-of-sinusoids fading channel simulators*, Communications, IEEE Transactions on, vol.49, no.4, pp.699-708, Apr 2001
- [132] M. F. Pop, N. C. Beaulieu, *Design of wide-sense stationary sum-of-sinusoids fading channel simulators*, Communications, 2002. ICC 2002. IEEE International Conference on, vol.2, no., pp. 709- 716 vol.2, 2002
- [133] C. Xiao, Y. R. Zheng, and N. C. Beaulieu, *Second-order statistical properties of the WSS Jakes fading channel simulator*, IEEE Trans. Commun., vol. 50, pp. 888891, June 2002
- [134] D. J. Young and N. C. Beaulieu, *The generation of correlated Rayleigh random variates by inverse discrete Fourier transform*, IEEE Trans. on Commun. vol. 48(7), pp. 1114-1127, 2000
- [135] C. Xiao, C. and Y. R. Zheng, *A statistical simulation model for mobile radio fading channels*, Proc. IEEE Wireless Commun. and Networking Conf. (1): pp. 144-149, 2002

- [136] Y. R. Zheng; C. Xiao, *Simulation models with correct statistical properties for Rayleigh fading channels*, Communications, IEEE Transactions on , vol.51, no.6, pp. 920- 928, June 2003
- [137] J. I. Smith, *A computer generated multipath fading simulation for mobile radio*, IEEE Transactions on , vol.24, no.3, pp. 39- 40, Aug 1975.
- [138] R. Wang and D. Cox, *Channel modeling for adhoc mobile wireless networks*, in Proc. IEEE Veh. Technol. Conf., vol. 1, Birmingham, AL, May 2002, pp. 21-25.
- [139] C. S. Patel, G. L. Stuber. and T. G. Pratt. *Simulation of Rayleigh faded mobile-to-miobile comimunication channels*, in Proc. 58th IEEE Veh. Technol. Conf: (VTC'03), Orlando. FL, USA, Oct. 2003, pp. 163-167.
- [140] B. O. Hogstad, M. Patzold, N. Youssef, and D. Kim. *A MIMO mobile to mobile channel model part II- The simulation model*, Personal, Indoor and Mobile Radio Communications, 2005. PIMRC 2005. IEEE 16th International Symposium on , vol.1, no., pp.562-567, 11-14 Sept. 2005
- [141] A. Petrolino, J. Gomes and G. Tavares. *A Mobile-to-Mobile Fading Channel Simulator Based on an Orthogonal Expansion*, Vehicular Technology Conference, 2008. VTC Spring 2008. IEEE , vol., no., pp.366-370, 11-14 May 2008
- [142] K. C. Borries, D. D. Stancil. *Efficient Simulation of Mobile-To-Mobile Rayleigh Fading using Gaussian Quadrature*, Vehicular Technology Confer-

- ence, 2007. VTC2007-Spring. IEEE 65th , vol., no., pp.534-538, 22-25 April 2007
- [143] A. G. Zaji and G. L. Stuber. *A New Simulation Model for Mobile-to-Mobile Rayleigh Fading Channels*, Wireless Communications and Networking Conference, 2006. WCNC 2006. IEEE , vol.3, no., pp.1266-1270, 3-6 April 2006
- [144] M. I. Akram, A. U. H. Sheikh, *Modeling Nakagami Hoyt Mobile to Mobile Fading Channel with Diffused Line of Sight* Wireless Communications and Networking Conference Workshops (WCNCW), 2012 IEEE , vol., no., pp.398-403, 1-4 April 2012
- [145] Signalware Corporation, *Documentation package of ORS-114 Wide bandwidth Microline Analog peripheral card*, Version 1.0, April 2005
- [146] *www.ti.com*
- [147] Texas Instruments SPRA455A, *Using the TMS320C6000 McBSP as a High Speed Communication Port*, Application report, August 2001.
- [148] Texas Instruments SPRA645A, *Circular Buffering on TMS320C6000*, Application report, April 2001.
- [149] Texas Instruments SPRU198K, *TMS320C6000 Programmer's Guide*, Reference manual, July 2011

- [150] U. Yun; B. Jeon, *Implementation of real-time high speed convolution using DSP*, New Trends in Information Science and Service Science (NISS), 2010
4th International Conference on , vol., no., pp.499-502, 11-13 May 2010

Vitae

- Muhammad Imran Akram
- Nationality: Pakistani
- Current Address: P.O. Box 8611, K.F.U.P.M., Dhahran 31261, Saudi Arabia
- Permanent Address: House 18, Street 1, Block 3D, Nazimabad, Karachi 74600, Pakistan
- Telephone: (+966) 50 411 6138
- Email: *miakram@kfupm.edu.sa*
- Born in Karachi, Pakistan on June 02, 1976
- Received Bachelor of Engineering (B.E.) in Electrical Engineering from NED University of Engineering & Technology, Karachi, Pakistan in 1998.
- Received Master of Science (M.Sc) in Systems Engineering from Quaid-e-Azam University, Islamabad, Pakistan in 2000.
- Joined King Fahd University of Petroleum and Minerals, Dhahran, Saudi Arabia as a Lecturer-B in October 2008.
- Completed Ph.D. in Electrical Engineering in September 2012.